Rhyolitic volcanism in the Onverwacht Group, Barberton Greenstone Belt.

by
Byron Nico Diergaardt

Thesis presented in partial fulfilment of the requirements for the degree Master of Science in Geology at the University of Stellenbosch

Supervisor: Prof. Gary Stevens
Co-supervisor: Prof. Jean-François Moyen
Faculty of Science
Department of Earth Sciences

March 2013

Declaration

By submitting this thesis/dissertation electronically, I declare that the entirety of the work contained therein is my own, original work, that I am the sole author thereof (save to the extent explicitly otherwise stated), that reproduction and publication thereof by Stellenbosch University will not infringe any third party rights and that I have not previously in its entirety or in part submitted it for obtaining any qualification.

September 2012

Acknowledgements

I would like to acknowledge and express my sincere gratitude to my supervisors, Prof. Gary Stevens and Prof. Jean-François Moyen for initiating this study and always having an open door for providing advice and guidance. This study was funded by the South African National Research Foundation (NRF) in the form of grant funding to Prof. Gary Stevens via the SARChI programme and in the form of an MSc. bursary to B.N. Diergaardt.

I'm also grateful to Johan Eksteen of the Mpumalanga parks board and Colin Wille for allowing me access to the Songimvelo Game Reserve for sampling. I also want to thank Sylvain Block for assisting me in sample collection in treacherous areas. Last but not least I want to especially thank Cynthia Sanchez-Garrido and Theo Pauw for getting me acquainted with new software, always providing help if needed and being great friends.

Abstract

The source of the K_2O in the K_2O-rich ~3.45 Ga felsic intrusive rocks of the H6 unit in the Hooggenoeg Formation of the Onverwacht Group in the Barberton Granite Greenstone Terrain (BGGT) is examined in this study. This is of particular research interest because the Paleoarchaean rock record is considered to lack K_2O-rich magmatic rocks. Previous studies on the felsic igneous rocks of the H6 unit have proposed that these rhyolites are K-metasomatised eruptive equivalents of the sodium-rich ~3.45 Ga TTGs of the BGGT and that the K-feldspar crystals in the rocks formed as a consequence of subsolidus replacement of plagioclase by K-feldspar. Furthermore, the timing of K-metasomatism has previously been related to the formation of the Buck Ridge Chert (BRC), which overlies the H6 unit. However, it has recently been demonstrated from granitic clasts in the conglomerate layer at the base of the Moodies sucession that K_2O-rich magmatic rocks formed concurrently with TTG magmas during each of three episodes of TTG magmatism observed in the BGGT. Consequently, the hypothesis of a metasomatic origin for the K_2O-rich character of the felsic rocks of the H6 unit requires further examination.

Previous studies of the chemistsry of felsic volcanic rocks within the H6 unit were based on relatively low numbers of samples. This study has examined a substantial set of the freshest material available. Two varieties of felsic volcanic rocks were identified; K_2O-rich, CaO-poor, Na_2O-poor rhyolites and Na_2O-rich, CaO-poor, K_2O-poor Na-rhyolites. The K_2O- rich rhyolite variety is dominant.

Consequently, it is possible that the K_2O-rich character of these rocks represents a primary magmatic signature. However, this judgment is complicated by the presence of a greenschist-facies metamorphic overprint at 3.2 Ga, which has resulted in complete replacement of micrystalline groundmass and partial replacement of the phenocryst assemblages by greenschist- and sub-greenschist-facies mineral assemblages, which undoubtedly allowed possible shifts in chemical compositions

In this thesis, I test the source of K_2O in these rocks by using the porphyritic textures of the rocks as an indication of the primary composition of the magmas they were formed from. These textures are typically defined by K-feldspar or albite and quartz phenocrysts within a microcrystalline groundmass. The rocks containing albite are Na-rich (Na-rhyolites) whereas the rocks defined by K-feldspar phenocrysts are rhyolites. XRD study of the structural state

of the K-feldspar phenocrysts in the rhyolites indicates that these crystals are orthoclase and intermediate microcline, i.e. medium temperature K-feldspar polymorphs. The modal proportions of K-feldspar, quartz and microcrystalline groundmass in the rhyolites were calculated by using image analysis software. The compositions of the feldspar minerals were determined by electron beam analysis. Minimum bulk rock K_2O content of the rhyolites were calculated from the proportions of K-feldspar crystals and their compositions. Even where the proportion of K-feldspar phenocrysts is relatively low (~ 30%), the calculated minimum bulk-rock K_2O content is still above 5 wt%. The HREE slope (GdN/LuN) of the felsic porphyritic rocks of the H6 rhyolites is similar to that of ~3.45 Ga TTG plutons and steeper than that of granitic clasts of identical age contained in the basal conglomerate of the Moodies Group.

Hence this study has illustrated that the rhyolites of the H6 unit were primary K-feldspar-rich, K_2O-rich magmas that formed contemporarily with the ~3.45 Ga TTGs. This implicitly means that rhyolitic volcanism was more wide spread than previously thought in the Paleoarchaean and that it occurred together with the intrusion of the ~3.45 Ga TTGs in the BGGT.

Uittreksel

Die bron van die K_2O in die K_2O-ryk ~ 3,45 Ga felsiese vulkaniese rotse van die H6-eenheid in die Hooggenoeg formasie van die Onverwacht Groep in die Barberton Graniet Groensteen Terrein (BGGT) is in hierdie studie ondersoek. Dit is van besondere navorsingsbelang omdat die Paleoargeïse gesteenterekord beskou word as vry van magmatiese K_2O ryke gesteentes. Vorige studies oor die felsiese vulkaniese rotse van die H6 eenheid het voorgestel dat hierdie rioliete K-gemetasomatiese eruptiewe ekwivalente van die natrium-ryke ~ 3,45 Ga TTGs van die BGGT is en dat die K-veldspaat kristalle in die gesteentes gevorm is as gevolg van subsolidus vervanging van plagioklaas deur K-veldspaat. Verder is die tydsberekening van K-metasomatisme voorheen gekoppel aan die vorming van die Buck Ridge Chert (BRC) wat die felsiese H6 eenheid bedek. Dit is egter onlangs aangetoon dat K_2O-ryke magmatiese rotse gelyktydig met TTG magmas gevorm is tydens elk van drie episodes van TTG magmatisme waargeneem in die BGGT. Gevolglik vereis die hipotese van 'n metasomatiese oorsprong vir die K_2O-ryke karakter van die felsiese gesteentes van die H6 eenheid verdere ondersoek. Vorige studies van die felsiese vulkaniese gesteentechemie in die H6 eenheid is gebaseer op 'n relatief klein getal monsters. Hierdie studie het ‘n aansienlike stel van die varsste materiaal beskikbaar vir analise ondersoek. Twee variëteite van peralumineuse felsiese vulkaniese gesteentes naamlik 'n K_2O-ryk, CaO-arm, Na_2O-arm rioliet en Na_2O-ryk, CaO-arm, K_2O-arm Na-rioliet. Die K_2O-ryke rioliet variëteit is meer oorheersend as die Na-rioliete.

Dit is dus moontlik dat die K_2O-ryk karakter van hierdie rotse 'n primêre magmatiese kenmerke verteenwoordig. Hierdie uitspraak is egter bemoeilik deur die teenwoordigheid van 'n groenskisfasies metamorfe oorprint op 3,2 Ga, wat gelei het tot die volledige vervanging van mikrokrisstalyne grondmassa en gedeeltelike vervanging van fenokrist samestellings deur groenskis en sub-groenskisfasies minerale samestellings en wat ongetwyfeld toegelaat het vir 'n moontlike verskuiwing in chemiese samestelling.

In hierdie tesis toets ek die bron van K_2O in hierdie gesteentes deur gebruik te maak van die vulkaniese teksture van die gesteentes as 'n aanduiding van die primêre samestelling van die magmas waaruit hulle gevorm het. Hierdie teksture word gewoonlik gedefinieer deur K-veldspaat of albiet en kwarts fenokriste binne 'n grondmassa van wat vroeërglasoorblyfsels was. Die rotse wat albiet bevat is Na-ryk (Na-rioliete) terwyl die rotse gedefinieer deur K-

veldspaat fenokriste rioliete is. XRD studie van die strukturele toestand van die K-veldspaat fenokriste in die rioliete dui aan dat hierdie kristalle ortoklaas en intermediêre mikroklien is, dit wil sê die hoër temperatuur K-veldspaat polimorfe. Die modale proporsies van K-veldspaat, kwarts en glasoorblyfsels in die rioliete is akkuraat bereken deur gebruik te maak van beeld analise sagteware. Verder is die samestellings van die veldspaat minerale bepaal deur die elektronstraal analise. Minimum grootmaat rots K_2O inhoud van die rioliet is berekén vanaf die fase verhouding van K-veldspaat en hul komposisies. Resultate dui daarop dat selfs waar die verhouding van K-veldspaat phenocrysts is relatief laag (~ 30%), die berekende minimum K_2O grootmaat rots samestelling is nog steeds bo 5 wt%. Die REE-helling (GDN / Lun) van felsiese porphyritic rotse van die H6 is soortgelyke relatief tot die REE helling van ~ 3,45 Ga TTGs en steiler REE helling relatief tot granitiese klaste vervat in die basale konglomeraat van die Moodies-groep.

Dus het hierdie studie getoon dat die rioliete van die H6-eenheid primêre K-veldspaat-ryke, K_2O-ryke en peralumineuse magmas was wat gevorm is terselfdertyd met die ~3,45 Ga TTGs. Dit beteken implisiet dat riolitiese vulkanisme meer wyd verspreid was as wat voorheen gedink is in die Paleoargeïkum en dat dit tesame met die indringing van die ~ 3,45 Ga TTGs in die BGGT plaasgevind het.

TABLE OF CONTENTS

List of Figures

List of tables

Chapter 1: Introduction

Research on felsic igneous rocks of the 3.55 to 3.10 Ga Barberton Granite Greenstone Terrain (BGGT) has mostly concentrated on the trondhjemite-tonalite-granodiorite (TTG) (Viljoen and Viljoen, 1969d; Anhaeusser et al., 1981, 1983; Robb and Anhaeusser, 1981; Kroner et al., 1996; Kisters et al., 2003; Moyen et al., 2006; 2007) and granite-monzonite-syenite (GMS) (Belcher and Kisters 2006a, 2006b; Westraat et al., 2004; Yearron, 2003) groups of rocks, with very few studies addressing the rare felsic lavas that exist within the Barberton Greenstone Belt (BGB). The TTG and GMS granitoid suites occur as large plutons around the belt and intrusive into it whereas felsic igneous rocks occur as volcanic rocks and are associated with smaller high-level intrusions within the stratigraphy of the belt.

Most studies that have addressed the felsic volcanic rocks have linked them to TTG magmatic events, as prominent TTG plutons have similar crystallisation ages. For example: Amphibolite facies ~3500 Ma felsic volcanic rocks of the Theespruit Formation have been proposed to be eruptive equivalents of the 3509 Ma rocks of the Steynsdorp Pluton (Armstrong et al., 1990; Kroner et al., 1992; Kroner et al., 1996); greenschist to sub-greenschist facies 3445 Ma felsic volcanic rocks of the Hooggenoeg Formation have been proposed to be genetically related to the ~3.45 Ga Stolzburg and Theespruit Pluton (de Wit et al., 1987; Hofmann and Harris., 2008) ; and, greenschist to sub-greenschist facies ~3223 Ma felsic volcanic rocks of the Fig Tree Group have been proposed to be comagmatic with the ~3.23 Ga Kaap Valley, Nelshoogte and Badplaas Plutons (Kroner et al., 1991a; de Ronde and Kamo, 2000). TTG plutons are mostly sodic and plagioclase-rich tonalities, trondjemites and granodiorites with low K_2O contents (K-feldspar < 10%). As the felsic volcanic rocks of the BGB are predominantly of rhyolitic composition, a general consequence of these proposed links with TTG magmatism has been that the rhyolites have been regarded as having undergone pervasive potassium metasomatism.

However a recent study by Sanchez-Garrido et al. (2011) provides reason to question this interpretation. Sanchez-Garrido et al. (2011) have demonstrated that K_2O-rich extrusive and high-level intrusive granitic rocks were produced during each of the three main TTG magmatic events in the BGGT and that the products of this rhyolitic magmatism are recorded as clasts within a conglomerate that marks the onset of coarse clastic sedimentation in response to ca 3.2 Ga terrane accretion. The generally peraluminous (A/CNK ~1 to 1.3) and

potassic character of the rocks described by Sanchez-Garrido et al., (2011), their flat REE patterns and monazite-bearing accessory mineral suite indicate that these are S-type granites that were derived from the partial melting of metasediments. These characteristics, as well as the very low CaO content of the rocks, coupled with significant Sr contents and lack of a pronounced negative Eu anomaly, rule out any petrogenetic link with TTG magmas of equivalent age. Consequently, Sanchez-Garrido et al. (2011) conclude that the anatectic events that produced the TTG magmas, by the melting of metamafic rocks, also involved the melting of metasediments to produce these granites and rhyolites. However the mantle-like $\delta^{18}O$ values of zircon in these rocks suggests that the peraluminous character is unlikely to be inherited from the source (C. Sanchez-Garrido pers. comm.). As this has been shown to have occurred during each of three TTG producing events, the production of rhyolites and high-level granites appears to be a fundamental part of the geodynamic process that produced TTG magmas in the BGB. Clearly these findings question the general interpretation that the K-rich signature in volcanic and volcaniclastic rocks within the BGB stratigraphy can be assumed to be a consequence of alteration.

The similar crystallization ages and similar chondrite-normalized REE patterns (Hofmann and Harris., 2008; Rouchon et al., 2009) of these felsic volcanic rocks (rhyolites) and the ~3445 Ma Stolzburg and Theespruit TTG Plutons has prompted previous workers to suggest that these rhyolites are the K_2O metasomatised eruptive equivalents of the Stolzburg and Theespruit plutons (de Wit et al., 1987a). In particular, the high K_2O content and lower concentrations of almost all other major elements except SiO_2 in the H6 rhyolites, in comparison with the ~ 3445 Ma TTG plutons, is proposed to be linked with formation of muscovite-bearing K_2O enriched chert horizons that cap the H6 layer (Hofmann and Harris, 2008; Rouchon et al., 2009). These chert horizons are closely related to volcanic activity within the Onverwacht Group and consist of >75% microcrystalline quartz, muscovite and plagioclase. The muscovite has a metasomatic origin that is interpreted to reflect pervasive hydrothermal alteration (Lowe et al., 1999). The possible origin of K_2O from primarily K_2O-rich felsic porphyritic layers directly in contact with chert layer was previously identified by Lowe and Knauth, (1977), but more recently overlooked in favour of the conclusion that K_2O in both rock types is of metasomatic origin, with an unspecified source (Hofmann and Harris, 2008; Rouchon et al., 2009).

The very well preserved volcanic character of the H6 rhyolites for the Archaean presents an opportunity to test the source of the K_2O-rich signature in the volcanic rocks. In particular,

the fact that the rocks are sufficiently undeformed to allow for the identification of phenocrysts and the magmatic structures defined by these crystals, allows the primary chemistry of the system to be partially constrained by information that is independent of bulk-rock chemical analysis. This study takes this approach of using 31 undeformed felsic igneous rocks that have undergone greenschist-facies metamorphism to test the validity of the metasomatism hypothesis to explain the K_2O-rich character of these rocks.

Chapter 2: Geological setting and locality

2.1. Stratigraphy of the Barberton Granite Greenstone Belt (BGGT)

The 3.55 to 3.10 Ga BGGT in South-Africa and Swaziland is one of the oldest, best preserved early crustal sections on Earth (Fig.2.1; Lowe and Byerly, 2007). Rocks of the BGGT can be subdivided into three constituents: 1. The BGB which consist mostly of supracrustal successions; 2. The 3.55 to 3.21 Ga trondhjemite-tonalite-granodiorite (TTG) group intrusions, which are characterised by their Na- rich and K-poor compositions; 3. The 3.14 to 3.10 Ga granite-monzonite-syenite (GMS) group. The rocks of the BGB and the TTG plutons are syngenetic, whereas the GMS plutons post-date the formation of the greenstone belt (Lowe and Byerly, 2007).

The rocks of the BGB form part of the Swaziland Supergroup and can be subdivided into three lithostratigraphic units, firstly the >3547 to ~3260 Ma Onverwacht Group at the base, secondly the ~3260 to 3225 Ma Fig Tree Group, which overlies the Onverwacht Group and finally the <3225 Ma Moodies Group at the top (Viljoen and Viljoen, 1969a, 1969b; Kröner et al., 1991a; Heubeck and Lowe, 1994a; Byerly et al., 1996; Lowe and Byerly, 1999).

The Onverwacht Group predominantly consists of komatiites, komatiitic basalts, basalts and cherts with minor amounts of dacite, rhyolite and clastic sedimentary rocks. The Onverwacht Group is divided into the Sandspruit, Theespruit, Komati, Hooggenoeg, Kromberg and Mendon Formations (Viljoen and Viljoen., 1969; Armstrong et al., 1990; Kröner et al., 1991; Kamo and Davis, 1994; Byerly et al., 1996; Lowe and Byerly, 1999b). The Hooggenoeg Formation, in particular the H6 unit of this formation, is the host of the felsic lavas that are the focus of this study (Fig. 2.1).

The Hooggenoeg Formation was subdivided into six informal members by Lowe and Byerly, (2007), and consists predominantly of a thick succession of tholeiitic basalts, komatiitic basalts and thin cherty units (Viljoen and Viljoen, 1969b). These six members are: The H1 known as the Middle Marker that consists of a thin (1 to 5m thick) sedimentary unit comprised of silicified komatiitic ash and carbonaceous material; the H2 is comprised of tholeiitic pillowed and massive basalts capped by chert; the H3 and H4 consist of units of komatiitic basalt, basalt and vestiges of silicified volcaniclastic units; the H5 is made up of spherulitic basalts and basalt capped by silicified volcaniclastic sediments; and the H6 forms

the top part of the Hooggenoeg Formation and consists of felsic volcanic and volcaniclastic rocks, as well as conglomerates, sandstone and 3445 ± 4Ma; and 3451 ± 5Ma felsic intrusive rocks (Viljoen and Viljoen, 1969; de Wit, 1982; Lowe et al., 1985; de Wit et al., 1987; Lowe and Byerly., 1999b; de Vries et al., 2006). The H6 is capped by the Buck Ridge Chert (BRC). Previous studies in the area have placed the BRC within Hooggenoeg Formation (Viljoen and Viljoen, 1969; Brandl and de Wit., 1997; de Vries et al., 2006) whereas others propose that it constitutes the basal part of the Kromberg Formation (Byerly et al., 1996; Lowe and Byerly, 1999a).

The Onverwacht Group is overlain by the Fig Tree Group, which consists of interstratified terrigenous clastic units and dacitic to rhyodacitic volcaniclastic and volcanic rocks (Lowe and Byerly, 2007). The youngest rocks of the BGB occur within the Moodies Group which consists of lithic, feldspathic and quartzose sandstones, conglomerates and siltstones. The evolution of the BGGT can systematically be described on the basis of the different groups that are the building blocks of the BGGT.

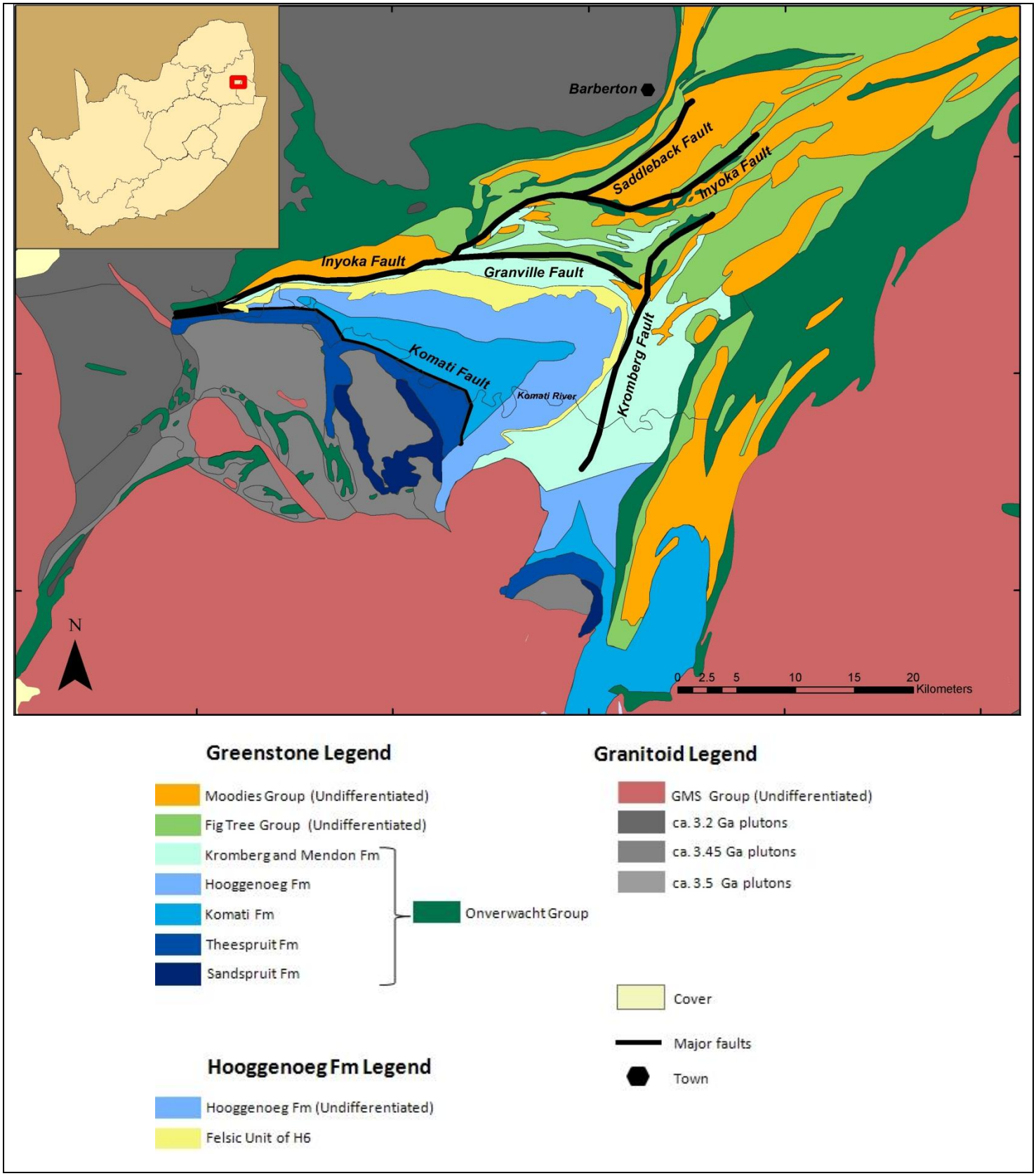

Figure 2.1 Geological map of the Barberton Greenstone Belt, illustrating the distribution of the different lithological units that make up the belt and their relationship with the surrounding TTG and GMS plutons to form the Barberton Granite Greenstone Terrain (BGGT) (Map modified after Anhaeusser et al., 1981; Kröner et al., 1996, Diener et al., 2006). The position of felsic H6 unit was modified after maps by de Wit et al., (1987) and de Vries et al., (2006).

2.2. Development of the BGGT

The development of the BGGT was grouped within four evolutionary stages by Moyen et al, 2007. Within the Onverwacht Group two events can be recognised on the basis of the intrusion of two generations of TTG plutonic rocks, in conjunction with comagmatic felsic volcanic layers within the stratigraphy of the Onverwacht group. The first stage of evolution is represented by voluminous mafic volcanism and subsequent felsic volcanism to form rocks of the Theespruit Formation, with the eruption of the felsic volcanic layers being broadly comagmatic with the 3.55 – 3.50 Ga Steynsdorp Pluton (Kröner et al., 1996) which intrudes the lower layers of the Theespruit Formation. The geological environment that is responsible for this evolutionary stage is unclear (Lowe and Byerly, 2007; Moyen et al., 2007).

The second stage of evolution of the BGGT is represented by voluminous mafic, ultramafic and minor amounts of felsic volcanism that formed the Komati, Hooggenoeg and Kromberg Formations of the Onverwacht Group. The felsic layer is located in the H6 unit of the Hooggenoeg Formation and consists of 3451 ± 5Ma (de Vries et al., 2006) felsic volcanic rocks that has the same age within error of the 3.46-3.44 Ga Stolzburg and Theespruit Pluton (Kröner et al., 1991; Dziggel et al., 2002; Kamo and Davis, 1994), clastic sediments and conglomerates. These clastic sediments together with conglomerates illustrate that topography existed at this time in Earth's history (Moyen et al., 2007). Furthermore the H6 unit contains direct evidence for D1 deformation. This is represented by listric normal faults that are mostly synchronous with the intrusions of ~3.45 Ga felsic igneous rocks and most likely represented an oceanic arc environment (Lowe, 1999b; de Ronde and Kamo, 2000; Lowe and Byerly, 2007; de Vries et al., 2006).

The third evolutionary event was followed by the tectonic amalgamation and suturing of tectono-stratigraphic suites to form a proto-continent that is well recorded by the ~3230 Ma metamorphism and deformation in the BGGT (Lowe, 1999; Lowe and Byerly, 1999). This metamorphic event is well characterised by high-grade metamorphic rocks in the south of the BGB and low-grade greenschist-facies metamorphism in the north of the BGB (Diener et al., 2005; Kisters et al., 2003; Moyen et al., 2006). The ~3258 – 3216 Ma event is also represented by the 3.23-3.21 Ga TTG plutons (Tegtmeyer and Kröner, 1987; Kröner et al., 1991a; Kamo and Davis, 1994; Armstrong et al., 1990; de Ronde and Kamo, 2000) and sediments of the Fig Tree and Moodies Groups. The Fig Tree Group is characterized by a transition from deep- to shallow marine terrigenous sediments that were deposited during the

closure of an ocean basin during convergence (Kröner et al., 1991a; Byerly et al., 1996; Lowe and Byerly, 2007), whereas the Moodies Group is typified by subaerially deposited conglomerates, feldspar- and quartz-rich sandstones which has been deposited into discrete contractional and extensional basins which reflects gradual orogenic uplift (Heubeck and Lowe, 1994a; 1994b; Lowe, 1999). 4) The last and continent forming stage of the ~3216 - <3100 Ma evolution of the BGGT is characterized by intraplate compression that in turn caused crustal melting from which the GMS group originated (Lowe, 1999; Belcher and Kisters, 2006a, 2006b).

The TTG plutons within the BGGT are very well preserved and contain valuable information concerning the development of the BGGT, in particular valuable constraints of the magma source conditions and consequently the geodynamic setting of magma formation. These rocks are particularly important to this study as some of them form at the same time as the felsic volcanic rocks of the H6 unit. Consequently, the characteristics of the TTG group, especially the ~3.45 Ga TTGs are described below.

2.3. TTGs from the BGGT

TTG plutons are the most common component of the Archaean continental crust today (Martin, 1994). TTG plutons are sodic and leucocratic igneous rocks with dominant plagioclase (55 -65% and quartz in their modal mineralogy (15-20%). Potassic minerals are subordinate and are usually represented by biotite. K-feldspar is either absent or makes up a relatively minor component (<10%) (Le Maitre, 2002). Mafic phases are represented by biotite (5-15%) and on rare occasions, hornblende. Accessory minerals are characterized by epidote, allanite, apatite, secondary chlorite and zircon (Moyen et al., 2007).

The genesis of the TTGs from the BGGT can be traced to three main generations that correspond to the first three of the four developmental (evolutionary) events discussed in Chapter2.2. 1) The 3.55-3.50 Ga TTGs of the BGGT are characterized by the tonalitic Steyndorp Pluton that has been deformed and metamorphosed to banded gneisses (Robb and Anhaeusser, 1983; Kröner et al., 1996). 2) The ~3.45 Ga generation is represented by the Stolzburg, Theespruit and smaller Theeboom, Eerstehoek and Doornhoek plutons, whereas the 3) ~3.23-3.21 Ga generation is represented by the Kaap Valley and Nelshoogte plutons,

and Badplaas gneissic unit. 4) The fourth plutonic event is represented by the 3.14-3.10 Ga granite-monzonite-syenite (GMS) group.

The felsic igneous rocks of the H6 unit have previously been proposed to be eruptive equivalents of the Stolzburg and Theespruit Plutons that have undergone K-metasomatism (de Wit et al., 1987a; Hofmann and Harris, 2008; Rouchon et al., 2009). This interpretation that the felsic igneous rocks of the H6 have undergone K- and Si-metasomatism was based on O-isotopes and comparisons between chemistry of a small group of H6 rocks with that of the synchronous Na-rich Theespruit and Stolzburg Plutons (Hofmann and Harris, 2008; Rouchon et al., 2009). Thus for the purposes of this study it is important to note the mineralogy and chemistry of the ~3.45 Ga Stolzburg and Theespruit plutons in the BGGT.

2.4. Geochemistry and petrogenesis of ~3.45 TTGs from the BGGT

The most favoured theory for TTG genesis is by high pressure partial melting of hydrous mafic lithologies such as either amphibolites (Foley et al., 2002) or eclogites (Rapp et al., 2003). This hypothesis is supported by substantial bodies of experimental and geochemical research (experimental work reviewed in Moyen and Stevens, (2006); geochemical work is reviewed in Martin, 1994).

The three generations of TTGs in the BGGT have been subdivided into three geochemical types by Moyen et al, (2007). These distinct geochemical types can also be subdivided into distinct subordinate series based on their Sr and K_2O/Na_2O relationship. The geochemical types are the 1) K_2O poor with “low” or “high” amounts of Sr; 2) a K_2O rich sub-series and 3) a positive Eu/Eu*, extremely low K_2O, lower Na_2O and higher Al_2O_3 contents than rocks of group 1, “melt depleted” sub series (Moyen and et al., 2007).

The mostly homogenous ~3.45 Ga leucocratic trondjemitic Stolzburg, Theespruit plutons are characterised by high Al_2O_3contents (>15%), similar to most TTGs in the BGGT, high SiO_2 (≥70%), high-Sr, relative to other TTGs of the BGGT, as well as flat HREE patterns and depleted HREE concentrations. The geochemistry of the ~3.45 TTGs is thus grouped within the K_2O poor and high Sr sub-series (Table 1) (Moyen et al., 2007; Moyen, 2011).

It is possible to constrain the likely pressure conditions of TTG magma genesis by using Al_2O_3, Na_2O, Sr, Y, Yb concentrations and consideration of the minerals most likely to retain these elements in the residuum during partial melting. Therefore the conditions for high SiO_2, Al_2O_3, Sr, Na_2O and depleted HREE TTG melts can be theoretically recreated by geochemical modelling. During geochemical modelling of partial melting for amphibolites it was observed that Al_2O_3, Na_2O, CaO and Sr prefer to be incorporated within plagioclase in the residuum if the pressure of melting is below 15kbar (Moyen and Stevens, 2006). This interpretation is supported by the observation that during high pressure melting of garnet and plagioclase containing amphibolites the melt produced is similar in composition to trondjemites with low Sr contents. At pressures above the plagioclase stability, the Sr content in the melt is boosted whereas the Ca from the plagioclase is accommodated within the pyroxene in the residuum (Zamora, 2000; Martin and Moyen, 2002; Moyen and Stevens, 2006).

Table 1. TTG plutons found within the BGGT subdivided into geochemical subordinate series based on their major and trace element geochemistry.

TTG plutons of the BGGT	K_2O poor sub-series		K_2O rich sub series	High Eu/Eu*, low K_2O, "melt depleted" subseries
	High Sr	Low Sr		
~3.55-3.50 Ga Steynsdorp pluton		x	x	
~3.45-3.44 Ga Stolzburg pluton	x			
~3.44 Ga Theespruit pluton	x			
~ 3.29-3.24 Ga Badplaas gneisses	x	x	x	x
~3.23-3.21 Ga Nelshoogte pluton		x		
~3.23-3.22 Ga Kaap Valley tonalite		x		

The HREE contents in the melt are generally controlled by the amount of garnet in the residue. In order to produce magmas with the HREE depletion observed in typical high Al_2O_3

TTGs, Moyen and Stevens, (2006) proposed that the residuum required at least 20% garnet fora tholeiitic basalt source. This equates to a depth of anatexis of at least 50 km (Moyen, 2011).

During modelling (model 3) in the study of Moyen and Stevens (2006) it was found that the ~3.45 TTGs possibly formed at above 20 kbar, where the Na_2O, Sr and Eu is incorporated in melt fraction whereas Ca is incorporated in the residuum within pyroxene (Moyen and Stevens, 2006; Moyen, 2010). At these pressures the amount of garnet in residuum would also deplete the HREE contents similar to ~3.45 TTGs HREE contents (Moyen and Stevens, 2006; Moyen, 2010).

2.5. Previous work on the Felsic volcanic rocks of the H6

Previous work on the rocks of the H6 unit mostly concentrated on the structure and stratigraphy of the Hooggenoeg Formation, with special attention to the measurement of U/Pb ages of the felsic volcanic rocks in the H6 unit and the formation of the BRC. A list of previous research on the felsic volcanic rocks of the H6 is provided in Table 2.

More recent studies on the felsic volcanic rocks have concentrated on their paleomagnetism and fluid inclusion characteristics (de Vries and Touret, 2007; Tarduno et al., 2010; Usui et al., 2009). The fluid inclusion studies on the Buck Ridge Chert samples illustrate that the H6 rocks have not experienced metamorphic temperatures higher than 300˚C (de Vries and Touret, 2007).

Three past studies have commented on the geochemistry of the felsic igneous rocks of the H6, i.e. de Wit et al., (1987a), Hofmann and Harris (2008) and Rouchon et al., (2009). The findings of these studies are discussed below.

Table 2.A list and short description of the previous research in the BGGT that included rocks within felsic unit of the Hooggenoeg Formation (H6).

Previous work reference	**Nature of study on the felsic igneous rocks of H6**
Hall, 1918	Structure and Stratigraphy which includes portions of the H6 felsic igneous rocks.
Visser, 1956	"
Viljoen and Viljoen, 1969a	"
Viljoen and Viljoen, 1969b	"
Anhaeusser, 1973	"
de Wit et al., 1987a	Structure, Stratigraphy, Geochemistry and Geochronology of H6 felsic igneous rocks.
Armstrong et al., 1990	Stratigraphy and Geochronology which included the calculation of ages from the H6 felsic igneous rocks.
Kröner et al., 1991a	"
Byerly et al., 1996	Stratigraphy and Geochronology which included the calculation of ages H6 felsic igneous rocks.
Xie et al., 1997	Metamorphic and fluid inclusion study that includes portions of the Hooggenoeg Formation.
Cloete, 1999	Metamorphic study which included portions of the H6 felsic igneous rocks.
Lowe and Byerly, 1999	Mapping and Stratigraphy which includes portions of the H6 felsic igneous rocks.
Lowe et al., 1999	Stratigraphy and Geochronology which included the calculation of agesfrom the H6 felsic igneous rocks.
Knauth and Lowe, 2003	Oxygen Isotope study on cherts, especially the BRC.
de Vries et al., 2006	Structural mapping and Geochronlogy of H6.
de Vries and Touret, 2007	Fluid inclusions of the BRC.
Hoffman and Harris, 2008	Geochemistry, metasomatism and oxygen isotope study on the felsic igneous rocks of the H6.
Usui et al., 2009	Paleomagnetic and rock magnetic study on the felsic igneous rocks of the H6.
Rouchon et al., 2009	Geochemistry and metasomatism study on the felsic igneous rocks of the H6.
Tarduno et al., 2010	Study of Earth's magnetic field ~3.45 Ga ago on dacites of the H6.
de Wit et al., 2011	Geology and tectonostratigraphy of the Onverwacht Group which includes rocks of the H6.

The first geochemical and U/Pb isotopic investigation of felsic igneous rocks of H6 by de Wit et al., (1987a), also included the felsic volcanic rocks found outside the H6 layer and concentrated on the upper 3.5- to 3.3 Ga Onverwacht Group. These authors calculated the zircon U/Pb ages of the shallow level felsic intrusions and domes at 3445 ±4 Ma from a felsic volcanic sample. The major and trace element geochemical data reported by this study includes information from 8 samples with a subset of HREE information reported from only 2 samples. The other 8 samples reported on by de Wit et al., (1987a), were sampled from locations stratigraphically above the BRC, most likely from within the Mendon Formation, since the Kromberg Formation lacks a felsic component (Lowe and Byerly, 2007).

The conclusion of the study by de Wit et al (1987a) was that the felsic volcanic rocks of the 3.3- to 3.5-Ga BGB can be grouped as volcanic equivalents of the trondjemites and tonalites that intrude the lower portions of the stratigraphy of the BGB. The volcanic equivalents of the trondjemites proposed by the de Wit et al (1987a) study are located within the H6. There was no correlation observed between the K_2O, Na_2O, CaO, Rb and Sr contents of the H6 felsic volcanic rocks and the contemporary ~3.45 Ga TTG rocks of the Theespruit and Stolzburg plutons. The cause for this disparity was proposed to be hydrothermal alteration of the volcanic rocks that enriched them in K_2O, Rb and depleted them in Na_2O, CaO and Sr (de Wit et al., 1987a). The similar U/Pb age constraints, P_2O_5 and TiO_2 contents and proposed similar chondrite normalized REE patterns between the felsic volcanics of the H6 and ~3.45 TTGs was the basis on which de Wit et al (1987a) concluded that the felsic volcanic rocks as eruptive equivalents of the ~3.45 Ga TTGs.

The Harker type diagrams below (Fig 2.2) present Al_2O_3 vs Zr, TiO_2, Y, Ce and Nb element ratios from the previous studies of de Wit et al., (1987a) and Rouchon et al., (2009) vs those for the ~3.45 Ga BGGT TTG. The TTG data is from the TTG database of Moyen, (2011). The plots show that the trace element chemistry is similar for the felsic volcanic rocks relative to the ~3.45 Ga TTGs for similar amounts of Al_2O_3 (Fig 2.2).

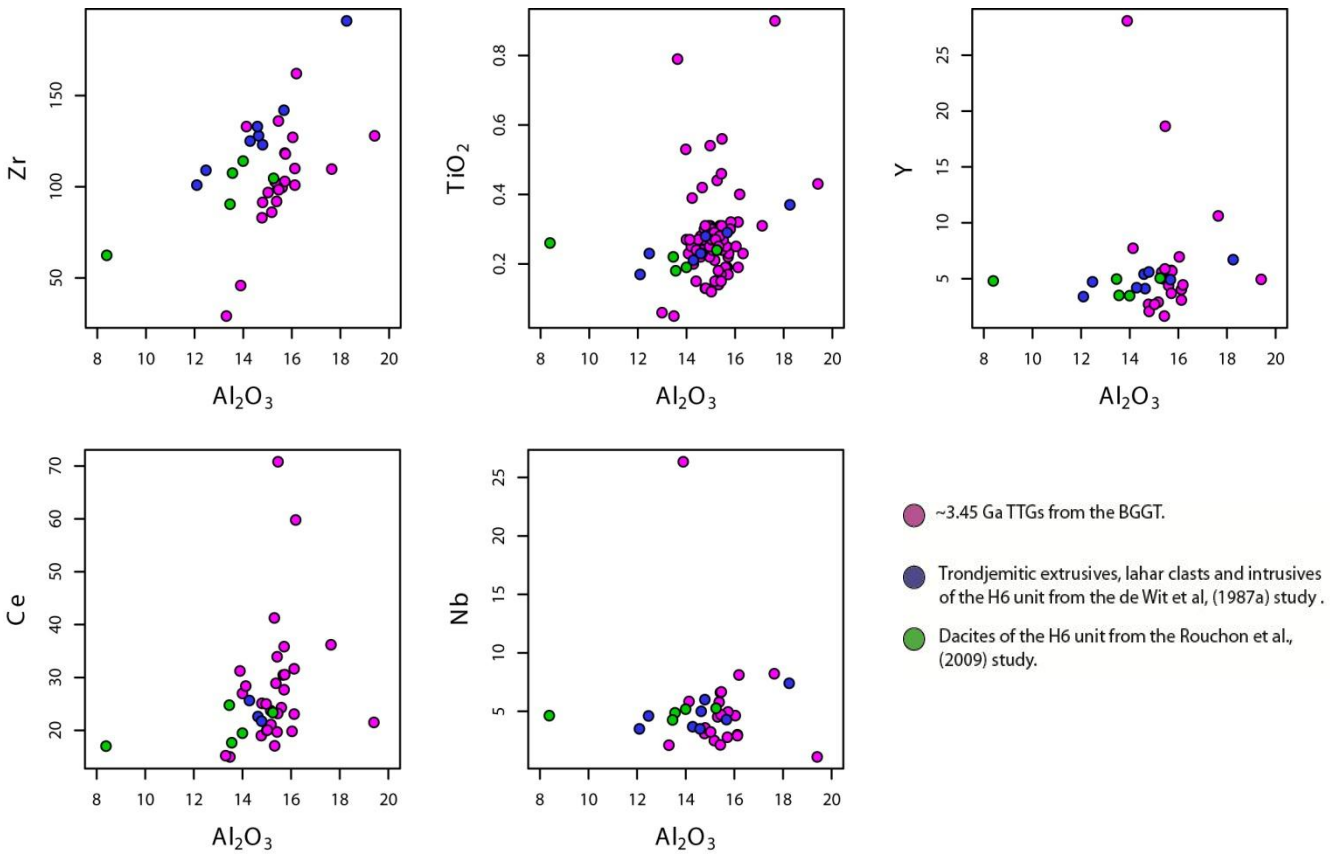

Figure 2.2. Harker type diagrams of Al2O3 vs Zr, TiO2, Y, Ce and Nb comparison of dacites of the H6 unit from previous studies by Rouchon et al., (2009) and de Wit et al., (1987a) vs ~3.45 Ga TTGs from the BGGT.

The Hofmann and Harris (2008) study examined 3 silicified dacite and 3 sandstone samples derived from the dacite in the H6 layer of the Onverwacht Group. This study concluded that the felsic igneous rocks of the H6 underwent pervasive silica and K-alteration. This conclusion was largely based on the high $\delta^{18}O$ values, more specifically the systematic increase in $\delta^{18}O$ and SiO_2 (decrease in most other elements) with increasing stratigraphic height that indicates a high water rock ratio of which the temperature of the water was between 100-150 ^{o}C. This conclusion was based on a comparison between 3 silicified dacite samples from the H6 and rocks of the Theespruit Pluton, in conjunction with the findings of the prior study by de Wit et al. (1987a). The results of this comparison illustrate K, Rb, Si and Ba enrichment in the volcanic rocks with the depletion of all other major elements in the felsic rocks relative to the average composition of the Theespruit pluton by using an isocon diagram (Fig. 2.3). A low temperature (100-150 ˚C) of alteration was proposed due to loss of Mg, and the enrichment of K, Rb and an increase of $\delta^{18}O$ (10.2% to 12.6%) together with an increase in SiO_2 content upwards towards the Buck Reef Chert (BRC). The source of silica

during alteration could be a result of olivine, pyroxene, feldspar and volcanic glass breakdown processes whereas the source of K is generally only speculated upon as being possibly derived from large continents that possibly existed in the Archaean (Hofmann and Harris, 2008). The granitic clasts in the Moodies Group and granite-like REE patterns of felsic volcanic units in the Theespruit Formation are seen as possible remnants of these continents (Hofmann and Harris, 2008).

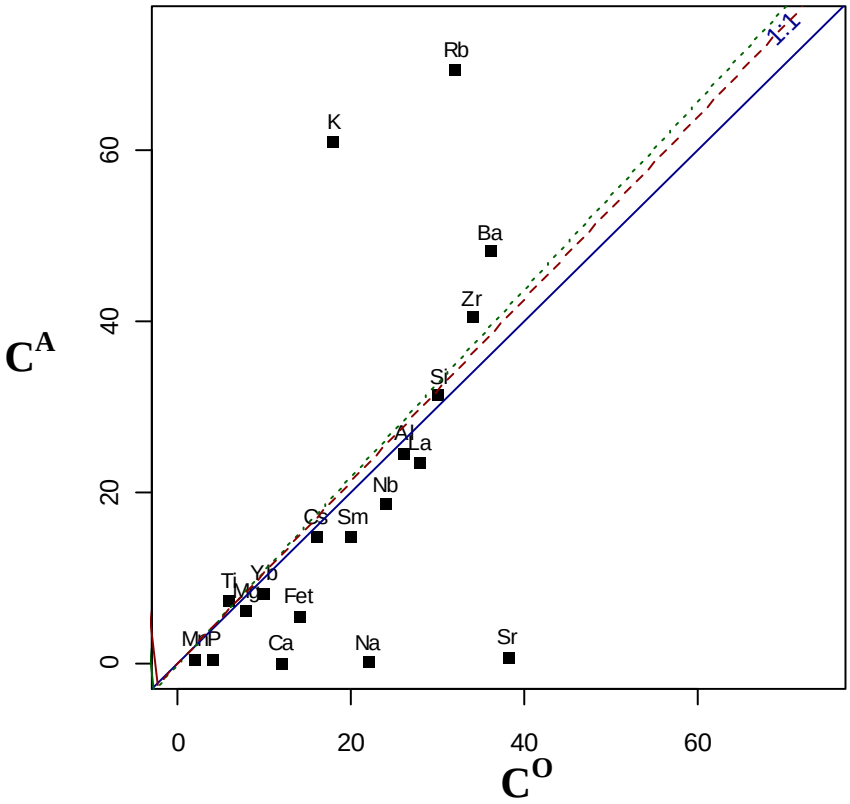

Figure 2.3 Isocon diagrams for least-altered sample (Theespruit pluton sample TTG 235 = CO) and most altered sample (felsic volcanic sample from the H6 = CA). Al, Si, Cs and Ti plot close to the 1:1 solid line or isocon, indicating that the concentration of these elements has not been "altered". Elements above the isocon line have been added during alteration whereas elements below isocon line have been removed during alteration.

In the study by Rouchon et al., (2009), the volcanic rocks of the H6 were compared to the rocks of the Theespruit pluton, in a manner similar to the comparison made by Hofmann and Harris (2008). Rouchon et al., (2009) studied 5 H6 igneous rock samples and concluded that the rocks had undergone K-, Si-metasomatism from an original dacitic composition that was depleted of all other major elements. Rouchon et al., (2009) propose that Na-feldspar in the lavas was replaced by assemblages of sericite + K-Feldspar + quartz and that volcanic glass was replaced by sericite + quartz. The K-feldspar identified in the Rouchon et al., (2009)

study is orthoclase with approximately 0.15 wt. % of Na_2O and 0.15 wt. % CaO. The siltstones in H6 contain detrital K-feldspar in a quartz muscovite matrix. This is interpreted to illustrate derivation from the associated metasomatised dacite. Therefore Rouchon et al., (2009) propose that the BRC formed from low temperature hydrothermal alteration from previously K-metasomatised felsic volcanic rocks.

The K-feldspar compositions documented in the study of Rouchon et al., (2009) have higher amounts of Cr (0-43 ppm), Zn (6-28 ppm), Cu (10-40 ppm), Co (1-17 ppm) and Ni (0-21 ppm) elements then K-feldspars in granites. Since the Cr, Zn, Cu, Co and Ni elements prefer to form complexes with Cl and OH, the origin of Cr, Zn, Cu, Co and Ni in K-feldspar is interpreted to be hydrothermal (Henley et al., 1984, Alfonso et al., 2003). The secondary formation of K-feldspar and muscovite is believed to have formed at low temperatures (100-150 ˚C) by the following reactions as listed in Rouchon et al., (2009):

3 Orthoclase + $4H^+$→ K-mica + K^+ (aq) + 12SiO2
Albite + $2K^+$ → orthoclase + $2Na^+$ (aq)
3 Anorthite + $2K^+$ +$4H^+$→ 2K-mica + $3Ca^{2+}$ (aq)
Anorthite + $2K^+$ + $4SiO_2$→ orthoclase + $2Ca^+$ (aq)

The findings of these previous studies are limited by a number of rather important shortcomings: 1) the nature and geochemistry of the felsic volcanic rocks of the H6 member was described from a limited amount of material (de Wit et al., 1987a = 8 samples; Hofman and Harris, 2008 = 3 samples; Rouchon et al., 2009 = 5 samples). In the Hofmann and Harris (2008) study 6 samples were used for geochemical analysis and 3 of these rocks were sedimentary rocks. The study of Rouchon et al., (2009) was mostly based on the sedimentary rocks of the H6 layer and included 5 samples that are interpreted to be igneous rocks with one of these samples having more than 85% SiO_2. Consequently, there are questions over the representivity of the material investigated in these studies, as well as the appropriateness of the material in some cases to show the processes that have shaped the igneous rocks.

2) Various geochemical studies by previous authors (Hofmann et al, 2008; Rouchon and Oberger, 2009) have named these felsic igneous rocks as dacites, based on the assumption that these igneous rocks start out as TTG-like compositions. This prejudges the issue of whether or not the rocks are altered. In essence if it is assumed that a rock of rhyolitic

composition originated as a dacite, then the finding will always be that the rock has undergone metasomatic K and Si enrichment. Consequently, the validity of the findings of all of these works, hinges on the correctness of the original finding of de Wit et al., 1987. On compositional grounds, the majority of the intrusive rocks of the H6 are rhyolites with minor amounts of dacites (Fig 2.4), but strictly speaking these are metamorphic not igneous rocks. The more correct collective term would be rhyodacites and this was indeed the term that de Wit et al., (1987a) used for these igneous rocks.

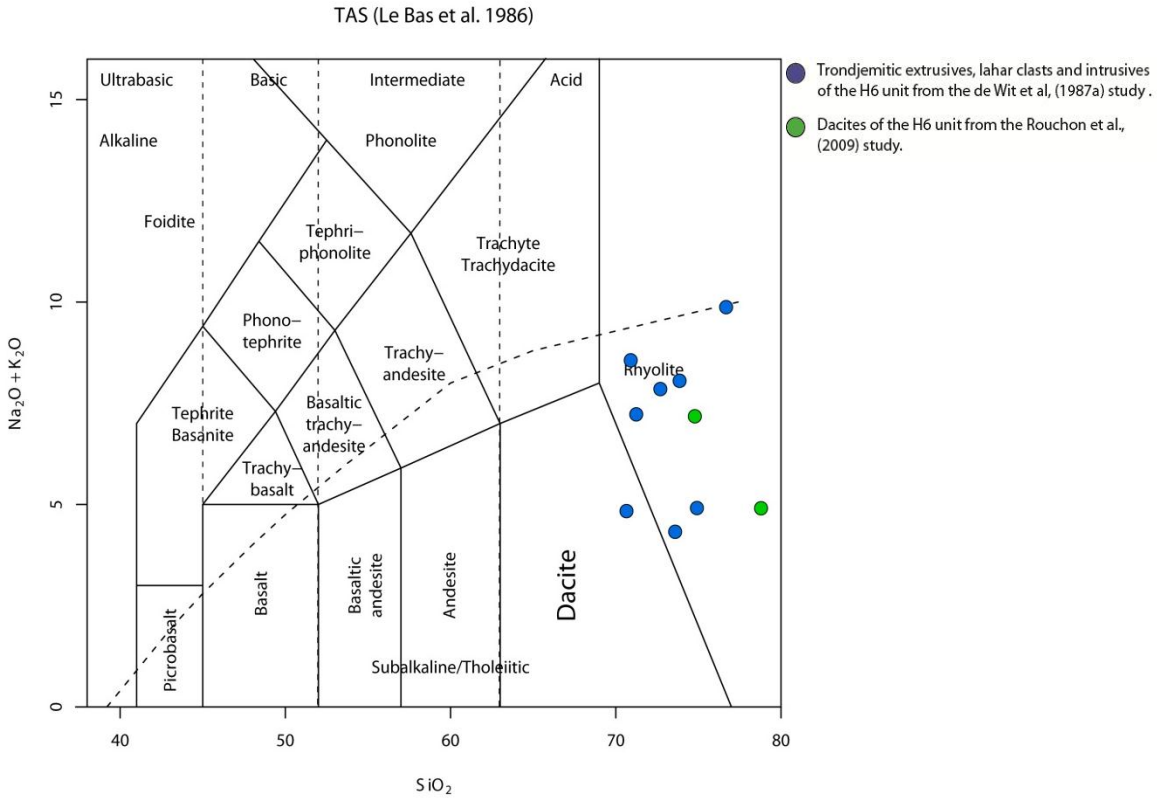

Figure 2.4 Total alkali vs silica (TAS) [Le Bas, 1986] diagram showing compositions acquired from elemental oxide data of previous papers on the felsic volcanic rocks of the H6 by de Wit et al., (1987a) and Rouchon et al., (2009). Values plotted represent 100% normalised anhydrous (i.e. excluding LOI) values.

3) The K-feldspar to form in low temperature (~70-150˚C) would be adularia. Additionally, no textural evidence of K-feldspar replacing albite has been identified in previous studies, and all the textural evidence presents white mica or SiO_2 replacement of K-feldspar which may simply reflect hydration and silicification of these rocks under low temperatures (~70-150˚C).

4) The study by Sanchez-Garrido et al., (2011) showed that the whole rock Ni and Cr contents of the granites and rhyolites she documents are elevated relative to younger peraluminous granites. This suggests that primary feldspars crystallizing from such magmas should have higher concentrations of these elements that would be considered typical for granites.

Chapter 3: Analytical Methods

70 samples were initially collected from the H6 member of the Hooggenoeg Formation from which a sub-set of 29 samples was selected on the basis that they contain clear volcanic textures in hand sample and have SiO_2 values lower than 76.5 %. Two additional samples were selected where the SiO_2 content is >78.50 and Loss of Ignition (LOI) of 9. These two samples were included because they showed field evidence for chert replacement and they were included to identify replacement textures in this section. Their compositions were not used in the whole rock major and trace element analysis that follows. The 31 volcanic rock samples were sampled on the western limb and eastern limb (Komati river type locality) of the Onverwacht anticline. Polished thin sections were made at the University of Cape Town (UCT) thin section lab. The rock textures were identified by optical microscope whereas mineralogical compositions were analyzed by scanning electron microscope (SEM).

The 31 volcanic samples were crushed using a jaw crusher and then pulverized to a fine powder by a tungsten carbide mill. After each volcanic rock was milled, the mill was cleaned using water and acetone after which a pure quartz fraction was milled and the mill cleaned again using water and acetone. The amount of Co cannot be accurately accounted for, due to contamination from tungsten carbide mill. The rock volcanic rock powders were then analyzed for major element bulk chemistry by X-ray fluorescence (XRF). A fraction of the fresh volcanic rock powders was also used for X-ray diffraction (XRD) analysis.

3.1. Sample preparation and X-ray fluorescence (XRF) methods

Major, minor and trace element analysis of 17 samples was carried out at Acme labs, whilst 15 samples were analysed by XRF and ICP-MS at Stellenbosch University Central Analytical Facilities (CAF). Major element analysis was carried out on fused glass beads that were made from powdered volcanic rock samples. These fusion beads were prepared from 1.0000g ±0.0009g of milled sample that was placed in an oven for 1hour at 110 ºC to determine the amount of H_2O^- loss. After this the sample was placed in an oven for 1 hour at 1000 ºC to determine LOI. The sample is then dissolved in 10.0000g ± 0.0009g of Ultrapure Fused

Anhydrous Li-Tetraborate-Li-Metaborate flux (66.67 $Li_2B_4O_7$ + 32.83% $LiBO_2$) with a releasing agent of Li-Iodide (0.5% Lil).

The XRF instrument used for major element analysis was an Axios from PANalytical with a 2.4kWatt Rh X-ray Tube. This instrument was calibrated with international (NIST®) and national (SARM®) standards for major and trace elements. These standards were also used to guarantee Quality Assurance of the major and trace element analysis. A local granitic sample (HG) was used for precision and quality control purposes.

Loss of Ignition (LOI) is defined as the mass difference of volatile compounds that escape when a sample is heated to 1000 ºC. The mass change reflects the loss of volatile components such as H_2O+, OH-, CO_2, F, Cl, S and the gain of mass due to oxidation of Fe in the Fe^{2+} state.

The composition of the standards analysed by XRF is presented in Table 2A. The same fused glass beads that were used during the XRF analysis was used for the determining of trace element concentrations by laser ablation inductively coupled plasma mass spectroscopy (ICP-MS).

Table 2A. Composition of the ACME STD SO-18 that was analysed at Acme Labs as a standard during the analyses of the rocks of the H6. Composition of in house granite standard analysed by XRF at different time intervals for quality control and precision purposes. The rocks of the H6 unit was analysed on two separate occasions (04/11/2009 and 13/05/2010), these dates falls within the time interval of the analysis of the in house granite.

Acme standards														
	Al2O3	**CaO**	**Cr2O3**	**Fe2O3**	**K2O**	**MgO**	**MnO**	**Na2O**	**P2O5**	**SiO2**	**TiO2**	**LOI**	**H_2O-**	**Sum**
	wt%	**wt%**	**wt%**	**wt%**	**wt%**	**wt%**	**wt%**	**wt%**	**wt%**	**wt%**	**wt%**	**wt%**	**wt%**	**wt%**
STD SO-18	14.12	6.38	0.55	7.62	2.16	3.33	0.39	3.69	0.83	58.05	0.69	1.90		99.71
STD SO-18	14.12	6.38	0.55	7.61	2.16	3.33	0.39	3.69	0.83	58.03	0.69	1.90		99.70
STD SO-18	14.12	6.37	0.55	7.61	2.16	3.33	0.39	3.69	0.82	58.07	0.69	1.90		99.71
STD SO-18	14.11	6.38	0.55	7.60	2.16	3.33	0.39	3.69	0.83	58.07	0.69	1.90		99.70
STD SO-18	14.14	6.38	0.55	7.61	2.15	3.33	0.39	3.68	0.82	58.06	0.69	1.90		99.70
STD SO-18	14.14	6.38	0.55	7.63	2.15	3.34	0.39	3.68	0.83	58.01	0.69	1.90		99.70
Average STD SO-18	**14.13**	**6.38**	**0.55**	**7.61**	**2.16**	**3.33**	**0.39**	**3.69**	**0.83**	**58.05**	**0.69**	**1.90**		**99.70**
STDEV	**0.01**	**0.00**	**0.00**	**0.01**	**0.01**	**0.00**	**0.00**	**0.01**	**0.01**	**0.02**	**0.00**	**0.00**		**0.01**
MIN	**14.11**	**6.37**	**0.55**	**7.60**	**2.15**	**3.33**	**0.39**	**3.68**	**0.82**	**58.01**	**0.69**	**1.90**		**99.70**
MAX	**14.14**	**6.38**	**0.55**	**7.63**	**2.16**	**3.34**	**0.39**	**3.69**	**0.83**	**58.07**	**0.69**	**1.90**		**99.71**
STD x2	0.02	0.01	0.00	0.02	0.01	0.01	0.00	0.01	0.01	0.05	0.00	0.00		0.01
STD x3	0.04	0.01	0.00	0.03	0.02	0.01	0.00	0.02	0.02	0.07	0.00	0.00		0.02
HG= House Granite Sample (Stellenbosch)														
hg	14.07	1.55	0.00	3.99	4.76	1.11	0.06	2.62	0.22	69.84	0.60	0.67	0.00	99.50
HG 28-10-9A	13.77	1.50	0.00	3.88	4.57	1.07	0.06	2.58	0.21	70.17	0.57	0.79	0.07	99.25
HG 28-10-9B	13.75	1.50	0.00	3.83	4.58	1.06	0.05	2.57	0.22	70.59	0.54	0.77	0.07	99.53
HG-1 A 4-11-9	13.84	1.49	0.00	3.85	4.55	1.06	0.06	2.54	0.22	69.92	0.57	0.79	0.07	98.95
HG B 4-11-9	13.87	1.50	0.00	3.83	4.56	1.04	0.06	2.54	0.21	70.50	0.54	0.77	0.07	99.50
2009/10/28	14.09	1.48	0.01	4.56	4.71	1.22	0.06	2.53	0.20	70.13	0.60	0.75	0.06	100.40
2009/12/14	13.95	1.52	0.00	3.80	4.59	1.07	0.06	2.58	0.21	70.96	0.55	0.74	0.05	100.09
HG 09-03-10	13.88	1.51	0.00	3.84	4.58	1.05	0.06	2.78	0.21	69.53	0.57	0.68	0.02	98.72
HG 25-3-10	13.97	1.52	0.00	3.84	4.59	1.05	0.06	2.55	0.22	69.52	0.54	0.71	0.03	98.58
HG 29-3-10	13.87	1.50	0.00	3.85	4.59	1.06	0.06	2.52	0.21	69.26	0.54	0.72	0.03	98.21
Hg 6-5-10	13.85	1.51	0.00	3.84	4.59	1.06	0.06	2.56	0.21	68.71	0.56	0.80	0.14	97.89
hg 7-5-10	13.76	1.52	0.01	3.81	4.62	1.06	0.06	2.62	0.21	68.58	0.57	0.80	0.14	97.75
hg 12-5-10	13.73	1.51	0.00	3.85	4.59	1.05	0.06	2.55	0.22	68.42	0.56	0.75	0.05	97.33
hg 26-5-10	13.85	1.54	BD	3.94	4.67	1.10	0.06	2.65	0.21	69.14	0.54	0.74	0.01	98.46
hg 27-5-10	14.01	1.55	0.00	3.94	4.69	1.06	0.06	2.63	0.21	69.76	0.54	0.73	0.07	99.25
Average HG	**13.88**	**1.51**	**0.00**	**3.91**	**4.62**	**1.07**	**0.06**	**2.59**	**0.21**	**69.67**	**0.56**	**0.75**	**0.06**	**98.90**
STDEV	**0.11**	**0.02**	**0.00**	**0.19**	**0.06**	**0.04**	**0.00**	**0.06**	**0.01**	**0.75**	**0.02**	**0.04**	**0.04**	**0.87**
MIN	**13.73**	**1.48**	**0.00**	**3.80**	**4.55**	**1.04**	**0.05**	**2.52**	**0.20**	**68.42**	**0.54**	**0.67**	**0.00**	**97.33**
MAX	**14.09**	**1.55**	**0.01**	**4.56**	**4.76**	**1.22**	**0.06**	**2.78**	**0.22**	**70.96**	**0.60**	**0.80**	**0.14**	**100.40**
STD x2	0.23	0.04	BD	0.38	0.12	0.09	0.01	0.13	0.01	1.51	0.04	0.08	0.08	1.74
STD x3	0.34	0.06	BD	0.56	0.19	0.13	0.01	0.19	0.02	2.26	0.06	0.12	0.12	2.62

3.2. Inductively coupled plasma mass spectroscopy (ICP-MS) analysis of trace elements techniques used

A New Wave 213nm laser ablation system that is connected to an Agilent 7500ce ICP-MS was used in the analysis of fusion disks for trace element data in counts per second (cps) parts per million (ppm). Ablation was performed in helium gas and mixed with argon after exciting the ablation cell, then passed through a mixing chamber before introduction into the ICP. The ICP-MS can analyze most isotopes on the periodic table; accept for C, H, O, N, halides and inert gasses. The spot size during analysis by laser ablation was 110µm, with laser warm-up taking 20 seconds and 50 seconds spot analysis for data acquisition.

The ICP-MS is calibrated by using NIST® 612 trace element standards and ^{29}Si as internal standard. Two measurements were obtained for each sample for disc inhomogeneity. The standard deviations of the the two analyses were generally below 1. The calibration standard, together with the quality control standard was analysed at the start of a series which is at the beginning or after each 12 analysis. The certified reference standard was a basaltic glass (BHVO-2G) that was produced by Dr Steve Wilson at the United States Geological Survey. Data processing was completed by using Glitter software, distributed by Access Macquarie Ltd., Macquarie University NSW 2109.

A fusion control standard, made from BCR-2 certified reference material, is prepared and analysed regularly to monitor matrix effects from the flux as well as any possible contaminants introduced (Appendix, Table I.1A). Claisse ultra-pure flux is used to prepare fusions for trace element analysis. During LA ICP-MS measurement on fusions, analysis is in'dry plasma', resulting in none of the problematic matrix based interferences typical from a solution containing chlorides, hydroxides, suphides etc. Oxides are controlled to be less than 0.5%, and masses suffering from direct interference of Argon oxides are not selected for analysis.

Trace element analysis of isotopes was completed within three different sessions. The analysis of the average standard was compared with accepted BHVO-2G certified values (Appendix, Table I.1B). The percentage difference between the accepted BHVO-2G values and average of the BHVO-2G values analysed in the lab was below 15%, accept for Cn111 and Sn118 that was above 20% (Appendix, Table I.1B). However, during the 3rd session the difference between the accepted values and lab values for Zn66 and Ga69 were between 15

and 20%. The relative standard deviation (RSD) is the measure of the precision of the average results and can also be the measure of reproducibility of the instrument during analysis of the same standard. The RSD for most isotope analysis was generally below 10%, accept for Zn66, Cd111, Sn118, Cs133 and U238 in the different sessions (Appendix, Table I.1B).

3.3. X-Ray Diffraction (XRD) analysis

XRD analysis was conducted on rock powders. The XRD used in this study is the PANalytical X'Pert Pro MPD (Multi-Purposes Diffractomator) with an X'Celerator detector at Stellenbosch University CentralAnalytical Facilities (CAF). The XRD in this study is used to identify the structural state of especially feldspars and other silicates within the rock powders. The diffraction patterns from the XRD are then transferred into the PDF-4 database supplied by the International Centre for Diffraction Data (ICDD). The ICDD contain over 180 000 references of diffraction patterns to identify the structural states of minerals present in the rock powders.

3.4. Scanning electron Microscope (SEM) techniques used

SEM analysis was conducted at Stellenbosch University Central Analytical Facilities (CAF). The SEM laboratory is equipped with a ZEISS EVO MA15VP SEM instrument. During this study the polished sections were coated by 15µm carbon. The Energy-dispersive X-ray Spectrometer (EDX) of the ZEISS EVO MA15VP SEM was used for quantitative in-situ elemental analysis of the different minerals. Major element analyses on minerals were completed at 20kV with10s counting times and a working distance of 8.5 mm. After every 5-10 analysis a standard was analysed to check for consistency.

Chapter 4: Field descriptions of the H6 member

The basal part of the H6 member consists of pillow basalts, komatiites and ultramafic rocks interspersed with distinct alternating white chert layers. The felsic unit within the H6 member occurs directly above these rocks (Fig. 4.2; de Wit et al., 1987a; de Vries et al., 2006). The felsic layer consists predominantly of massive sandstones, felsic volcaniclastic (polymict and monomict conglomerates) and igneous rocks (Fig. 4.1 C-E). Minor amounts of carbonate rocks are also observed in this layer.

The ~3.45 Ga felsic igneous intrusions are synchronous with NE-trending faults that occur at ~ 2-4 km intervals within the western limb of Onverwacht anticline of the H6 layer (de Vries et al., 2007). The maximum thickness of these felsic intrusions is approximately 2 km. Volcaniclastic and porphyritic rocks of the H6 can be traced for approximately 16 km along the western limb of the Onverwacht anticline in the H6 unit and thins out, toward the east, to about ~20 m in some places. The eastern limb of the H6 unit is made up of breccias and conglomerates containing the felsic volcanic rocks as clasts. In this study, the felsic igneous rocks were sampled along the eastern and western limb of the Onverwacht Anticline. The sample numbers are listed on the map (Fig 4.2) with the GPS coordinates stragraphical position below the top of the H6 unit and sample area presented in Table 2B.

The volcanic and porphyritic rocks in the western area were distinguished from granular light green silicified sandstone by the small 0.5 to 2mm euhedral feldspar and quartz phenocrysts within a microcrystalline groundmass. The phenocryst content varies from 30 to 70% in different samples. The apparent orientation of feldspars observed in some samples was interpreted as flow lineation. Two samples were also collected from thin layers of monomict orthoconglomerate consisting of clasts of these felsic volcanic rocks and fine sand matrix was locally observed (Fig. 4.1E). The Mtsoli River cuts through the stratigraphy in the eastern sampling area, exposing a cobble oligomict conglomerate containing clasts of felsic volcanic rocks (Fig. 4.1D and E). These clasts were sampled from the conglomerate, but were generally finer grained relative to the western area with no crystals identifiable within handsample. A short description of each hand sample appears in Appendix 1 (Table I.2).

Late cross-cutting features were also observed in the H6, including quartz veining, developed predominantly in the first 100 m below to the Buck Reef Chert (BRC), as well as 3228 ± 3 Ma (de Vries et al., 2006) mafic dykes cutting through the stratigraphy. The felsic rocks

described above are capped by the Buck Reef Chert (BRC) which was identified as the contact between the H6 unit and the Kromberg Formation (Fisher-Worrel, 1999).

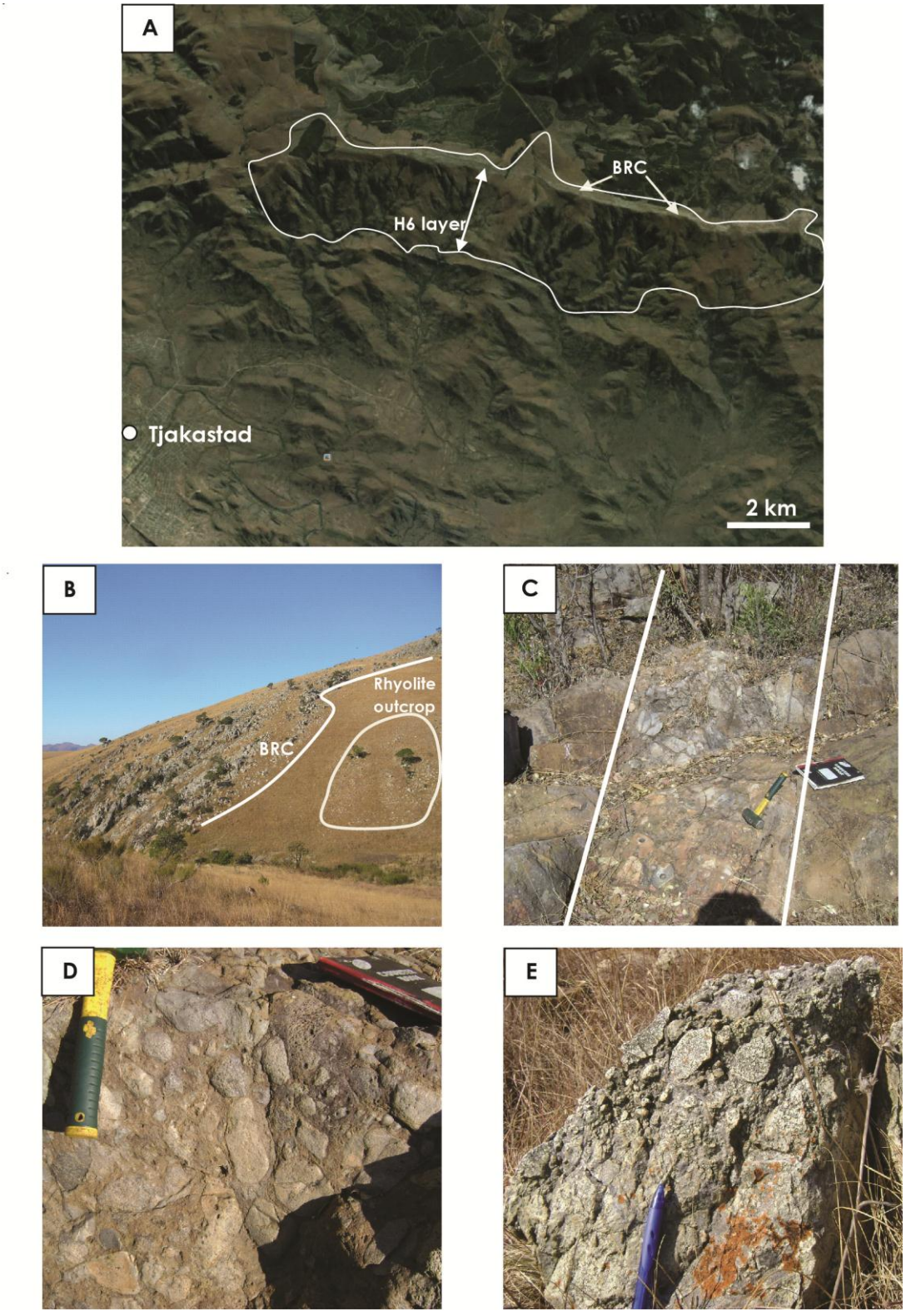

Figure 4.1A) Aerial photograph of the western limb section of the Onverwacht anticline illustrating the Buck Ridge Chert (BRC) and H6. B) Photograph illustrating a relationship between BRC and a rhyolite outcrop of the H6 on the western limb of the Onverwacht anticline. C) Polymict conglomerate containing felsic volcanic clasts on the eastern limb of the H6 layer of the Onverwacht anticline. D) Zoomed in view of the clasts that make up the cobble oligomict conglomerate. These conglomerates consist of felsic volcanic, sandstones with a silicified sand matrix. E) Monomict orthoconglomerate containing only felsic volcanic rocks of the H6 unit on the western limb of the Onverwacht anticline.

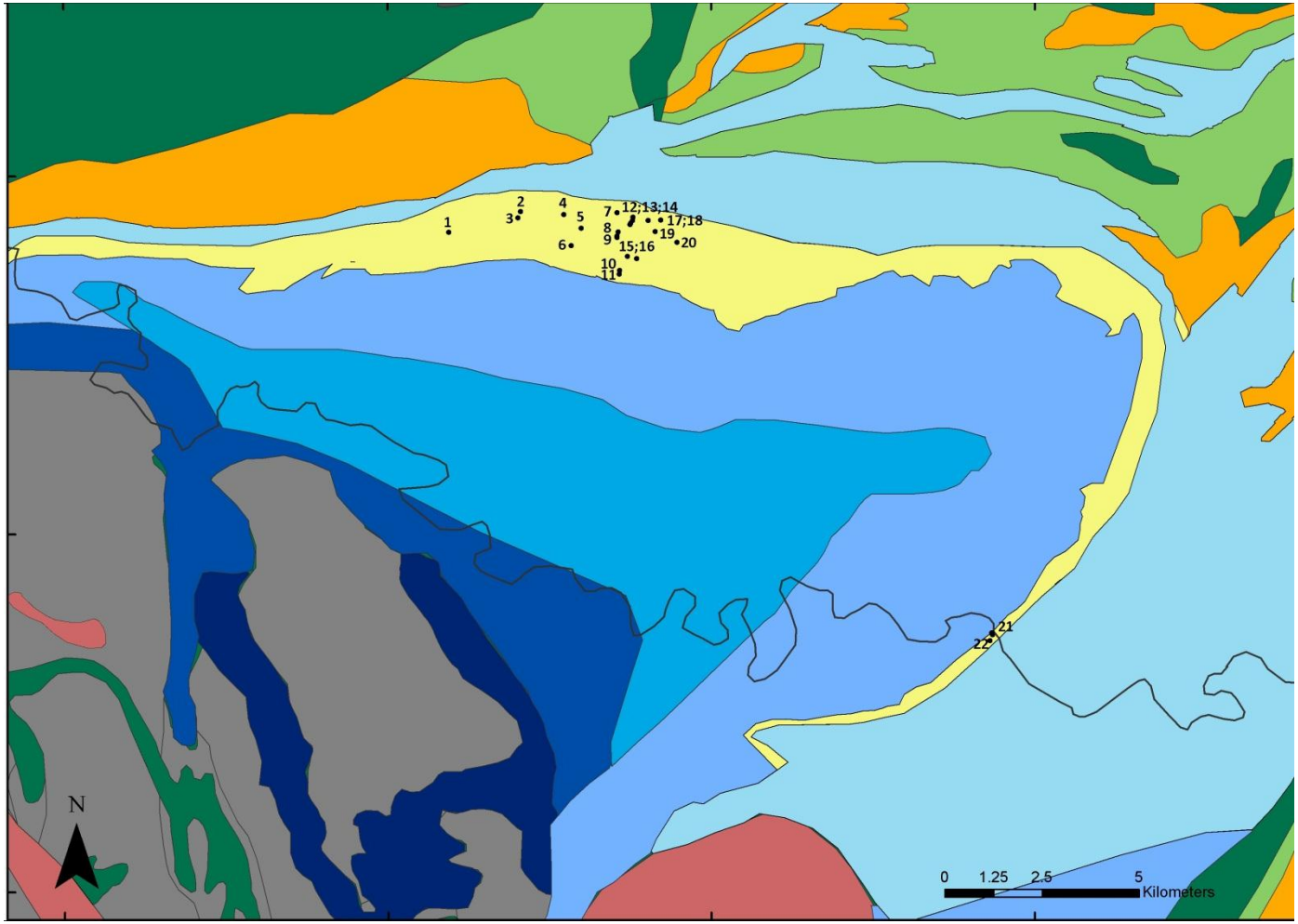

Figure 4.2 Geological map of the BGGT (Map modified after Anhaeusser et al., 1981; Kröner et al., 1996, Diener et al., 2006). The felsic unit was modified from De Wit et al., (1987) and De Vries et al., (2006).. The legend corresponds to the legend of Figure 2.1.

Table 2B. The sample name with GPS coordinates that correlate with locations of samples on Figure 4.2, depth of samples below the top of H6 unit and also the area where the sample was collected from.

Nr.	Sample_Nam	GPS coordinates		Depth below top of H6 layer (m)	Sample area
		South	East		
1	DHG 02-10	-25.929783	30.849217	750	Western Area
2	DHG 02-12	-25.924983	30.867650	553	Western Area
3	DHG 01-12	-25.926383	30.866983	700	Western Area
4	DHG 06-13	-25.925650	30.878833	500	Western Area
5	SHG 02-14	-25.928817	30.883333	780	Western Area
6	DHG 04-14	-25.932850	30.880767	1260	Western Area
7	CHG 03-07	-25.925233	30.892500	310	Western Area (Volcanic clast from monomict orthoconglomerate)
8	DHG 05-05	-25.929717	30.892867	820	Western Area
8	CHG 05-03	-25.929717	30.892867	820	Western Area (Volcanic clast from monomict orthoconglomerate)
9	DHG 05-06	-25.930650	30.892550	940	Western Area
9	SHG 05-04	-25.931033	30.892500	940	Western Area
10	SHG 03-16	-25.938683	30.893200	1800	Western Area
11	DHG 02-16	-25.939500	30.893067	1900	Western Area
12	CHG 03-02	-25.926267	30.896633	410	Western Area (Volcanic clast from monomict orthoconglomerate)
13	SHG 03-02	-25.927083	30.896517	500	Western Area
13	SHG 03-02B	-25.927083	30.896517	500	Western Area
14	DHG 05-04	-25.927650	30.896083	930	Western Area
14	DHG 05-04A	-25.927967	30.895833	930	Western Area
15	DHG 01-16	-25.935417	30.895217	1420	Western Area
16	DHG 03-16	-25.935933	30.897600	1320	Western Area
17	DHG 03-01A	-25.927033	30.900567	300	Western Area
18	DHG 03-02	-25.927000	30.903733	250	Western Area
19	SHG 03-01	-25.929600	30.902300	530	Western Area
20	DHG 01-09	-25.932150	30.908000	710	Western Area
21	DHG 03-18	-26.023017	30.988983	150	Eastern Area (Volcanic clasts from polymict conglomerate)
21	DHG 04-18 A	-26.023500	30.989200	150	Eastern Area (Volcanic clasts from polymict conglomerate)
21	DHG 05-18 A	-26.023500	30.989200	150	Eastern Area (Volcanic clasts from polymict conglomerate)
21	DHG 05-18 B	-26.023500	30.989200	150	Eastern Area (Volcanic clasts from polymict conglomerate)
22	DHG 01-18	-26.024883	30.988533	100	Eastern Area (Volcanic clasts from polymict conglomerate)
22	DHG 02-18 D	-26.024883	30.988533	100	Eastern Area (Volcanic clasts from polymict conglomerate)

Chapter 5: Petrography

5.1. General statements

The felsic volcanic unit of the H6 is comprised of 2 varieties of felsic igneous rocks that were examined in thin section: 1. Predominant porphyritic rhyolitic rocks that contain K-feldspar and quartz phenocrysts within a microcrystalline groundmass that could have represented fine-grained quenched crystals or devitrified glass; 2. Subordinate rhyolites consisting of lamellar twinned albite and quartz phenocrysts within a similar groundmass as that described for the igneous rocks containing K-feldspar (Fig. 5.1A and B). Feldspar phenocrysts are euhedral to subhedral with the modal abundance of feldspar phenocrysts (0.2 – 3 mm) varying between 28 and 61% whereas the modal abundance of the smaller euhedral to anhedral quartz phenocrysts (0.05 – 1mm) varies between 1 and 10%. Petrographic details of individual samples are provided in the appendix Table I.3. The primary igneous texture defined by these rocks is a phenocryst-rich (33 – 65%) porphyritic texture, characterized by quartz and feldspar phenocrysts surrounded by a groundmass that consists of muscovite, microquartz and minor clays. These magmatic textures are overprinted by metamorphic and low temperature alteration-related textures. Rhyolites containing albite and quartz phenocrysts are normally called quartz keratophyres (Schermerhorn, 1973). These albite-rich rocks can also be called Na-rhyolites. The latter name will therefore be applied to these rocks in this study. Biotite occurs as a minor mineral in the felsic igneous rocks together with rutile, monazite, zircon and apatite as accessory phases.

5.2. Preserved magmatic textures

The magmatic textures in the porphyritic felsic igneous rocks that were examined in thin section are characterized by smaller euhedral quartz relative to larger feldspar phenocrysts within a microcrystalline groundmass (Fig. 5A and B). Intact feldspar domains can be observed in thin sections of felsic igneous rocks where the feldspar minerals are extensively replaced by muscovite (Fig.5 G-H). In one sample, the K-feldspar crystals contain small spots of perthitic exsolution of albite.

5.3. Metamorphic textures

In felsic igneous rocks in which a metamorphic overprint is pronounced, the feldspars are either partially or completely replaced by muscovite (pseudomorphs) with the euhedral shape of original feldspar preserved (Fig.5G, H and I). Additionally, minor amounts of clays are observed in thin section within these muscovite pseudomorphs. The muscovite pseudomorphs also contain quartz inclusions (Fig.5C, D, E and F) whereas the groundmass observed in thin section mostly consists of phyllosillicates such as muscovite and minor clays. In the view of the close association of muscovite and clays within euhedral K-feldspar, these minerals can be regarded as products that formed from water-present breakdown of K-feldspar. This assemblage of K-feldspar-muscovite-kaolinite is stable between 0 and 300°C (Berman, 1988) and therefore demonstrates that these rocks have undergone water present greenschist to sub-greenschist facies metamorphism. The chemical equation for the breakdown of K-feldspar to muscovite to kaolinite is illustrated below:

$$6\ KAlSi_3O_8 + 2\ H_2O = K_2Al_4(Si_6Al_2O_{20})(OH)_4 + 2\ K_2O + 12\ SiO_2 \quad \text{(K-feldspar} \rightarrow \text{muscovite)}$$

($6K\text{-}feldspar + 2\ H_2O = Muscovite + 2K_2O + 12Quartz$)

$$2\ K_2Al_4(Si_6Al_2O_{20})(OH)_4 + 4\ H^+ + 6\ H_2O = 4\ K^+ + 3\ Al_4Si_4O_{10}(OH)_8 \quad \text{(Muscovite} \rightarrow \text{clays)}$$

($2Muscovite + 2H^+ + 6\ H_2O = 4K^+ + 3\ Kaolinite$)

These equations illustrate that the rhyolites in the H6 unit are net exporters of K_2O during water-present sub-greenschist to greenschist-facies metamorphism.

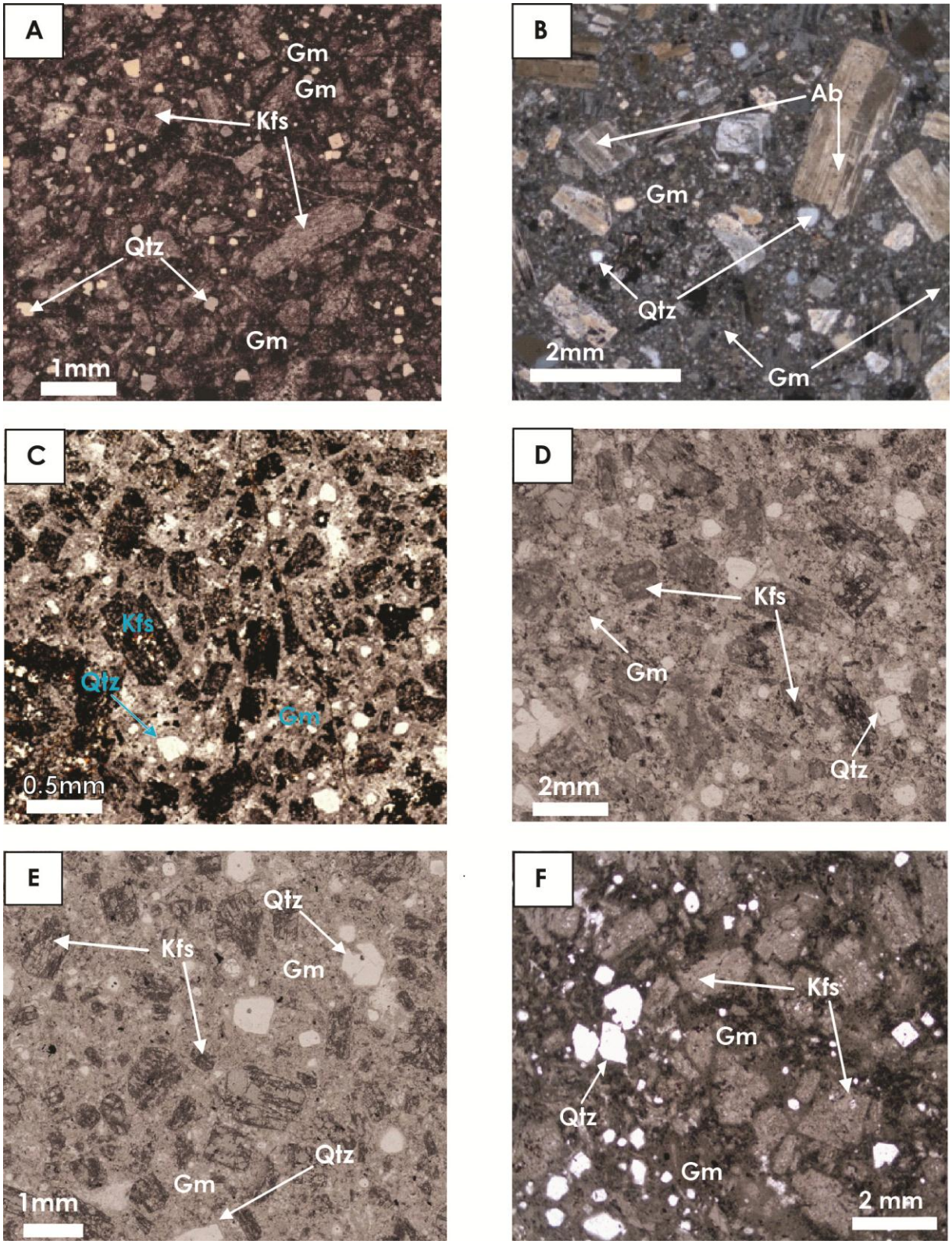

Figure 5.1 Transmitted cross polarised (A,B and F) and plane polarised light (A, D and E) photomicrographs of textures of the felsic igneous rocks of the H6 unit. A) Rhyolite illustrating euhedral K-feldspars with smaller euhedral quartz within a microcrystalline groundmass (SHG 03-02B). B) Na-rhyolite that contains lamellar twinned euhedral albite and subhedral quartz (DHG 04-14). C-F) Rhyolite samples containing euhedral K-feldspar replaced by mica and quartz phenocrysts identified in different samples. Sample C=DHG 05-06, D= CHG 05-03, E=DHG 03-02 and F=DHG 03-04. Abbreviations: Kfs = K-feldspar; Qtz = quartz; Gm = groundmass

5.4. Textural features produced by Alteration

Replacement features related to post-depositional hydrothermal alteration in the felsic igneous rocks that can be observed in thin section are mostly quartz veins, replacement cherts and calcite. In the field and in thin section, quartz veins are seen as cross cutting features and related to replacement cherts that increase in abundance towards the BRC (Fig. 5J). Microcrystalline quartz is mostly observed on the rims of some of the quartz phenocrysts. Despite all these alteration features, preserved remnant K-feldspar domains were still observed in thin section images (Fig.5 G, H, I and J). These preserved domains occupy an area of almost 40% of the entire mineral grain whereas muscovite domains occupy about 60% of mineral grain (Fig.5 G and H).

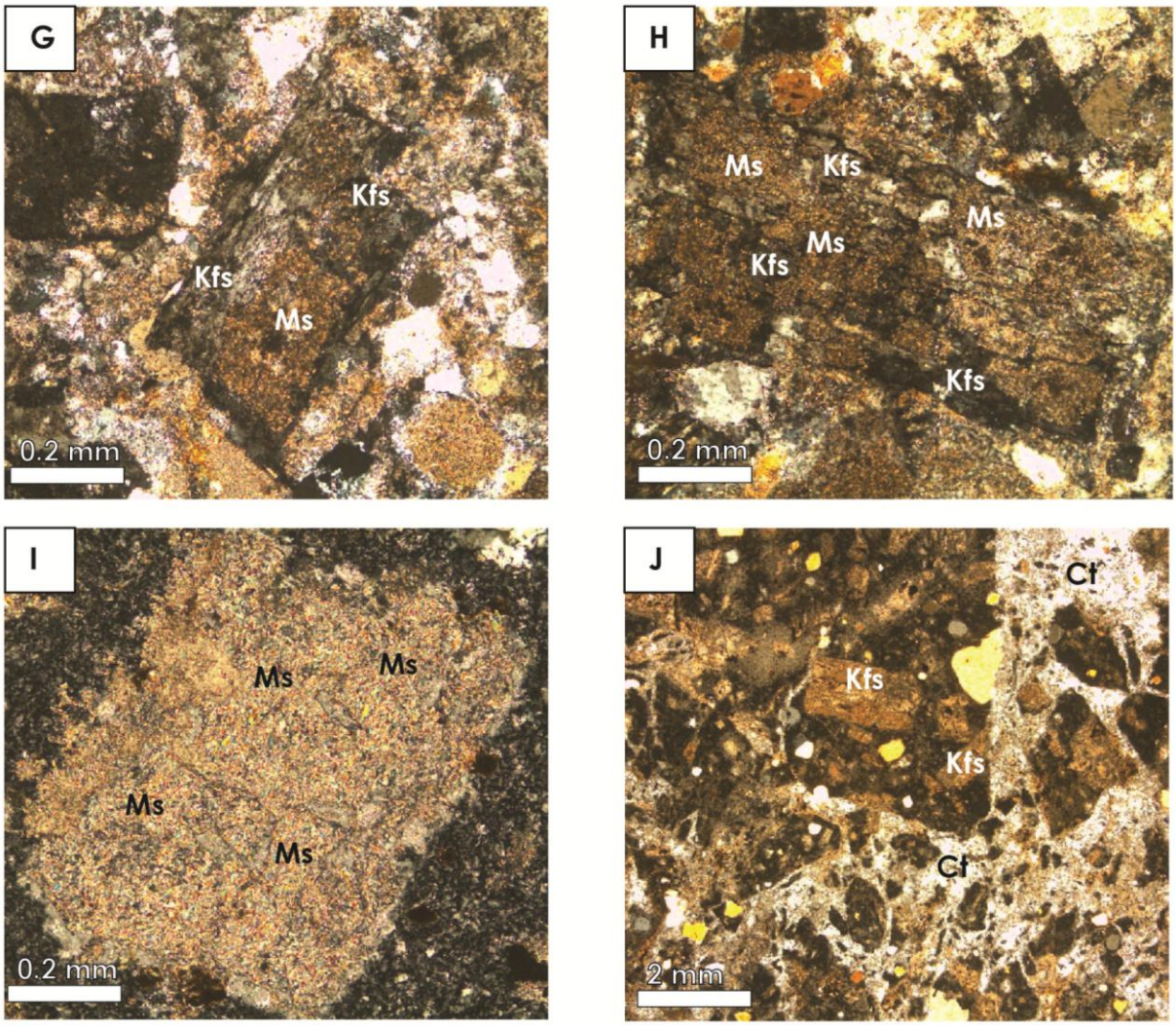

Figure 5.2 Transmitted cross polarised light (G, H, I and J) of K-feldspars in rhyolites. G-H) Euhedral K-feldspar being partially replaced by muscovite with fresh K-feldspar still visible. I) Euhedral remnant K-feldspar (muscovite pseudomorph) being totally replaced by muscovite with small fresh spots of K-feldspar still observed. J) Chert replacement of especially the groundmass with remnant K-feldspar visible (SHG 03-02).

Chapter 6: Mineralogy of the felsic igneous rocks

The magmatic textures in the rhyolites of the H6 unit are characterized by K-feldspar phenocrysts. K-feldspar phenocrysts can represent up to 61% of the total mineral modal proportion in samples. It is therefore an important contributor of K_2O to the overall bulk composition of the rhyolites. Previous studies (de Wit et al., 1987a; Hofmann and Harris, 2008; Rouchon et al., 2009) proposed that the feldspars that are completely replaced by muscovite in rhyolites of H6 member were initially plagioclase. This observation is in disagreement with the occurrence of remnant domains of K-feldspar that are replaced by muscovite and clearly shows that K-feldspar is not the product of replacement (Fig. 5G and H).

Generally the structural state of K-feldspar can be used as an estimate for the temperature environment in which the K-feldspar crystallized. Thus, the identification of the structural state of feldspars, and in particular K-feldspar, is critical for this study. The method used to identification of the structural state and chemistry of the feldspars and K-feldspars in particular was X-ray diffraction (XRD) in conjunction with EDX analysis on the scanning electron microscope (SEM).

6.1. Relict K-spar in altered grains

The feldspar phenocrysts in the felsic igneous rocks of the H6 unit vary from being partially to completely replaced by muscovite (Fig. 5 G, H and I). Within these replaced feldspar phenocrysts remnant K-feldspar domains were analyzed for major and trace elements by EDX electron beam analyses. The major- and trace- element data generated by the electron beam analysis are presented together with the structural formulae of the feldspars, calculated on the basis of 8 oxygens, in Table 3A. The compositions of the K-feldspars in rhyolites vary between Or_{92} and Or_{99} whereas the plagioclase compositions of Na-rhyolites are Ab_{99}.

Table 3A.Electron beam analysis of major and minor elements in feldspars of different felsic volcanic rock samples.

Sample Name	**SHG 05-03**				**CHG 03-02**			**SHG 03-02B**			**DHG 04-14**		
Feldspar variety	**Albite inclusion in K-feldspar**	**Alkali feldspar inclusion in K-feldspar**	**K-feldspar**								**Albite**		
Analysis Number	**1**	**2**	**2C**	**8**	**3b**	**3c**	**5b**	**4**	**15**	**16**	**3**	**6**	**17**
SiO_2	70.76	68.95	65.20	65.48	64.62	64.64	64.27	63.77	64.70	64.51	68.35	69.17	68.75
Al_2O_3	19.37	18.92	17.72	16.82	17.54	17.57	17.13	17.47	17.59	17.58	19.01	18.95	18.92
FeO	0.14	0.07	0.02	0.01	0.03	0.03	0.07	0.09	0.01	0.04	0.04	0.00	0.12
CaO	0.04	0.10	0.00	0.12	0.17	0.12	0.06	0.05	0.03	0.03	0.09	0.03	0.13
Na_2O	11.40	7.78	0.23	0.78	0.63	0.54	0.65	0.12	0.28	0.14	11.93	12.46	11.91
K_2O	1.30	6.16	16.65	15.91	16.00	16.00	15.73	16.45	16.54	16.60	0.05	0.04	0.03
BaO	0.00	0.00	0.14	0.04	0.00	0.16	0.00	0.12	0.10	0.03	0.00	0.00	0.00
Totals	**103.01**	**101.98**	**99.96**	**99.17**	**98.99**	**99.06**	**97.92**	**98.07**	**99.25**	**98.94**	**99.47**	**100.63**	**99.86**
Si	3.01	3.01	3.02	3.05	3.02	3.02	3.03	3.01	3.02	3.02	3.00	3.01	3.01
Al	0.97	0.98	0.97	0.92	0.97	0.97	0.95	0.97	0.97	0.97	0.99	0.97	0.98
Fe2+	0.01	0.00	0.00	0.00	0.00	0.00	0.00	0.00	0.00	0.00	0.00	0.00	0.00
Ca	0.00	0.00	0.00	0.01	0.01	0.01	0.00	0.00	0.00	0.00	0.00	0.00	0.01
Na	0.94	0.66	0.02	0.07	0.06	0.05	0.06	0.01	0.03	0.01	1.02	1.05	1.01
K	0.07	0.34	0.98	0.95	0.95	0.95	0.95	0.99	0.98	0.99	0.00	0.00	0.00
Ba	0.00	0.00	0.00	0.00	0.00	0.00	0.00	0.00	0.00	0.00	0.00	0.00	0.00
Totals	**5.01**	**5.00**	**5.00**	**5.00**	**5.00**	**5.00**	**5.00**	**5.00**	**5.00**	**5.00**	**5.01**	**5.03**	**5.01**

Cations were calculated on the basis of 8 oxygens.

6.2. XRD analyses of whole rock powders

Whole-rock powders were analysed by X-ray diffraction (XRD) at Stellenbosch University to determine the minerals and their structural states present in the felsic igneous rock samples, particularly the variety of feldspar in these samples. The XRD analyses of Na-rhyolites and rhyolites is presented in Table 4. K-feldspars were only identified in rhyolites and consist of orthoclase, intermediate microcline and microcline whereas albite was identified in the Na-rhyolites (Table 4). The feldspar variety identified by XRD in the different samples is presented in Table 4. Furthermore different phyllosilicates were identified in the rhyolites and Na-rhyolites and mainly consists of muscovite and kaolinite (Table 4). Graphical representation of reflection peaks indexed, list of d-spacings with relative intensity of each mineral is presented in the Figure I.1 in the appendix.

Table 4. Qualitative phase identification was carried out by using X'Pert High Score Plus software that matches the XRD patterns to the PDF-4 database supplied by the International Centre for Diffraction Data (ICDD). The ICDD contain over 180 000 references of diffraction patterns to identify the structural states of minerals present in the rock powders.

Sample Name	Reference Code	Compound Name	Chemical Formula
CHG 03-02	01-085-0335	Quartz low, syn	SiO_2
	00-019-0932	Microcline, intermediate	$KAlSi_3O_8$
	01-089-7536	Muscovite-2M1, ferroan	$K(Al,Fe)_2AlSi_3O_{10}(OH)_2$
	00-001-0527	Kaolinite	$Al_2Si_2O_5(OH)_4$
DHG 03-16	01-070-8054	Quartz-á	SiO_2
	01-071-6219	Albite	$Na(AlSi_3O_8)$
	01-086-1384	Muscovite-2M1	$K_{0.932}Al_2(Al_{0.932}Si_{3.068}O_{10})(OH)_{1.744}F_{0.256})$
	01-074-1786	Kaolinite 1A	$Al_2Si_2O_5(OH)_4$
DHG 04-14	01-085-0504	Quartz	SiO_2
	01-070-3752	Albite	$(Na_{0.98}Ca_{0.02})(Al_{1.02}Si_{2.98}O_8)$
	00-001-1098	Muscovite	$H_2KAl_3(SiO_4)_3$
	01-074-1786	Kaolinite 1A	$Al_2Si_2O_5(OH)_4$
DHG 05-04A	01-070-7345	Quartz	SiO_2
	01-083-1895	Microcline	$K_{0.96}Na_{0.04}AlSi_3O_8$
	01-082-0576	Muscovite-2M1	$KAl_2(AlSi_3O_{10})(OH)_2$

DHG 05-18A	01-070-7345	Quartz	SiO_2
	01-076-0824	Microcline, sodian	$(K_{0.931}Na_{0.055})(Al_{0.97}Si_{3.03}O_8)$
	01-082-2450	Muscovite 2M1	$(Na_{0.07}K_{0.90}Ba_{0.01})(Al_{1.84}Ti_{0.04}Fe_{0.07}Mg_{0.04})(Si_{3.02}Al_{0.98})O_{10}(OH)_2$
SHG 03-02	01-070-7344	Quartz	SiO_2
	01-089-7536	Muscovite-2M1, ferroan	$KAl_2(AlSi_3O_{10})(OH)_2$
	00-001-0527	Kaolinite	$Al_2Si_2O_5(OH)_4$
	01-071-0955	Microcline	$KAlSi_3O_8$
SHG 03-02B	01-083-0539	Quartz	SiO_2
	01-075-1592	Orthoclase	$KAlSi_3O_8$
	01-089-7536	Muscovite-2M1, ferroan	$KAl_2(AlSi_3O_{10})(OH)_2$
DHG 03-02	01-085-0794	Quartz low, syn	SiO_2
	00-019-0932	Microcline, intermediate	$KAlSi_3O_8$
	00-019-0932	Muscovite-2M1	$K(Al,Fe)_2AlSi_3O_{10}(OH)_2$
DHG 05-05	01-085-0865	Quartz-á	SiO_2
	01-071-1543	Orthoclase	$KAlSi_3O_8$
	01-089-5401	Muscovite 2M1	$KAl_{2.20}(Si_3Al)_{0.975}O_{10}(OH)_{1.72}O_{0.28}$
	01-075-1593	Kaolinite 1A	$Al_2Si_2O_5(OH)_4$

Chapter 7: Geochemistry

7.1. Major-element chemistry

The bulk chemical analyses of the felsic igneous rocks of the H6 are presented in Table 5A and Figure 7.1. SiO_2 ranges from 66.09 to 76.49 wt%, K_2O varies between 0.45 to 9.69 wt%, Na_2O varies from 0 (below detection) to 6.63 wt% and CaO is often below 1% but is as high as 4.74 wt% in one sample. LOI range mostly between 1.35 and 3.8 wt%, but as high as 7.84 wt% in one sample. A/CNK ratios range between 0.89 and 2.55 with one sample having a value of 3.78. These igneous rocks are mostly peraluminous and have Mg # between 0.41 and 0.80. FeOt + MgO are low and range from 0.45 to 3.16 wt% with two samples respectively 4.27 and 9.97 which explains the leucocratic nature of most these rocks. The rock compositions plotted on a K_2O or Na_2O vs SiO_2 Harker diagrams (Fig. 7.1), define two distinct groups; rocks rich in Na_2O and those rich in K_2O. A distinct separation exists between these two populations (Fig 7.1). Only one trend was observed in the major element Harker Type diagrams that is defined by TiO_2 that decreases with increasing SiO_2 (Fig 7.1). No trends were observed when LOI was plotted against SiO_2 and K_2O which suggests that the high LOI was not influenced by the addition of K_2O or SiO_2 (Fig 7.1). The consistently high LOI is most likely caused by the loss of H_2O^+ and possibly F during ignition. H_2O^+ and F is readily accomadated within the crystal structure of muscovite, which is also the most abundant mineral in the felsic igneous rocks of the H6.

7.1.1. Trace element chemistry

The average transition metal concentrations are generally lower than 30 ppm with average values for Ni = 20.11 ppm, Sc = 5.54ppm, V = 19.62ppm, Cr = 37.66 ppm, Cu = 15.35ppm and Zn = 20.34 ppm. The high field strength element (HFSE) concentration is generally low with average Zr = 109.2 ppm, Nb = 5.20ppm and Hf = 2.91ppm. The large ion lithophile element (LILE) concentrations vary for Ba and Rb, with the Ba concentration ranging mostly between 99.4and 595 ppm, Rb values range between 41.8 and 160.5ppm and Sr values are generally very low (<32.4 ppm) with one sample having an Sr concentration equal to 119 ppm (Table 5B; Fig 7.2). Two trends was observed in trace element Harker Type diagrams

with Zr that increases with increasing Hf and Nb, whereas extreme scatter is observed in plots between Zr and K, Rb, Ba and Sr (Fig. 7.2).

The rare earth element (REE) analysis of the felsic igneous rocks in the H6 unit show high light rare earth element (LREE) contents (La_N= 30.93-171.73) and low HREE contents (Yb_N = 1.68–7.95).The average LREE slope is typified by $(La/Sm)_N$ = 4.90 with the average HREE $(Gd/Lu)_N$ slope =2.50 and average $(La/Yb)_N$ = 20.90. These felsic igneous rocks in the H6 unit have a slightly negative Eu anomaly (Eu /Eu*= 0.97) and a slight negative Ce anomaly (Ce/Ce* = 0.90) (Table 5B; Fig 7.3) that could indicate interaction of these rocks with suboxic seawater (DeBaar et al., 1985, 1988; DeBaar, 1991). The scatter in regards to most trace and major elements plots suggests the absence of magmatic characteristics (Fig. 7.1 and 7.2). Tables showing the raw major- and trace element chemistry, lowest limit of detection and the chemistry of the samples reported in this thesis are presented in the appendix Table I.4.

Table 5A. Bulk-rock major element data by sample number from felsic igneous rocks of the H6 unit. All major elements are in wt%. Abbreviations: Lab = laboratory; Acme = Samples analysed at Acmelabs; Stel = Samples analysed at Stellenbosch University CAF with the number following Stel indicating the session the sample was analysed at.LOI = loss of ignition; FeOt = Total iron; A/CNK = molecular ratio Al/(Ca+Na+K); BDL = 3 * below detection limit. * Sample SHG 03-02 and SHG 05-03 were not described in geochemistry section and were only used for describing replacement chert (Fig. 5J) and feldspar analysis (table 3A; appendix 1).

Sample name	Lab	SiO_2	TiO_2	Al_2O_3	FeOt	MnO	MgO	CaO	Na_2O	K_2O	P_2O5	LOI	Total	A/CNK	FeOt + MgO
DHG 03-04	Acme	75.02	0.20	14.09	1.09	BDL	0.54	BDL	0.04	6.44	BDL	2.40	99.82	2.00	1.63
DHG 03-01A	Acme	73.85	0.22	15.24	0.63	BDL	1.40	BDL	0.04	5.66	BDL	2.80	99.84	2.46	2.03
DHG 03-02	Acme	75.77	0.20	13.94	0.97	BDL	0.53	0.06	0.04	6.14	0.06	2.10	99.81	2.06	1.50
DHG 05-04A	Acme	76.49	0.19	12.93	0.81	BDL	0.89	BDL	0.04	6.15	BDL	2.30	99.80	1.92	1.70
DHG 05-04	Acme	74.95	0.19	12.99	0.94	BDL	0.57	0.05	0.07	8.57	0.06	1.40	99.79	1.38	1.51
DHG 05-06	Acme	70.43	0.23	15.87	1.51	BDL	0.71	BDL	0.27	8.58	0.05	2.10	99.75	1.63	2.22
CHG 03-02	Acme	74.46	0.20	13.62	1.30	BDL	0.61	BDL	0.06	6.77	0.05	2.70	99.77	1.83	1.91
CHG 05-03	Acme	74.40	0.21	13.66	0.83	BDL	0.54	BDL	0.18	7.94	BDL	2.00	99.76	1.54	1.37
SHG 03-01	Acme	71.48	0.23	15.99	1.26	BDL	0.87	BDL	BDL	6.56	BDL	3.40	99.79	2.25	2.13
SHG 03-02	Acme	68.63	0.18	12.37	1.45	BDL	0.63	BDL	BDL	4.48	BDL	9.50	97.24	2.55	2.08
SHG 03-02B	Acme	73.89	0.22	14.54	0.71	BDL	0.49	BDL	0.06	7.73	BDL	2.10	99.74	1.72	1.20
SHG 05-04	Acme	69.48	0.24	16.03	1.84	BDL	1.21	BDL	0.11	7.01	0.05	3.80	99.77	2.06	3.05
DHG 05-05	Acme	70.95	0.23	15.85	1.24	BDL	0.72	BDL	0.06	7.50	BDL	3.20	99.75	1.93	1.96
CHG 03-07	Stel2	75.95	0.21	14.16	1.04	BDL	0.55	0.05	BDL	5.95	0.08	2.33	100.32	2.18	1.59
DHG 01-09	Stel1	73.27	0.22	14.60	1.55	BDL	0.97	BDL	BDL	6.88	BDL	2.59	100.08	1.96	2.52
DHG 01-12	Stel1	72.30	0.22	14.88	1.41	0.09	0.69	BDL	BDL	7.66	0.04	2.50	99.79	1.79	2.10
DHG 01-16	Stel1	69.85	0.23	14.57	2.27	BDL	0.89	1.79	6.30	0.87	0.06	2.35	99.18	1.13	3.16
DHG 02-10	Stel2	71.68	0.22	15.81	1.69	BDL	0.86	BDL	BDL	7.29	0.05	2.86	100.46	2.00	2.55
DHG 02-12	Stel2	70.54	0.27	12.45	7.59	0.1	2.38	BDL	BDL	3.04	0.07	3.53	99.97	3.78	9.97
DHG 02-16	Stel1	72.97	0.20	14.56	1.74	BDL	1.13	0.62	4.03	1.59	0.06	2.62	99.52	1.63	2.87
DHG 03-16	Stel2	66.82	0.28	14.00	2.08	0.04	1.08	3.61	2.34	3.51	0.06	5.43	99.25	1.28	3.16
DHG 04-14	Stel2	71.92	0.19	14.73	1.58	BDL	1.34	0.53	4.60	2.23	0.06	2.35	99.53	1.41	2.92
DHG 06-13	Stel3	76.34	0.18	13.03	0.23	BDL	0.22	0.09	BDL	8.48	0.11	1.35	100.03	1.41	0.45
SHG 03-16	Stel3	71.15	0.25	15.03	2.07	BDL	0.88	0.25	6.63	0.45	0.06	2.77	99.54	1.29	2.95
DHG 05-18a	Stel2	70.67	0.24	14.46	0.31	BDL	0.41	0.53	BDL	10.10	0.08	1.59	98.39	1.27	0.72
DHG 05-18b	Stel2	71.39	0.22	13.25	0.37	0.04	0.60	1.11	0.04	9.32	0.07	2.12	98.53	1.19	0.97
DHG 03-18	Stel1	70.99	0.24	13.53	0.55	BDL	0.61	1.61	0.04	7.97	0.08	2.92	98.54	1.33	1.16
DHG 01-18	Stel3	66.09	0.36	9.68	1.74	0.20	2.53	4.74	BDL	6.11	0.08	7.84	99.37	0.89	4.27
DHG 04-18a	Stel3	70.81	0.28	14.05	0.57	0.05	0.51	0.58	BDL	9.69	0.08	1.88	98.50	1.28	1.08
DHG 02-18d	Stel2	71.10	0.27	13.87	0.74	BDL	0.68	1.28	BDL	8.04	0.07	2.64	98.69	1.41	1.42
SHG 05-03*	Acme	78.50	0.21	13.26	0.42	BDL	0.57	BDL	0.04	4.52	BDL	2.30	99.82	2.67	0.99

Table 5B. Bulk-rock minor and trace element data by sample number from felsic igneous rocks of the H6 unit.Trace elements are in ppm.

Sample name	Sc	V	Cr	Ni	Cu	Zn	Ga	Rb	Sr	Y	Zr	Nb	Mo	Sn	Cs	Ba
DHG 03-04	BDL	BDL	BDL	BDL	1.5	BDL	15.5	120.8	6.6	4.2	108.4	4.4	0.3	BDL	1.4	183.0
DHG 03-01A	BDL	28	BDL	BDL	0.9	BDL	18.5	122.4	9.6	7.9	114.6	4.9	BDL	BDL	2.4	302.0
DHG 03-02	BDL	BDL	BDL	BDL	3.4	BDL	16.3	114.6	8.4	4.6	103.2	4.5	BDL	BDL	1.4	395.0
DHG 05-04A	BDL	BDL	BDL	BDL	0.5	BDL	16.8	139.6	16.7	6.1	102.6	4.3	BDL	BDL	2.0	319.0
DHG 05-04	BDL	BDL	BDL	BDL	2.0	5	14.7	136.2	10.1	4.9	96.5	4.2	0.2	BDL	2.2	389.0
DHG 05-06	BDL	BDL	BDL	BDL	1.7	4	19.4	160.5	23.7	6.2	129.8	5.5	BDL	BDL	3.0	360.0
CHG 03-02	BDL	BDL	BDL	BDL	1.0	BDL	15.6	126.8	9.1	4.6	105.6	4.3	BDL	BDL	2.9	279.0
CHG 05-03	BDL	BDL	BDL	BDL	0.6	3	16.8	144.6	22.8	13.5	116.8	5.0	BDL	BDL	2.4	365.0
SHG 03-01	BDL	BDL	BDL	BDL	4.7	4	19.3	129.4	5.8	4.6	118.5	4.6	BDL	BDL	2.1	204.0
SHG 03-02	9	BDL	BDL	BDL	5.5	1338	14.9	112.7	9.7	5.4	91.0	2.6	0.4	BDL	2.5	234.0
SHG 03-02B	BDL	BDL	BDL	BDL	1.4	BDL	17.0	128.7	11.7	4.4	109.3	4.5	BDL	BDL	1.4	497.0
SHG 05-04	BDL	BDL	BDL	BDL	1.2	9	17.5	147.3	19.6	6.9	124.7	5.0	BDL	BDL	4.0	371.0
DHG 05-05	BDL	BDL	BDL	BDL	3.2	4	18.7	149.1	9.9	4.9	134.8	5.4	BDL	BDL	2.9	243.0
CHG 03-07	6.03	20.3	28.83	16.06	5.7	17	19.4	92.7	8.2	4.3	83.0	3.8	0.5	1.8	1.8	164.1
DHG 01-09	7.74	34.74	54.58	73.23	20.0	104	23.1	85.8	4.2	14.1	125.8	5.5	0.4	3.4	1.9	310.5
DHG 01-12	5.91	20.12	30.04	26.17	14.5	33	26.9	144.4	12.0	5.6	123.7	5.9	0.6	2.1	2.5	392.8
DHG 01-16	5.22	24.75	72.11	20.47	39.1	26	13.5	71.7	20.6	4.1	78.9	2.5	0.3	5.1	1.4	151.7
DHG 02-10	5.98	20.95	70.21	17.58	24.6	19	19.0	105.6	25.7	3.9	84.8	3.6	0.5	2.4	2.1	209.1
DHG 02-12	5.83	21.45	34.27	25.5	8.9	22	21.0	146.2	4.7	5.3	120.9	4.9	0.8	3.0	3.5	186.9
DHG 02-16	3.7	17.52	37.21	11.77	11.0	14	24.2	139.3	10.8	6.7	115.1	7.4	0.5	1.8	3.1	387.9
DHG 03-16	4.13	15.57	29.9	16.52	31.4	16	23.9	115.1	10.2	8.1	130.4	7.8	0.4	2.8	3.0	442.7
DHG 04-14	4.24	12.41	16.66	19.06	4.2	15	15.2	41.8	32.4	3.3	75.6	3.1	0.7	1.6	1.6	99.4
DHG 06-13	8.05	22.09	31.01	25.23	9.0	26	22.9	87.4	7.0	6.4	114.4	5.0	1.1	3.0	3.0	190.7
SHG 03-16	6.35	18.91	28.35	6.39	5.2	11	15.0	45.8	11.5	5.9	87.0	6.5	0.4	1.5	1.3	215.6
DHG 05-18a	3.71	14.94	46.68	9.24	10.3	15	21.7	141.1	6.4	5.3	77.0	5.8	0.5	0.7	1.9	165.7
DHG 05-18b	8.17	30.98	33.6	12.23	18.9	19	15.0	95.3	15.6	10.8	115.6	7.1	0.6	3.4	1.1	127.3
DHG 03-18	3.92	13.11	30.44	14.84	4.7	22	28.5	120.2	17.5	7.8	128.8	7.5	0.4	7.6	2.7	595.1
DHG 01-18	3.95	10.74	42.17	7.78	5.1	12	20.3	121.2	9.0	3.5	86.0	4.6	0.4	2.5	1.4	171.4
DHG 04-18a	6.11	12.41	25.04	9.44	13.5	18	23.5	124.5	12.0	8.3	141.8	8.5	0.4	2.3	1.9	237.9
DHG 02-18d	5.14	22.55	29.07	30.28	35.0	51	28.0	94.9	119.1	4.8	112.5	4.8	0.9	2.3	3.0	357.2
SHG 05-03*	BDL	BDL	BDL	BDL	0.3	BDL	16.1	86.3	4.3	4.4	101.7	4.0	BDL	BDL	1.3	257.0

Table 5B (continued) Abbreviations: LaN=normalized REE values according to McDonough and Sun, (1995). Eu/Eu* is Eu anomaly that is calculated by Eu/Eu* = EuN/ (0.5*(SmN + GdN)). Ce/Ce* is Ce anomaly that is calculated by CeN / (0.5*(LaN + PrN)).

Sample name	La	Ce	Pr	Nd	Sm	Eu	Gd	Tb	Dy	Ho	Er	Tm	Yb	Lu	Hf	Ta	La_N	Yb_N	La_N/Yb_N	Eu/Eu*	Ce/Ce*
DHG 03-04	14.60	28.90	2.85	9.80	1.78	0.49	1.25	0.18	0.72	0.15	0.40	0.07	0.39	0.06	2.90	0.40	61.60	2.42	25.43	0.96	1.02
DHG 03-01A	22.90	34.30	4.70	17.00	3.03	0.82	2.67	0.35	1.56	0.27	0.71	0.12	0.62	0.11	3.20	0.50	96.62	3.85	25.09	0.87	0.76
DHG 03-02	13.10	25.30	2.77	10.10	1.80	0.50	1.31	0.17	0.79	0.14	0.40	0.06	0.39	0.06	2.90	0.50	55.27	2.42	22.82	0.95	0.97
DHG 05-04A	12.80	23.50	2.50	8.80	1.49	0.46	1.23	0.17	0.89	0.18	0.53	0.08	0.51	0.07	3.00	0.40	54.01	3.17	17.05	1.01	0.95
DHG 05-04	12.90	23.20	2.51	9.20	1.55	0.48	1.28	0.17	0.86	0.15	0.43	0.06	0.43	0.06	2.80	0.40	54.43	2.67	20.38	1.02	0.93
DHG 05-06	18.30	31.00	3.71	13.30	2.19	0.65	1.82	0.24	1.17	0.19	0.54	0.08	0.47	0.07	3.60	0.50	77.22	2.92	26.45	0.97	0.86
CHG 03-02	12.50	22.50	2.50	8.70	1.49	0.48	1.18	0.16	0.82	0.15	0.44	0.06	0.40	0.06	3.00	0.50	52.74	2.48	21.23	1.07	0.92
CHG 05-03	39.60	31.80	7.58	27.30	4.18	1.18	3.75	0.50	2.39	0.42	1.12	0.15	0.86	0.12	3.50	0.50	167.09	5.34	31.28	0.90	0.42
SHG 03-01	19.00	30.30	3.62	13.50	2.17	0.63	1.71	0.21	0.98	0.16	0.42	0.07	0.43	0.06	3.50	0.40	80.17	2.67	30.02	0.97	0.83
SHG 03-02	17.50	29.80	3.57	13.20	2.19	0.71	1.76	0.23	1.06	0.19	0.50	0.08	0.44	0.06	2.60	0.40	73.84	2.73	27.02	1.07	0.87
SHG 03-02B	13.40	24.50	2.56	9.00	1.41	0.52	1.16	0.15	0.76	0.15	0.42	0.07	0.38	0.06	3.20	0.40	56.54	2.36	23.96	1.21	0.95
SHG 05-04	40.70	52.10	8.61	31.40	5.34	1.37	3.72	0.45	1.93	0.27	0.70	0.11	0.69	0.10	3.40	0.50	171.73	4.29	40.07	0.89	0.64
DHG 05-05	17.30	26.20	3.43	12.60	2.19	0.58	1.86	0.24	1.05	0.18	0.48	0.08	0.45	0.07	3.50	0.50	73.00	2.80	26.12	0.86	0.78
CHG 03-07	12.01	21.04	1.93	6.93	1.20	0.50	0.91	0.13	0.80	0.15	0.47	0.07	0.46	0.07	2.15	0.37	50.68	2.86	17.74	1.41	0.96
DHG 01-09	13.63	25.13	2.74	11.97	2.72	0.89	2.61	0.32	2.19	0.50	1.42	0.23	1.28	0.17	3.47	0.55	57.51	7.95	7.23	1.01	0.94
DHG 01-12	14.43	25.06	2.52	9.75	1.75	0.46	1.32	0.18	0.99	0.20	0.54	0.08	0.52	0.09	3.15	0.60	60.89	3.23	18.85	0.89	0.93
DHG 01-16	7.33	14.07	1.65	6.89	1.42	0.33	0.92	0.14	0.84	0.14	0.47	0.09	0.45	0.08	2.07	0.23	30.93	2.80	11.07	0.83	0.94
DHG 02-10	10.54	17.85	1.83	6.52	1.52	0.44	1.09	0.13	0.78	0.17	0.45	0.05	0.31	0.05	2.10	0.32	44.47	1.93	23.10	1.00	0.91
DHG 02-12	14.66	23.86	2.61	9.69	1.67	0.59	1.30	0.19	1.02	0.21	0.45	0.09	0.49	0.09	2.95	0.55	61.86	3.04	20.32	1.18	0.87
DHG 02-16	12.92	25.07	2.53	9.05	1.81	0.59	1.42	0.20	1.28	0.27	0.73	0.10	0.68	0.10	2.98	0.64	54.51	4.22	12.91	1.09	1.00
DHG 03-16	15.66	26.99	2.84	11.64	1.86	0.55	1.68	0.22	1.81	0.32	0.82	0.13	0.82	0.14	3.45	0.86	66.08	5.09	12.97	0.94	0.91
DHG 04-14	9.52	18.64	2.03	7.20	1.28	0.35	0.86	0.13	0.55	0.13	0.29	0.03	0.28	0.04	1.93	0.29	40.17	1.74	23.10	0.96	0.98
DHG 06-13	14.99	26.14	2.63	9.83	1.81	0.50	1.45	0.19	0.97	0.22	0.72	0.10	0.57	0.09	2.88	0.54	63.25	3.54	17.87	0.92	0.93
SHG 03-16	13.52	25.60	2.82	10.93	2.10	0.62	1.63	0.21	1.18	0.23	0.62	0.09	0.52	0.09	2.02	0.53	57.05	3.23	17.66	0.99	0.96
DHG 05-18a	8.47	19.20	1.81	6.55	1.32	0.42	1.18	0.16	0.98	0.19	0.46	0.07	0.43	0.07	1.99	0.46	35.74	2.67	13.38	1.01	1.13
DHG 05-18b	15.38	27.82	3.03	11.72	2.45	0.64	2.14	0.33	1.81	0.40	1.06	0.15	1.04	0.12	2.88	0.61	64.89	6.46	10.05	0.84	0.93
DHG 03-18	16.43	27.91	2.96	11.32	2.08	0.59	1.70	0.21	1.40	0.25	0.82	0.14	0.66	0.11	3.25	0.65	69.32	4.10	16.91	0.93	0.90
DHG 01-18	10.57	19.59	1.82	7.01	1.20	0.37	1.07	0.12	0.65	0.12	0.35	0.06	0.27	0.04	2.23	0.38	44.60	1.68	26.59	0.98	1.00
DHG 04-18a	15.80	29.60	3.06	11.74	2.38	0.54	1.84	0.28	1.66	0.29	0.87	0.13	0.78	0.11	3.61	0.73	66.67	4.84	13.76	0.76	0.97
DHG 02-18d	16.27	28.17	2.97	10.97	2.22	0.61	1.46	0.18	0.91	0.15	0.48	0.08	0.42	0.07	2.91	0.47	68.65	2.61	26.32	0.98	0.91
SHG 05-03*	12.40	23.50	2.35	8.00	1.25	0.28	0.98	0.15	0.79	0.14	0.42	0.07	0.40	0.06	3.20	0.40	52.32	2.48	21.06	0.75	0.99

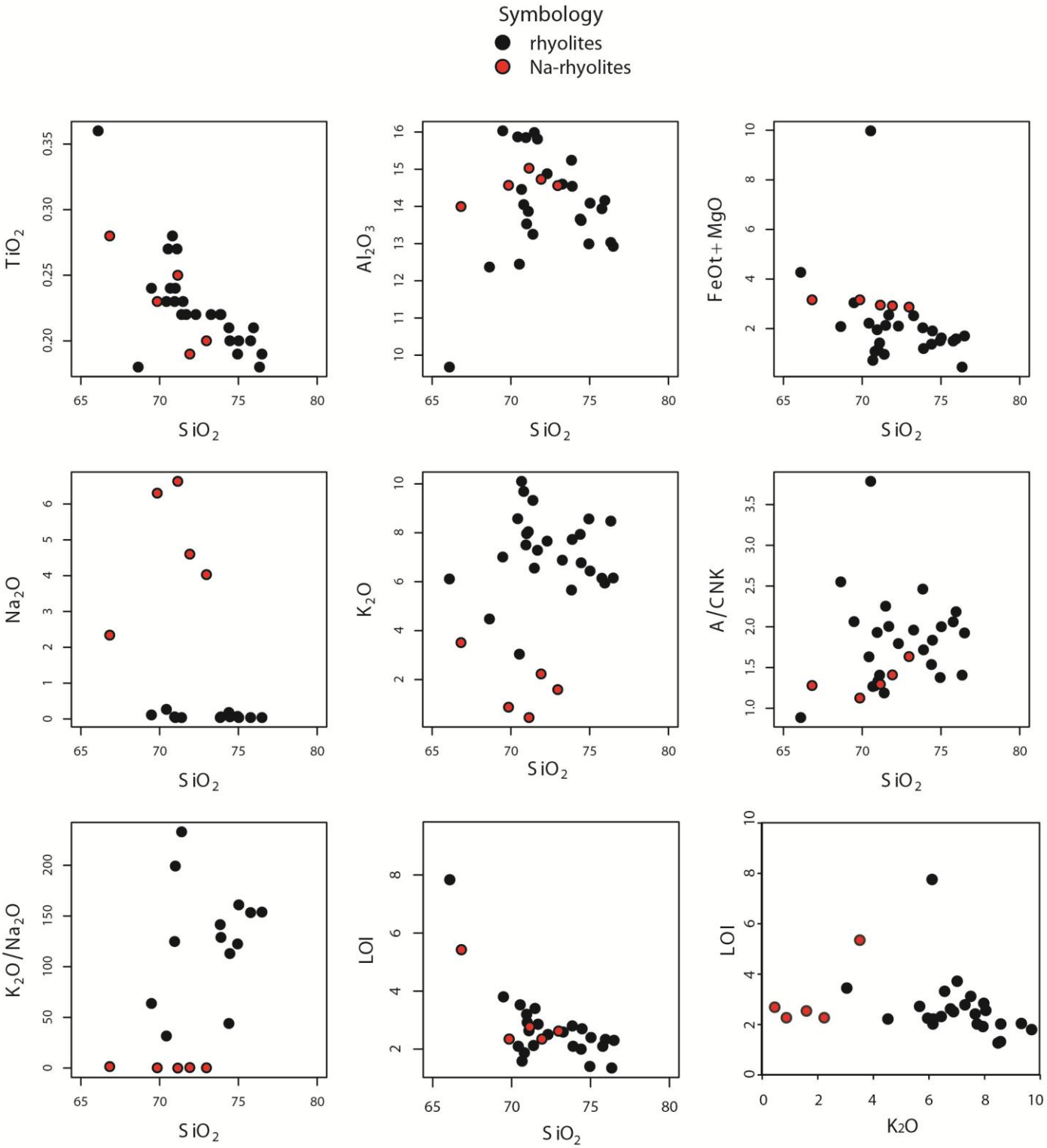

Figure 7.1 Harker diagrams for selected major element chemistry and LOI of the felsic igneous rocks of the H6 unit, comparison element plots of SiO_2 vs K_2O, CaO, MgO + FeO, TiO_2, K_2O/Na_2O, A/CNK (Al/(Ca+Na+K)), LOI and a Harker-type diagram of K_2O vs LOI. Values plotted represent 100% normalised anhydrous (i.e. excluding LOI) values.

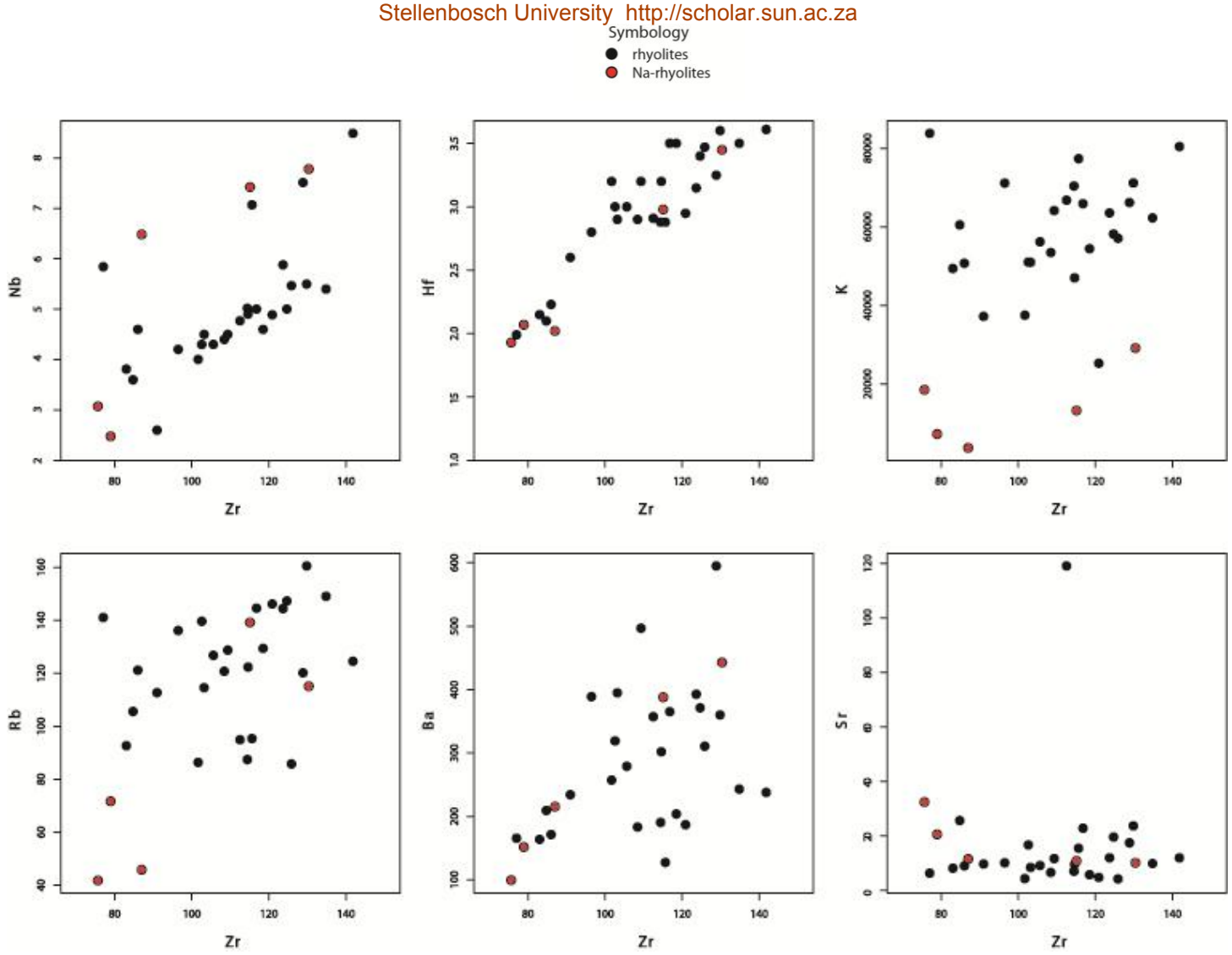

Figure 7.2 Harker-type diagrams of trace element chemistry of the felsic volcanic rocks of the H6 unit, comparison element plots of Zr vs Nb, Hf, K, Rb, Ba and Sr.

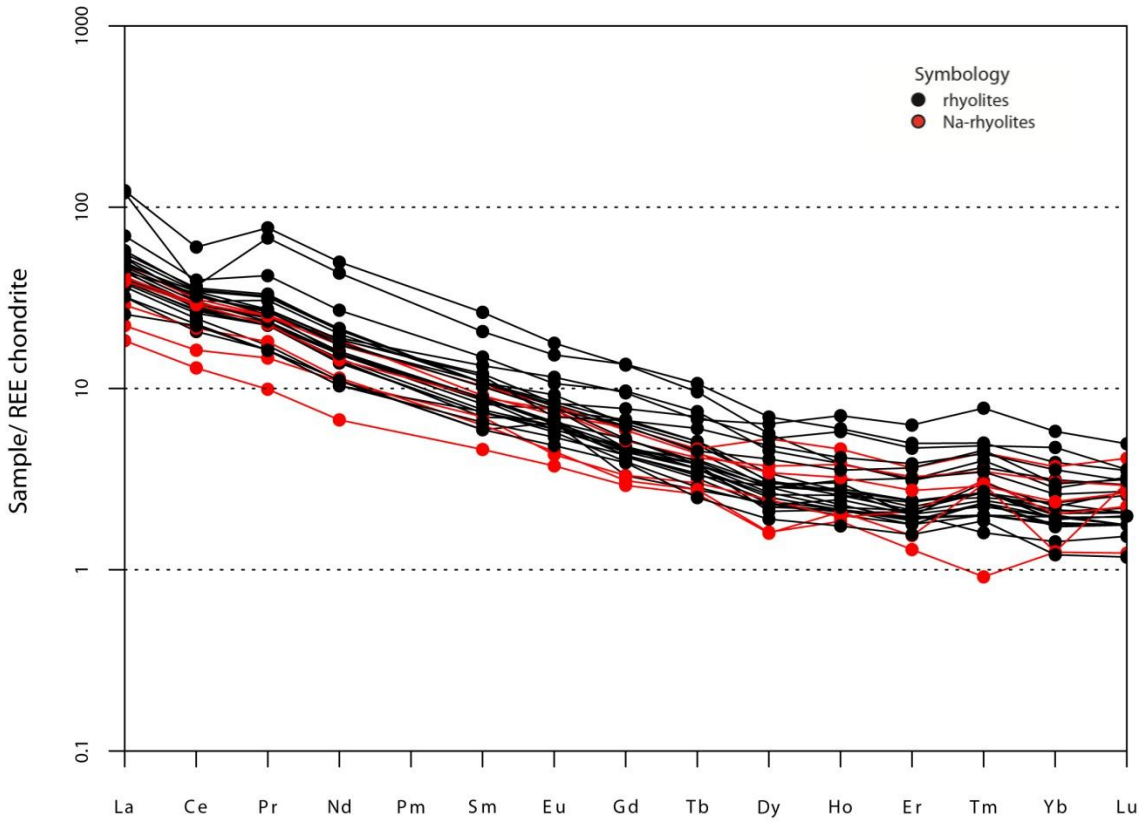

Figure 7.3 Chondrite (Nakamura 1974) normalized REE element composition of felsic volcanic of the H6.

7.2. Geochemical variation as a function of depth beneath the BRC

Rouchon et al., (2009) investigated the felsic volcanic rocks of the H6 unit and concluded that low temperature K-metasomatism occurred concurrently with silica alteration (formation of chert horizon). To test this hypothesis, samples were collected at different depths below the BRC to investigate if there is geochemical variation in K_2O and SiO_2 within rhyolites with an increase in depth below the BRC (Figure 4.2 A1). This method of testing geochemical variation is somewhat similar to the method Hofmann and Harris, (2008) used in their study of the felsic rocks of the H6 unit. However, the difference between the methods is that samples collected for this study were rhyolites 35 to 620 m beneath the BRC (Table 4C), whereas Hofmann and Harris, (2008) collected silicified felsic volcanic rocks and sandstones at different intervals up to 100m below the BRC.

Table 5C) Depth of rhyolite samples beneath the Buck Ridge Chert (BRC) unit in meters. Major element chemistry of corresponding samples is presented in Table 4A and trace element chemistry in Table 4B.

Sample name	Meters below BRC
CHG 03-07	35
CHG 03-02	70
SHG 03-02B	161
DHG 05-04	234
DHG 05-04A	275
CHG 05-03	471
DHG 05-05	580
DHG 05-06	580
SHG 05-04	620

Results presented in Fig. 7.4 illustrate no correlation between SiO_2 and K_2O with increasing distance towards the BRC. Furthermore SiO_2 does increase (from 69 to 76%) with increasing distance towards the BRC whereas no relationship is observed between K_2O with increasing distance towards the BRC (Fig 7.4).

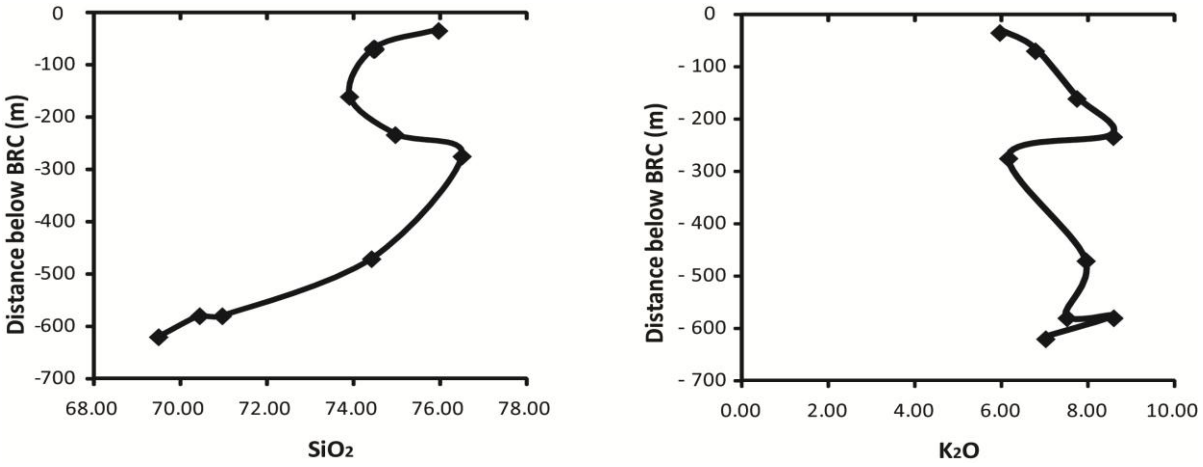

Figure 7.4 Plots illustrating geochemical variation in SiO_2 and K_2O in felsic volcanic samples as a function of depth below the BRC in meters.

Chapter 8: Discussion

Chert horizons are generally associated with volcano-sedimentary sequences within Archaean terrains, i.e. Onverwacht Group of the BGB, the Nondweni Greenstone Belt and the Warrawoona Group in the Pilbara Craton (Paris et al., 1985; Lowe and Byerly, 1986a; Duchac and Hanor, 1987; Hofmann, 2005a; Kitajima et al., 2001; Terabayashi et al., 2003; Van Kranendonk and Pirajno, 2004; Rouchon et al., 2008). These chert horizons form as a consequence of silicification that also silicifies the underlying volcano-sedimentary rocks, with the original textures of these underlying rocks sometimes still preserved as ghost textures. The silicification of these underlying rocks is associated with an increase of SiO_2 and K_2O content, a consequent decrease in FeOt, MnO, MgO, CaO and Na_2O and similar immobile element ratios relative to the unaltered underlying rocks. The source of SiO_2 in these cherts is proposed to be leached from the underlying volcano-sedimentary rocks by low temperature hydrothermal fluids (Hofmann and Harris, 2008 and references therein) whereas the source of K_2O (Rb and Ba) in these cherts is unresolved, as the Paleoarchaean rock record is considered to lack K_2O-rich granitoids that could have been a source. The timing of K_2O and SiO_2 alteration is proposed to be synchronous, as a result of selective K-uptake by phyllosillicates that also favours the uptake of SiO_2 in these minerals under specific conditions, as outlined in Rouchon et al., (2008).

The felsic rocks of the H6 unit are overlain by the Buck Ridge Chert (BRC) and almost all previous work completed on these rhyolites argued from the premise that they started out as dacites. Thus, previous studies stand on the de Wit et al., (1987a) observation that since these rhyolites have the same age as the ~3.45 Ga TTGs and that their REE patterns are alike, they therefore represent K-metasomatised eruptive equivalents of the ~3.45 Ga Stolzburg and Theespruit plutons. The observation that the dominant feldspar in the felsic rocks of the H6 were orthoclase and not adularia, calls into question the findings of previous studies. This study proposes an alternative hypothesis for the origin of the K_2O on the basis of examining magmatic and metamorphic textures in thin section and comparing all these observations with contemporary ~3.45 Ga felsic magmatic rocks of the BGGT.

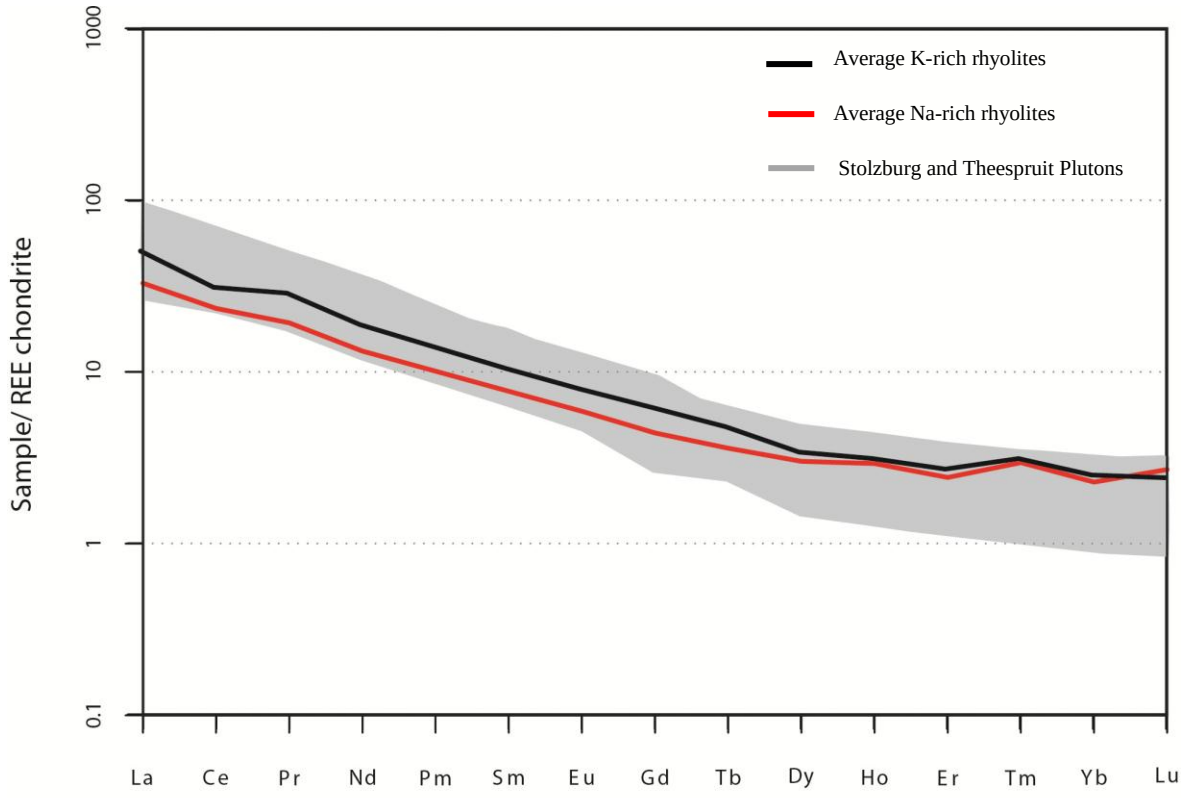

Figure 8.1 Chondrite (Nakamura 1974) normalized REE element composition for felsic volcanic rhyolites, Na-rhyolite from the H6 and ~3.45 Ga TTG plutons. (Red line = Average Na-rich rhyolites; Black line = Average K-rich rhyolites; Light grey shaded area = Stolzburg and Theespruit Plutons which represents the ~3.45 Ga TTGs in the BGGT.

8.1. The merits of alkali feldspar in rhyolites being a consequence of K-metasomatism

The chemistry of most of the felsic rocks in the H6 unit is that of peraluminous K-rich rhyolites with REE characteristics similar to the ~3.45 Ga TTGs of the BGGT (Fig.8.1). Importantly though, the pervasive replacement of microcrystalline groundmass and feldspar by hydrous phases during water-present metamorphism, together with silicification observed in textures (Fig. 5 J) and extreme scatter observed in most major and trace elements plots (Fig 7.1 and 7.2) makes it certain that the chemistry of these rhyolites has been altered. Consequently, the question as to what the original chemical composition of these rhyolites was remains. To try and solve this question, we examine the mineralogy of these rhyolites to determine whether the textures provide any clues to this original composition of these rocks.

The main mineralogical difference between the rhyolites of the H6 unit and ~3.45 Ga Stolzburg and Theespruit pluton is that the dominant mineral in these rhyolites is K-feldspar

(orthoclase or microcline abundance > 30%), whereas the dominant mineral in the Stolzburg and Theespruit plutons is plagioclase along with minor amounts of microcline (~ <10%). The occurrence of K-feldspar in these rhyolites has mostly been attributed to K-metasomatism due to the fact that these rocks are contemporaneous with the ~3.45 Ga Stolzburg and Theespruit TTGs (de Wit et al., 1987a; Hofmann and Harris, 2008; Rouchon et al., 2009). This observation is inconsistent with textures documented in thin sections of these rhyolites.

The rhyolite textures observed in thin section are characterized by feldspar crystals and quartz phenocrysts within a microcrystalline groundmass (Fig. 5A, C, D, E and F). Phenocrysts generally crystallized before the lava was quenched or before it erupted. Furthermore the quartz-feldspar porphyritic nature of the rocks with up to 70% phenocryst content could also indicate that these rocks crystallized at shallow levels. Most of the feldspar crystals are partially to completely replaced by muscovite (Fig. 5G, H and I). The fact that remnant K-feldspar domains exist within ghost feldspar phenocrysts suggests that in most of these rocks, this feldspar was K-feldspar (Fig. 5G and H; Table 3A).

The amount of the feldspar crystal that is replaced by muscovite was previously interpreted to represent the amount of K-metasomatism these rocks had undergone (de Wit et al., 1987a), hence the replaced feldspar was interpreted to have been plagioclase (de Wit et al., 1987a; de Vries et al., 2006; Rouchon et al., 2009). This observation is in contrast with the fact that remnant K-feldspars domains that cover an area of up to 40% of the ghost feldspar phenocrysts mineral grain, whereas the rest of the ghost feldspar phenocryst is covered by muscovite (Fig. 5G and H). Therefore the replacement of feldspar by muscovite most likely represent hydrothermal breakdown of K-feldspar during greenschist to sub-greenschist facies metamorphism (Fig. 5G, H and I).

The high potassium content within alkali feldspar (Or99) is thought to be an indication of metasomatic alteration given that feldspar with this chemistry are unlikely to form in igneous rocks (Deer, Howie and Zussman, 1992, pp. 220). However, this conclusion has been called into question by the occurrence of alkali feldspar inclusions within zircons of the K_2O-rich extrusives and high-level granites that has Or98 content, similar to the Or content of alkali feldspars phenocrysts found within these rocks.

The XRD analysis of whole rock powders demonstrate that the feldspar identified in rhyolites is K-feldspar whereas the feldspar identified in Na-rhyolites is albite (Table 4). The structural

state of these feldspars, in particular K-feldspar can be used to estimate the temperature in which the K-feldspar crystallized.

The XRD analysis of the structural state of the K-feldspars in the rhyolites in the H6 unit identified orthoclase (2 samples), intermediate microcline (2 samples) and microcline (3 samples) (Table 4). The intermediate microcline belongs to the triclinic crystal system whereas orthoclase belongs to the monoclinic crystal system. Al, Si ordering in the feldspar crystal structure together with microscopic evidence show intermediate microcline feldspar stability between 450 ˚C and ~500 ˚C (Mergoil-Daniel and Chevalier, 1984), whereas the transformation in crystal system from triclinic to monoclinic is characterized by the formation of orthoclase at ~ 500 ˚C (Smith and Brown, 1988, pp. 223-224). Adularia has mixture of Al, Si ordering variations within a single mineral, this lack of ordering is interpreted to indicate that the mineral has formed in a low-temperature environment (Smit and Brown, 1988, pp. 220).

The crystal structure of albite is similar to that of K-feldspars. Most albites in nature, even in volcanic rocks belong to the low albite group and therefore belong to the triclinic crystal system (Smith and Brown, 1988, pp. 221). Albite minerals in the monoclinic crystal system has only been observed in experimental labs where it forms at ~980 ˚C (Smith and Brown, 1988, pp. 221). The main reason for the existence of a wider variety of K-feldspar polymorphs relative to albite is due to the fact that between 550– 450˚C, a “tweed texture” develops in K-feldspar. This texture creates a buffer against higher Al, Si ordering, and thus against the formation of low microcline (Smith and Brown, 1988, pp 223-224). This buffer can only be broken down by fluids or deformation (Smith and Brown, 1988, pp 223-224). The rhyolites of the H6 member have only undergone sub greenschist to greenschist facies metamorphism and hydrothermal alteration below 300 ˚C (de Vries and Touret, 2007), therefore the formation of orthoclase and intermediate feldspar in these conditions are unlikely. Thus the presence of orthoclase and intermediate microcline polymorphs in the rhyolites from the H6 unit indicate that these minerals crystallized in medium temperature conditions of magma or in magma where the cooling magma was not extremely fast.

The high transition element concentrations documented in K-feldspars by Rouchon et al., (2009) could be the result of that study having analysed adularia. The other feature documented by Sanchez-Garrido et al., (2011) is that the peraluminous potassic granite magmas in the BGB were characterised by unusually high concentrations of transition

elements, therefore these elements could have been incorporated in the crystal structure of the K-feldspar during crystallization of these minerals from these magmas.

The presence of medium-temperature K-feldspar varieties indicates that the original igneous rocks contained K-feldspar. In addition compositions of these rocks may still be a product of K-metasomatism. However, rocks that contain quartz and K-feldspar phenocrysts cannot have been TTG dacites.

8.2. Minimum bulk rock K_2O content compositions based on the proportion of K-feldspar phenocrysts and the measured composition of these minerals.

The magmatic textures in the rhyolites of the H6 unit that can be observed in thin section are well preserved in some samples (Fig 5). These magmatic textures make it possible to determine the modal proportions of the minerals and groundmass accurately, with the assistance of special image analysis software, eCognition Developer version 8.0. The calculated feldspar mineral proportion of the rhyolites, in conjunction with major element compositions of K-feldspar can be used to determine the minimum bulk rock K_2O content of the rhyolites. This calculated minimum bulk rock K_2O content is thus determined based only on the K-feldspar proportion observed in the rhyolites and is independent of metamorphic or hydrothermal overprint and XRF-bulk data.

Calculation methods are based on selecting representative thin sections illustrating igneous textures from the H6 unit and acquiring their thin section images. The major requirement with regards to the choice of thin sections is that they must have variable modal proportions with groundmass content always being higher than the sum of K-feldspar and quartz phenocrysts content. The other requirement is that K-feldspar must be partially to completely replaced by muscovite. Three rhyolite samples meeting these requirements have been selected and presented in Fig. 8.2 A, C, E.

The modal proportion of the minerals and groundmass in the original volcanic rocks was determined by using image analysis software. The spectral (colour level) thresholds separating the different classes were determined through visual observation, and use to

classify pixels. It is possible to divide the thin section images of rhyolites into three classes that are consistent with the magmatic textures observed in the rhyolites. These three classes are K-feldspar, quartz and groundmass (Fig 8.2A and B; C and D; E and F). The calculated area of each class represents the modal proportion of each phase in the rhyolites. Some areas were unclassified, but this percentage of unclassified pixels is low (smaller than 10%). These unclassified pixels represent pixels in which overlap between different mineral thresholds occur, hence these unclassified pixels could be K-feldspar, quartz or groundmass. The modal proportion of the rocks can be normalized to 100 to exclude the unclassified pixels during the calculations. Modal proportions (excluding unclassified pixels) calculated by the software for the 3 different samples is presented in Table 6 below.

Table 6. Illustrating modal proportions calculated by eCognition developer software excluding the unclassified pixels. The modal proportion of glass is always higher than 50% and is as high as 63% in SHG 03-02B whereas K-feldspar modal proportion is between 43 and 30%. Quartz modal proportion is generally lower than 6%. Percentage phenocrysts are normalized to exclude the unclassified %.

Classification	**DHG 05-06**	**DHG 03-02**	**SHG 03-02B**
K-feldpar (%)	42.79	43.03	30.52
Albite (%)	0.00	0.00	0.00
Quartz (%)	0.87	5.01	5.68
Groundmass (%)	56.34	51.96	63.8
Unclassified (%)	10.87	9.68	10.22

The second step is to determine the minimum bulk K_2O content of the rhyolites by using the modal proportions in conjunction with the measured mineral chemistry of the feldspar phenocrysts. The major element chemistry of the K-feldspar is collected from electron beam analysis of orthoclase in sample SHG 03-02B (Table 3A, Analysis number 15). The groundmass in the felsic igneous rocks of the H6 could have been microcrystalline groundmass or volcanic glass that has undergone devitrification similar to all volcanic glass in the Archaean on earth.

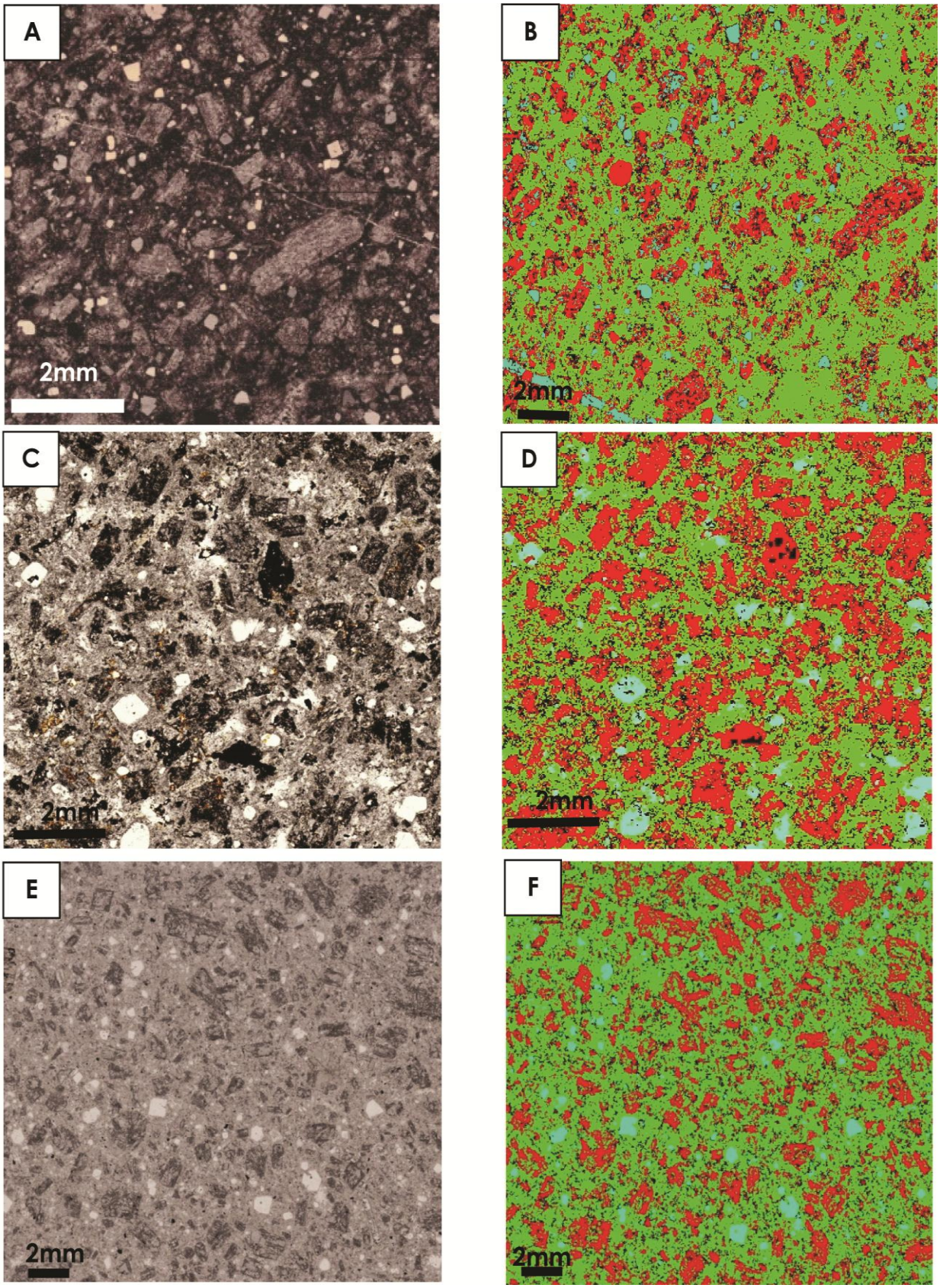

Figure 8.2 Transmission plane polarised (E) and cross polarised light (A and C) of the rhyolites of the H6 unit and images representing the classified thresholds (B, D and F) of the rhyolites. B is the classified image of A; D is the classified image of C; F is the classified image of E. Image analysis of representative thin sections indicates that many of these rocks contained upwards of 30% K-feldspar crystals. Symbology: Red = K-feldspar, Blue = quartz, Green = remnant glass and Black = unclassified pixels.

The minimum bulk rock K_2O content calculations were performed on a spreadsheet that works on the principle that minimum bulk rock K_2O content in wt% can be determined by multiplying the modal proportions (%) of K-feldspar and the mineral chemistry. The difference in density between K-feldspar, quartz and experimental glass is quite small. Therefore, the influence of mineral density in the calculation of minimum bulk rock K-content is negligible. The calculation can mathematically be expressed as:

- $\{X1, X2, X3, \ldots, Xn\}$ Where X equals the percentage of a particular element (e.g. Al_2O_3) in a particular mineral ($X1$ = percentage Al_2O_3 in K-feldspar)

- $\{W1, W2, W3, \ldots, Wn\}$ Where W equals the modal proportion (e.g. $W1$ = 30% K-feldspar) of the mineral in the rock.

Then the calculation for the estimated bulk is expressed as: estimated bulk =

$$\frac{(X1(W1) + X2(W2) + \ldots + Xn)Al2O3}{(W1, W2, W3, \ldots, Wn)Al2O3} + \frac{(X1(W1) + X2(W2) + \ldots + Xn)K2O}{(W1, W2, W3, \ldots, Wn)K2O} + \ldots$$

The minimum bulk rock K_2O content calculated from mode (Table 6) and mineral chemistry of K-feldspar (Table 3A, Analisys number 15). The results indicate that the minimum amount of K_2O these rocks contained prior to alteration range between 5.05 and 7.08 wt% (Table 8). These results suggest that these rocks were primary rhyolites prior to alteration.

Table 7. Minimum bulk rock major element content of three samples determined by using the proportion of K-feldspar phenocrysts and the mineral chemistry of K-feldspar.

	DHG 05-06	DHG 03-02	SHG 03-02B
SiO_2	27.69	27.84	19.75
Al_2O_3	7.53	7.57	5.37
FeO	0.00	0.00	0.00
CaO	0.01	0.01	0.01
Na_2O	0.12	0.12	0.09
K_2O	7.08	7.12	5.05
BaO	0.04	0.04	0.03

The fact that the granitic clasts in the Moodies Group, Stolzburg and Theespruit plutons and the felsic volcanic rocks of the H6 unit all have the same magmatic age, a geochemical comparison between these rocks are relevant. In particular a comparison between the major and trace element chemistry of the rhyolites of felsic volcanic rocks of the H6 unit and granitic clasts from the Moodies Group that has not been previously compared.

8.3. Comparison between the major and trace element chemistry of the ~3.45 Ga felsic magmatic rocks of the BGGT.

The similarity in Na_2O content and magmatic age of the Na-rhyolites and ~3.45 Ga TTGs indicates that they could be eruptive equivalents of these TTGs (Fig. 8.3). Alternatively the similarity between the magmatic origin of K-feldspar, K_2O-composition and the magmatic age of the rhyolites and K_2O-rich felsic granitic clasts contained within the Moodies Group conglomerate demonstrates that these rocks could be equivalents.

The major difference in K-Na-Ca chemistry between these potassic rocks is shown by the rhyolites of the H6 unit that has K >> Na = Ca whereas the granitic rocks from the Moodies Group has K ≥ Na >> Ca (Fig. 8.4). The K-Na-Ca chemical composition of the granitic rocks in the Moodies Group also plots between the rhyolites and Na-rhyolites felsic volcanic varieties of the H6 unit on the Feldspar triangle in Figure. 8.3. These differences in K-Na-Ca chemistry between these potassic magmatic rocks could be explained by the fact that the

rhyolites in the H6 unit have undergone low temperature hydrothermal alteration by the selective extraction or addition of Na_2O, CaO and K_2O from volcanic glass as mentioned by work on these rocks by Rouchon et al., (2009). Further work on trace element chemistry of accessory minerals in these rhyolites in the H6 unit could define the original chemistry of these rhyolites more conclusively and therefore define a better major element comparison with the contemporary granitic rocks in the Moodies Group.

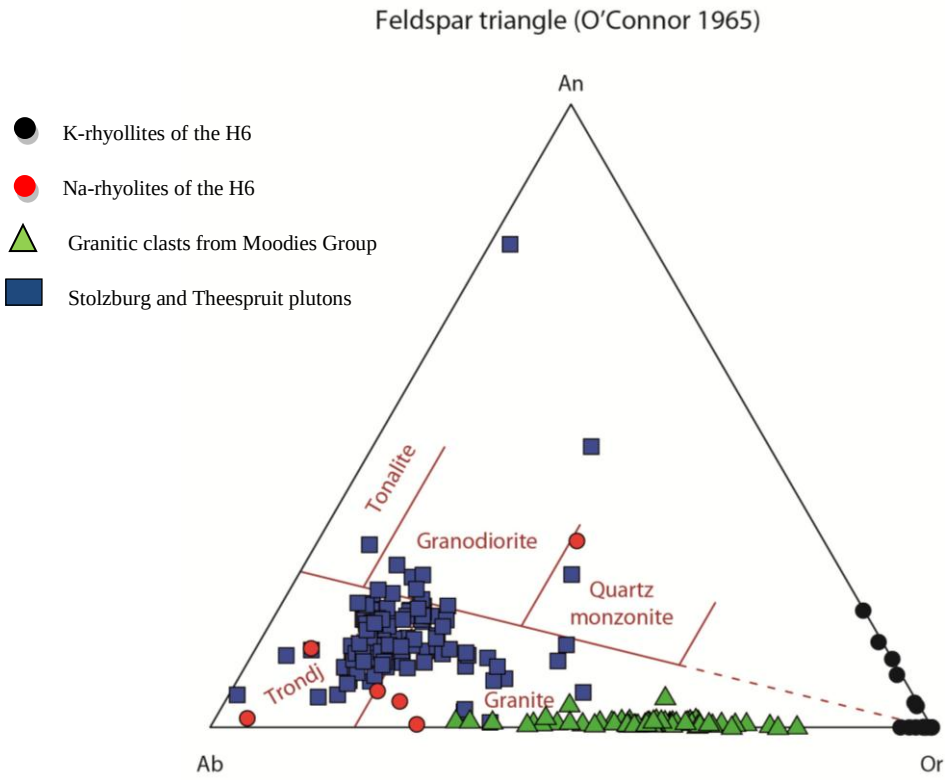

Figure 8.3 Normative feldspar triangle by O'Connor 1965 of the XRF data of the rhyolites (black circles) and Na-rhyolite (red circles) of the H6, Stolzburg and Theespruit plutons (blue squares) and granitic clasts from Moodies Group (green triangles). Only the least altered samples of the granitic clasts from Moodies Group were used in this diagram (Sanchez-Garrido et al., 2011). The least altered samples were classified on the basis of the Chemical Index of Alteration by Nesbit and Young, (1982) and LOI values. Samples with CIA > 60 and LOI > 2 was removed (Sanchez-Garrido et al., 2011). Abbreviation: Trondj = trondhjemite, Ab =Albite, An = anorthite, Or = orthoclase.

The rhyolites of the H6 unit were affected by hydrothermal alteration that caused the high A/CNK and mostly scattered major and trace element plots (Fig. 7.1; Fig. 7.2) in the rhyolites. Therefore, it is more adequate to compare the ~3.45 Ga felsic magmatic rocks by using HFS elements concentrations and ratios of TiO_2, Nb/Y, Zr and Zr/TiO_2 vs Al_2O_3 plots, given that these elements and ratios are not easily mobilized during alteration and thus

reliable elements to identify pre-alteration relationships between the ~3.45 Ga felsic magmatic rocks (Fig. 8.4).

The element concentrations and ratios presented in Figure 8.4 are similar for the ~3.45 Ga felsic magmatic rocks; except that Zr concentrations is more scattered and higher within the granitic clasts from the Moodies Group relative to the other ~3.45 Ga felsic magmatic rocks (Fig. 8.5). As mentioned in earlier chapters, the proposed similarity of REE patterns of the rhyolites and ~3.45 Ga TTGs have caused previous workers to identify the rhyolites as eruptive K-metasomatised equivalents of the ~3.45 Ga TTGs (de Wit et al., 1987a; Hofmann and Harris, 2008; Rouchon et al., 2009).

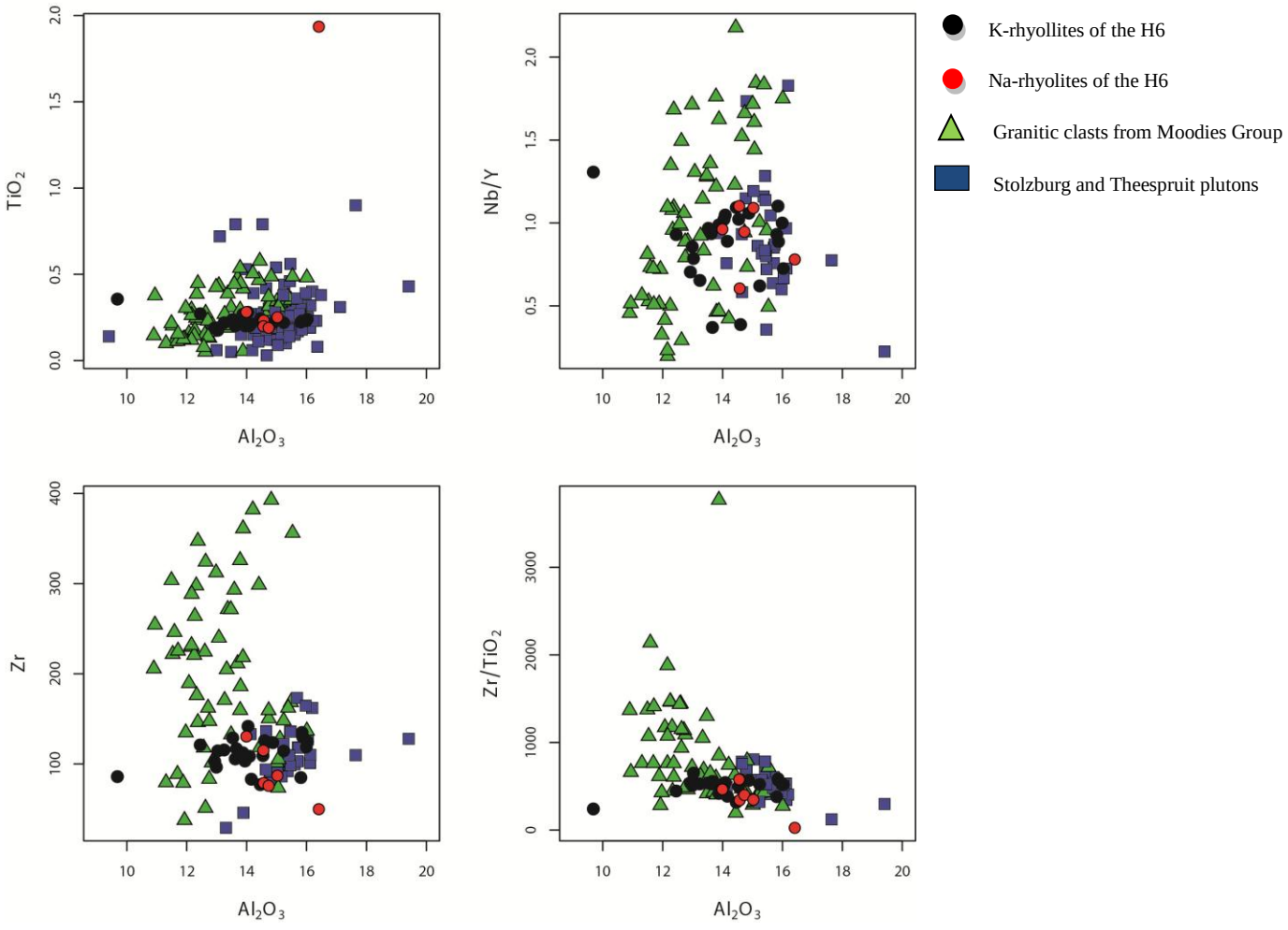

Figure 8.4 HFS element in concentrations (Zr in ppm whereas TiO2 in wt%) and ratios (Nb/Y and Zr/TiO2) is plotted against Al2O3. HFS elements are highly charged and will not be altered easily from a rock during metasomatism. Symbology: red circles = Na-rhyolites, black circles = rhyolites, green triangles = granitic clasts from Moodies Group, blue squares = ~3.45 Ga TTGs from the BGGT.

The conclusion by previous authors on the similarity of the REE patterns of the ~3.45 Ga TTGs and rhyolits of the H6 needs to be examined in more detail by also examining the REE patterns of the synchronous primary K_2O-rich volcanic rocks from the Moodies Group. The REE chemistry of rocks is generally considered to be immobile e.g. experiments by Petit et al, (1989) show that even when rhyolitic glasses have undergone extensive metasomatism, the REE chemistry remained insoluble and similar to the original composition of the glass (Petit et al., 1989). Therefore REE patterns can be used as good tool to differentiate between the different ~3.45 Ga felsic igneous rocks of the BGGT.

A comparison of the REE chemistry of ~3.45 Ga felsic magmatic rocks of the BGGT illustrate that differences in REE patterns exist (Fig. 8.5). These differences in REE patterns show that the granitic rocks from the Moodies Group are more enriched in HREE relative to the depleted HREE patterns of the rhyolites, Na-rhyolites and ~3.45 Ga TTGs. This difference in REE patterns between the contemporaneous felsic igneous rocks can be amplified by examining the slope of the REE diagram.

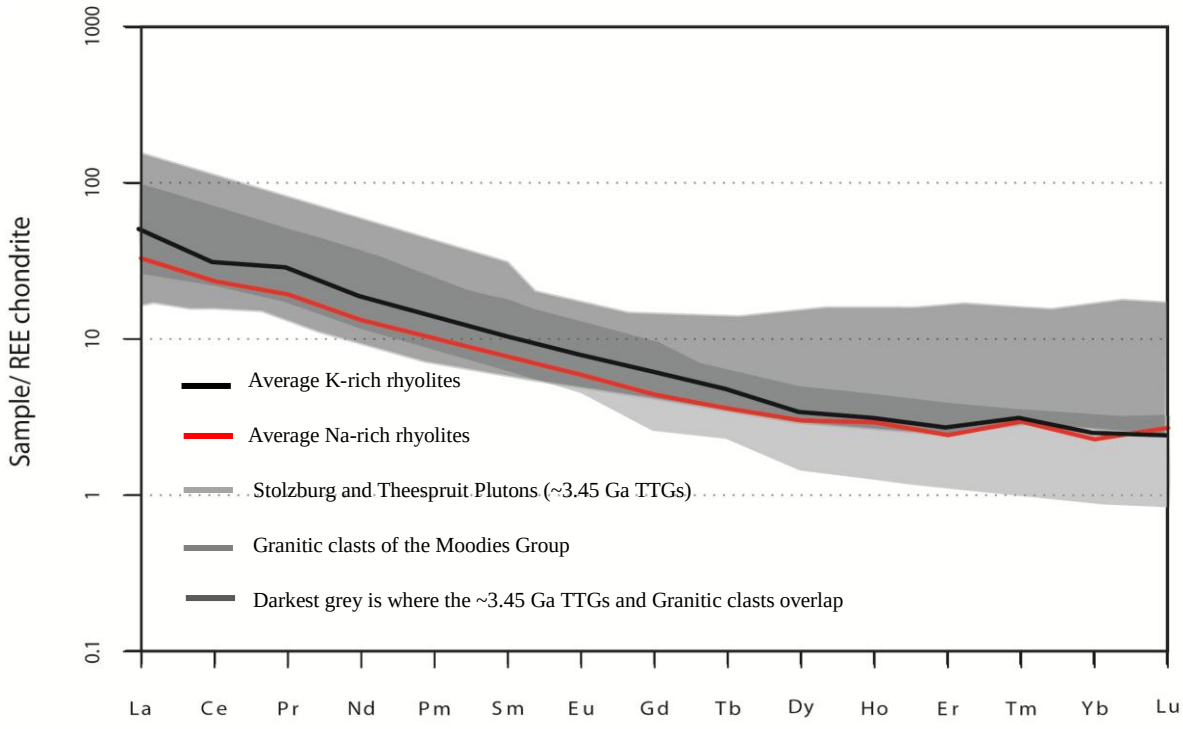

Figure 8.5 Chondrite (Nakamura 1974) normalized REE element composition of felsic volcanic rhyolites, Na-rhyolite from the H6 and ~3.45 Ga TTG plutons.

The slope of a REE patterns is calculated by dividing a normalized LREE (La_N) by normalized HREE (Lu_N) and can be mathematically expressed as La_N/Lu_N. To illustrate this slope graphically the La_N/Lu_N is compared with immobile oxide TiO_2 (Fig 8.6A). The difference in slope demonstrates that TTGs having the steepest slope relative to felsic volcanics of the H6 unit and granitic clasts from the Moodies Group. Overlap between slopes of the REE patterns occur and can be reduced by only comparing the HREE slope (Gd_N/Lu_N) vs TiO_2 of these ~3.45 Ga felsic magmatic rocks (Fig. 8.6B). These slopes expressed as points on a La_N/Lu_N and Gd_N/Lu_N vs TiO_2 plots clearly shows that the granitic rocks in the Moodies Group have a flatter HREE slope relative to the rhyolites of the H6 unit and ~3.45 Ga TTGs.

A)

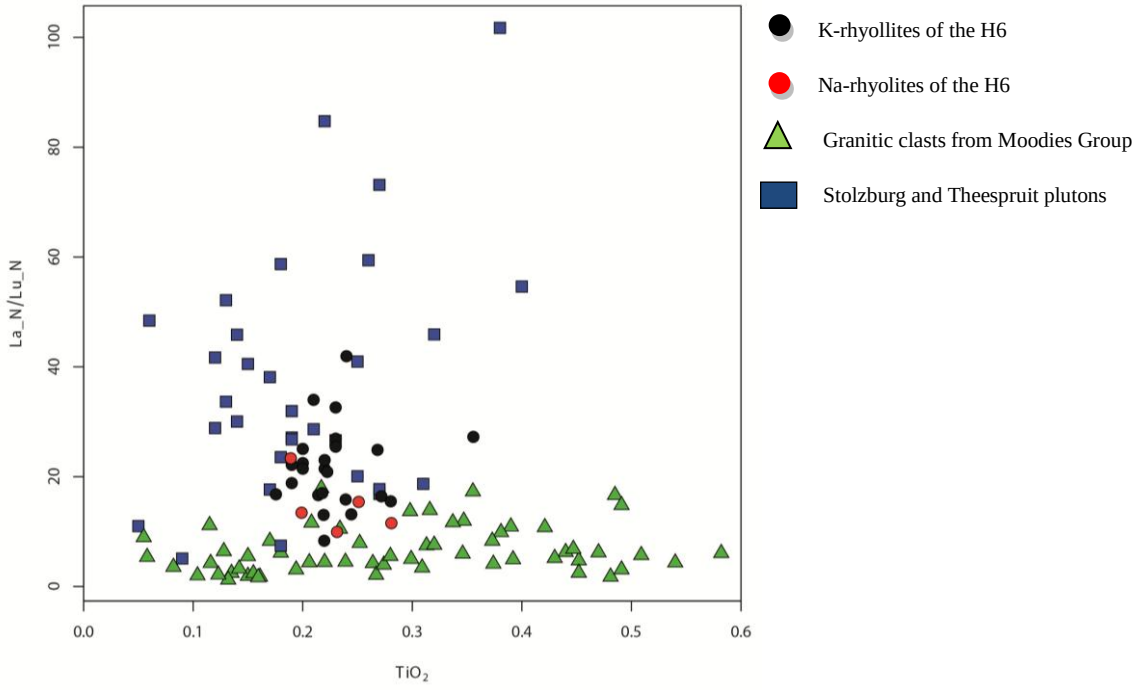

B)

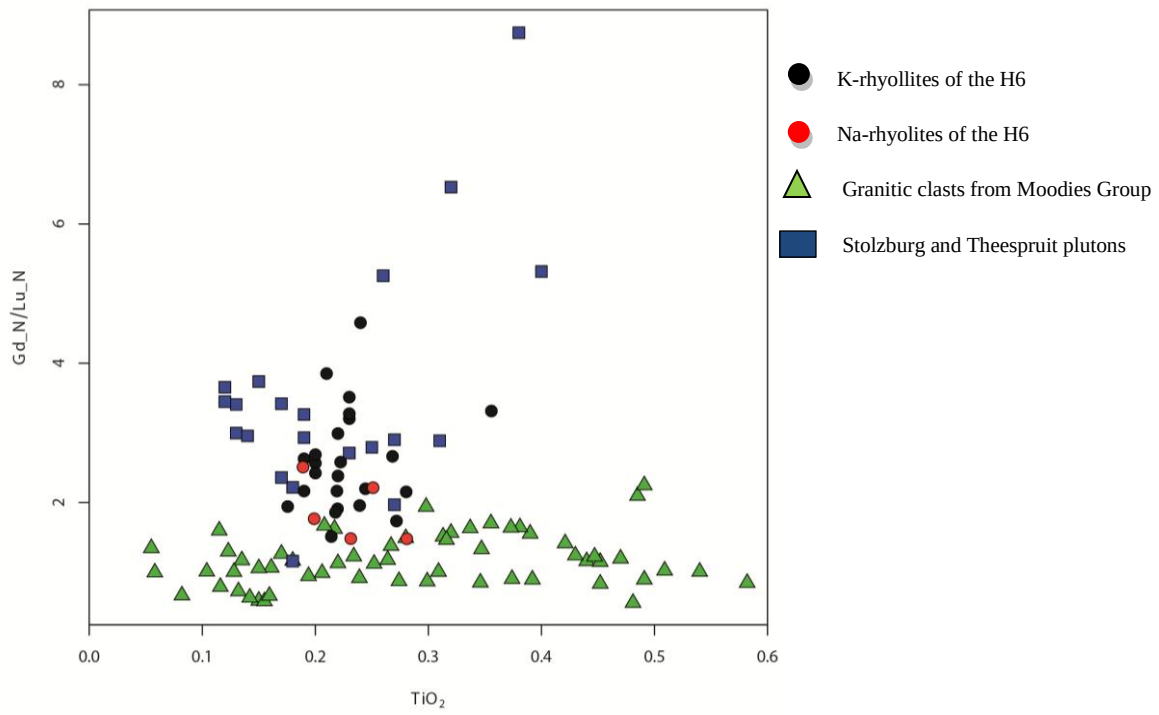

Figure 8.6A) Comparison element LaN/LuN vs TiO2 of the rhyolites (black circles), Na-rhyolite (red circles) of the H6 layer (green), Stolzburg and Theespruit plutons (blue squares) and granitic clasts from Moodies Group (green triangles). The La and Lu is normalized to chondrite to Nakamura, (1974) and represent the slope of the REE patterns. B) Comparison element GdN/LuN vs TiO2 of the rhyolites (black circles) and Na-rhyolites (red circles) of the H6 layer, Stolzburg and Theespruit plutons (blue squares) and granitic clasts from Moodies Group (green triangles). The Eu and Lu are normalized to chondrite of Nakamura, (1974).

The fact that the primary chemistry in these rhyolites of the H6 unit is not preserved makes it difficult to constrain the original composition with accuracy. Therefore basing the conclusions on a petrogenetic model would be inconclusive. In addition findings in this study indicate that these orthoclase bearing rhyolites were at least originally K_2O-rich magmas in regards to major elements chemistry. This feature that the rhyolites of the H6 unit are primary K_2O-rich magmas demonstrates that these rocks formed from the melting of biotite or melting of a sedimentary source (Patino-Douce and Johnston, 1991; Montel and Vielzeuf, 1997), whereas the chemistry of the ~3.45 Ga TTGs indicate that they formed from the high pressure melting of amphibolites (Foley et al., 2002; Rapp et al., 2003; Moyen and Stevens, 2006 and references therein; Martin, 1994 and references therein).

The REE patterns of the rhyolites in the H6 and ~3.45 TTGs are both depleted in HREE in regards to LREE (similar) (Fig.8.5 and Fig. 8.6A and B). This observation demonstrates that these rhyolites and ~3.45 Ga TTGs could have formed in the same geodynamic setting with the difference in major element chemistry being a consequence of melting of different sources. Therefore these rhyolites could represent high pressure (>20kbar) K-rich potassic melts that formed at the same time and in similar conditions as the ~3.45 Ga TTGs.

Conclusion

1) Magmatic textures of the K_2O rich rhyolites in conjunction with mineral chemistry of remnant K-feldspar crystals and presence of orthoclase indicates that these rhyolites were once K_2O-rich magmatic rocks. Therefore this thesis shows that these rhyolites could not have been K-metasomatised eruptive equivalents of the Stolzburg and Theespruit plutons as de Wit et al., (1987) originally proposed.

2) The fact that these K_2O-rich rhyolites of the H6 unit in conjunction with granitic clasts of the Moodies Group have the same magmatic age as the ~3.45 Ga Stolzburg and Theespruit plutons illustrates clearly that high pressure melting of amphiboltes to form the ~3.45 Ga TTGs occurred concurrently with the melting of a sedimentary source or a source that contained biotite during the ~3.45 Ga magmatic event in the BGGT.

3) This thesis demonstrates that rhyolitic volcanism during the ~3.45 Ga magmatic event in the BGGT was not only represented by granitic rocks contained as clasts in basal conglomerate of the Moodies Group. Thus the presence of K_2O-rich magmatic rocks was more extensive during the ~3.45 Ga magmatic event than previously thought.

Appendix 1: **Table I.1A. LA ICP-MS comparison between the certified BCR-2 powder and average BCR-2 fusions.**

	Fusion control std Certified BCR powder	Average Analysed	*% Deviation*
Sc	**33**	36.26	***9.9***
V	**416.00**	441.52	***6.1***
Cr	**18**	18.02	***0.1***
Co	**37**	37.84	***2.3***
Ni	**18**	14.60	***18.9***
Cu	**21**	19.95	***5.0***
Zn	**127**	131.33	***3.4***
Rb	**46.9**	46.43	***1.0***
Sr	**340**	353.73	***4.0***
Y	**37**	34.35	***7.2***
Zr	**184**	185.57	***0.9***
Nb	**12.6**	12.85	***2.0***
Mo	**250**	273.23	***9.3***
Cs	**1.1**	1.14	***3.4***
Ba	**677**	697.41	***3.0***
La	**24.9**	25.89	***4.0***
Ce	**52.9**	54.23	***2.5***
Pr	**6.7**	6.75	***0.8***
Nd	**28.7**	29.80	***3.8***
Sm	**6.58**	6.91	***5.1***
Eu	**1.96**	2.01	***2.8***
Gd	**6.75**	6.78	***0.4***
Tb	**1.07**	1.02	***4.7***
Dy	**6.41**	6.63	***3.4***
Ho	**1.28**	1.33	***3.9***
Er	**3.66**	3.76	***2.8***
Tm	**0.54**	0.55	***1.9***
Yb	**3.38**	3.55	***5.1***
Lu	**0.503**	0.53	***4.6***
Hf	**4.9**	4.84	***1.1***
Ta	**0.74**	0.83	***11.7***
Pb	**11**	10.40	***5.5***
Th	**5.7**	6.55	***14.9***
U	**1.69**	1.77	***4.7***

Table I.1B. Trace element data for certified value for BHVO-2G standard together with Stellenbosch lab analyses of the same standard during session 1 (Stel 1), session 2 (Stel 2) and session 3 (Stel3). This table also shows the standard deviation between the different analyses of the same standard during the first session, average value of analysis, percentage difference between accepted BHVO – 2G and average BHVO – 2G analysed in the Stellenbosch lab and the relative standard deviation (RSD) between the analysis in the Stellenbosch lab.

Accepted value for BHVO-2G			**Lab Stel 1**								
	Value	**Uncertainty**		**BHVO_1**	**BHVO_2**	**BHVO_3**	**BHVO_4**	**BHVO_5**			**Percentage difference between accepted BHVO-2G values and BHVO-2G lab values (%)**	**RSD (%)**
				Standard	**Standard**	**Standard**	**Standard**	**Standard**	**STDEVA**	**Average**		
Sc45	33	2	Sc45	31.14	31.48	31.42	32.18	32.33	0.52	31.71	-3.91	1.63
V51	308	19	V51	320.35	324.85	325.03	335.44	340.73	8.46	329.28	6.91	2.57
Cr53	293	12	Cr53	250.95	254.08	262.48	280.46	300.46	20.67	269.69	-7.96	7.67
Co59	44	2	Co59	43.62	44.4	44.33	46.13	46.49	1.25	44.99	2.26	2.77
Ni60	116	7	Ni60	117.41	119.23	119.74	123.11	121.94	2.26	120.29	3.69	1.88
Cu63	127	11	Cu63	110.47	112.99	117.84	125.6	136.34	10.50	120.65	-5.00	8.70
Zn66	102	6	Zn66	105.05	105.58	108.15	130.65	122.37	11.53	114.36	12.12	10.08
Ga69	22	3	Ga69	23	23.04	23.1	23.25	23.26	0.12	23.13	5.14	0.52
Rb85	9.2	0.04	Rb85	8.69	8.69	8.85	9.26	9.36	0.32	8.97	-2.50	3.56
Sr88	396	1	Sr88	380.9	387.72	384.94	399.9	406.06	10.62	391.90	-1.03	2.71
Y89	26	2	Y89	21.26	21.52	21.4	22.52	22.48	0.61	21.84	-16.02	2.81
Zr90	170	7	Zr90	143.06	144.46	145.74	152.39	157.25	6.02	148.58	-12.60	4.05
Nb93	18.3	0.8	Nb93	17.72	17.88	17.86	18.83	18.81	0.55	18.22	-0.44	3.03
Mo95	3.8	0.2	Mo95	3.81	3.96	3.98	4.18	4.39	0.22	4.06	6.95	5.53
Cd111	0.1	0.02	Cd111	0.139	0.178	0.151	0.244	<0.00	0.09	0.18	78.00	50.21
Sn118	2.6	0.6	Sn118	1.37	1.48	1.48	1.65	1.8	0.17	1.56	-40.15	10.87
Cs133	0.1	0.02	Cs133	0.0777	0.1056	0.0901	0.111	0.096	0.01	0.10	-3.92	13.64
Ba137	131	2	Ba137	127.61	127.62	128.08	136.64	135.36	4.53	131.06	0.05	3.46
La139	15.2	0.2	La139	14.31	14.61	14.51	15.32	15.14	0.43	14.78	-2.78	2.92
Ce140	37.6	0.2	Ce140	35.88	36.33	36.39	39.2	39.16	1.64	37.39	-0.55	4.40
Pr141	5.35	0.22	Pr141	4.85	4.94	4.91	5.29	5.25	0.21	5.05	-5.64	4.08
Nd146	24.5	0.2	Nd146	23.61	23.2	23.34	24.68	25.23	0.89	24.01	-1.99	3.73
Sm147	6.1	0.03	Sm147	5.95	5.74	5.68	6.22	5.83	0.21	5.88	-3.54	3.63
Eu153	2.07	0.01	Eu153	1.857	1.93	1.895	2.01	2.06	0.08	1.95	-5.78	4.27

Gd157	6.16	0.05	Gd157	5.37	5.44	5.36	6.14	6.06	0.39	5.67	-7.89	6.89
Tb159	0.92	0.04	Tb159	0.745	0.745	0.748	0.772	0.795	0.02	0.76	-17.28	2.91
Dy163	5.28	0.05	Dy163	4.51	4.79	4.65	5.12	5.1	0.27	4.83	-8.45	5.60
Ho165	0.98	0.04	Ho165	0.847	0.885	0.835	0.869	0.899	0.03	0.87	-11.53	3.04
Er166	2.56	0.02	Er166	2.223	2.218	2.176	2.38	2.27	0.08	2.25	-11.98	3.47
Tm169	0.34	0.02	Tm169	0.281	0.31	0.28	0.327	0.293	0.02	0.30	-12.29	6.75
Yb172	2.01	0.02	Yb172	1.785	1.87	1.827	1.86	2.01	0.08	1.87	-6.95	4.53
Lu175	0.279	0.003	Lu175	0.245	0.24	0.241	0.263	0.247	0.01	0.25	-11.40	3.76
Hf178	4.32	0.18	Hf178	3.43	3.49	3.61	3.9	4.01	0.26	3.69	-14.63	6.92
Ta181	1.15	0.1	Ta181	1.08	1.129	1.093	1.182	1.219	0.06	1.14	-0.82	5.17
Pb208	1.7	0.2	Pb208	1.7	1.699	1.635	1.9	1.74	0.10	1.73	2.05	5.75
Th232	1.22	0.05	Th232	1.1	1.15	1.132	1.307	1.194	0.08	1.18	-3.56	6.84
U238	0.403	0.003	U238	0.382	0.366	0.373	0.428	0.437	0.03	0.40	-1.44	8.28

Accepted values for BHVO-2G											
	Value	Uncertainty	BHVO_1	BHVO_2	BHVO_3	BHVO_4	BHVO_5			Percentage difference between accepted BHVO-2G values and BHVO-2G lab values (%)	RSD (%)
			Standard	Standard	Standard	Standard	Standard	STDEVA	Average		
Sc45	33	2	31.95	32.42	32.56	34.06	32.83	0.79	32.76	-0.72	2.42
V51	308	19	325.29	326.73	331.47	344.91	319.06	9.69	329.49	6.98	2.94
Cr53	293	12	272.94	278.44	276.36	276.65	266.16	4.87	274.11	-6.45	1.78
Co59	44	2	43.75	44.68	44.59	44.85	43.74	0.53	44.32	0.73	1.21
Ni60	116	7	111.37	112.33	110.86	111.82	107.91	1.74	110.86	-4.43	1.57
Cu63	127	11	113.96	116.45	111.32	111.63	111.41	2.24	112.95	-11.06	1.98
Zn66	102	6	108.47	114.16	112.09	128.3	108.47	8.20	114.30	12.06	7.17
Ga69	22	3	25.52	25.14	23.04	23.78	22.85	1.21	24.07	9.39	5.04
Rb85	9.2	0.04	8.67	8.93	8.82	10.03	8.72	0.57	9.03	-1.80	6.26
Sr88	396	1	383	391.08	396.93	432.88	380	21.26	396.78	0.20	5.36
Y89	26	2	22.31	22.68	22.78	24.17	22.81	0.71	22.95	-11.73	3.10
Zr90	170	7	152.81	158.68	157.9	165.7	156.33	4.72	158.28	-6.89	2.98
Nb93	18.3	0.8	17.76	18	18.26	19.03	18.09	0.48	18.23	-0.39	2.65
Mo95	3.8	0.2	4.08	4.15	4.18	4.45	4.17	0.14	4.21	10.68	3.37
Cd111	0.1	0.02	0.1	0.14	0.156	0.27	0.071	0.08	0.15	47.40	51.72
Sn118	2.6	0.6	1.612	1.862	1.806	1.53	1.611	0.14	1.68	-35.22	8.44
Cs133	0.1	0.02	0.0921	0.1023	0.0933	0.126	0.0832	0.02	0.10	-0.62	16.45
Ba137	131	2	124.84	130.46	130.59	142.23	127.46	6.65	131.12	0.09	5.07
La139	15.2	0.2	14.45	14.71	15.03	16.89	14.72	0.99	15.16	-0.26	6.52
Ce140	37.6	0.2	35.65	36.75	37.71	40.23	35.77	1.88	37.22	-1.01	5.04
Pr141	5.35	0.22	4.87	4.96	5.12	5.6	4.87	0.31	5.08	-4.97	6.02
Nd146	24.5	0.2	23.04	24.16	24.58	26.81	23.52	1.46	24.42	-0.32	5.98
Sm147	6.1	0.03	5.82	5.84	6.1	6.71	5.96	0.37	6.09	-0.23	6.02
Eu153	2.07	0.01	1.945	1.914	2.098	2.18	1.934	0.12	2.01	-2.70	5.86
Gd157	6.16	0.05	5.57	5.56	5.86	6.52	5.64	0.40	5.83	-5.36	6.93
Tb159	0.92	0.04	0.787	0.819	0.842	0.861	0.825	0.03	0.83	-10.13	3.34
Dy163	5.28	0.05	4.95	5.08	5.12	4.96	5.01	0.07	5.02	-4.85	1.48
Ho165	0.98	0.04	0.905	0.899	0.906	1.027	0.874	0.06	0.92	-5.90	6.51
Er166	2.56	0.02	2.24	2.28	2.33	2.55	2.37	0.12	2.35	-8.05	5.10
Tm169	0.34	0.02	0.299	0.31	0.306	0.309	0.323	0.01	0.31	-9.00	2.82
Yb172	2.01	0.02	1.854	1.861	1.897	2.06	2.01	0.09	1.94	-3.66	4.81
Lu175	0.279	0.003	0.244	0.261	0.261	0.288	0.28	0.02	0.27	-4.37	6.52
Hf178	4.32	0.18	3.86	4.07	4.09	4.45	4.02	0.22	4.10	-5.14	5.28
Ta181	1.15	0.1	1.105	1.16	1.152	1.163	1.149	0.02	1.15	-0.37	2.05
Pb208	1.7	0.2	1.696	1.832	1.728	1.84	1.696	0.07	1.76	3.44	4.10
Th232	1.22	0.05	1.134	1.164	1.182	1.383	1.19	0.10	1.21	-0.77	8.16
U238	0.403	0.003	0.445	0.439	0.428	0.552	0.41	0.06	0.45	12.85	12.30

Accepted values for BHVO-2G			BHVO_1	BHVO_2	BHVO_3			Percentage difference between accepted BHVO-2G values and BHVO-2G lab values	
	Value	Uncertainty	Standard1	Standard1	Standard1	STDEVA	Average	(%)	RSD (%)
Sc45	33	2	31.6	31.19	31.94	0.38	31.58	-4.31	1.19
V51	308	19	321.88	320.78	326.66	3.13	323.11	4.90	0.97
Cr53	293	12	265.42	264.08	269.13	2.62	266.21	-9.14	0.98
Co59	44	2	43.95	42.91	43.96	0.60	43.61	-0.89	1.38
Ni60	116	7	116.51	117.64	117.5	0.62	117.22	1.05	0.53
Cu63	127	11	114.15	110.81	114.53	2.05	113.16	-10.90	1.81
Zn66	102	6	117.72	125.89	120.91	4.12	121.51	19.12	3.39
Ga69	22	3	27.07	25.87	24	1.55	25.65	16.58	6.03
Rb85	9.2	0.04	8.68	8.33	8.8	0.24	8.60	-6.49	2.84
Sr88	396	1	377.42	372.59	386.83	7.24	378.95	-4.31	1.91
Y89	26	2	22.13	21.83	22.78	0.49	22.25	-14.44	2.18
Zr90	170	7	154.71	154.18	158.54	2.38	155.81	-8.35	1.53
Nb93	18.3	0.8	17.5	17.47	18.26	0.45	17.74	-3.04	2.52
Mo95	3.8	0.2	4.09	4.08	3.94	0.08	4.04	6.23	2.08
Cd111	0.1	0.02	0.096	0.187	0.199	0.06	0.16	60.67	35.06
Sn118	2.6	0.6	1.667	1.631	1.634	0.02	1.64	-36.77	1.22
Cs133	0.1	0.02	0.0923	0.0967	0.0907	0.00	0.09	-6.77	3.33
Ba137	131	2	127.71	125.89	132.11	3.20	128.57	-1.85	2.49
La139	15.2	0.2	14.58	14.52	14.79	0.14	14.63	-3.75	0.97
Ce140	37.6	0.2	36.17	36.14	36.98	0.48	36.43	-3.11	1.31
Pr141	5.35	0.22	4.83	4.81	4.9	0.05	4.85	-9.41	0.98
Nd146	24.5	0.2	23.17	22.88	23.7	0.42	23.25	-5.10	1.79
Sm147	6.1	0.03	5.86	5.82	5.96	0.07	5.88	-3.61	1.23
Eu153	2.07	0.01	1.878	1.892	1.986	0.06	1.92	-7.31	3.06
Gd157	6.16	0.05	5.31	5.61	5.83	0.26	5.58	-9.36	4.68
Tb159	0.92	0.04	0.802	0.799	0.842	0.02	0.81	-11.49	2.95
Dy163	5.28	0.05	4.9	4.83	5.02	0.10	4.92	-6.88	1.95
Ho165	0.98	0.04	0.887	0.86	0.904	0.02	0.88	-9.83	2.51
Er166	2.56	0.02	2.289	2.223	2.376	0.08	2.30	-10.31	3.34
Tm169	0.34	0.02	0.293	0.282	0.323	0.02	0.30	-11.96	7.09
Yb172	2.01	0.02	1.786	1.809	1.897	0.06	1.83	-8.92	3.20
Lu175	0.279	0.003	0.252	0.2379	0.242	0.01	0.24	-12.56	2.97
Hf178	4.32	0.18	3.89	3.84	3.95	0.06	3.89	-9.88	1.41
Ta181	1.15	0.1	1.101	1.116	1.116	0.01	1.11	-3.39	0.78
Pb208	1.7	0.2	1.62	1.612	1.79	0.10	1.67	-1.53	6.01
Th232	1.22	0.05	1.155	1.208	1.183	0.03	1.18	-3.11	2.24
U238	0.403	0.003	0.389	0.406	0.433	0.02	0.41	1.57	5.42

Table I.2 The appearance of hand samples that includes the colour of hand sample, visible phenocrysts, visible quartz veins together with vein thickness and if sample originates as a clast from a conglomerate.

Sample Name	Colour of hand sample after being opened by hammer	Visible phenocrysts	Presence of visible quartz veins (thickness of veins in mm)	Clast from a conglomerate
DHG 02-10	dark grey	yes	no	no
DHG 02-12	dark blue	no	no	no
DHG 01-12	brownish grey	yes	no	no
DHG 06-13	grey	yes	no	no
SHG 02-14	dark blue	yes	no	no
DHG 04-14	grey	yes	no	no
CHG 03-07	grey	yes	yes (< 0.5 mm)	yes
DHG 05-05	light grey	yes	no	no
CHG 05-03	greenish grey	yes	no	yes
DHG 05-06	grey	yes	no	no
SHG 05-04	brown	yes	yes (< 0.5 mm)	no
SHG 03-16	grey	yes	no	no
DHG 02-16	dark grey	yes	no	no
CHG 03-02	brownish grey	yes	yes (< 0.5 mm)	yes
SHG 03-02	dark grey	yes	yes (abundant > 3 mm)	no
SHG 03-02B	dark grey	yes	no	no
DHG 05-04	grey	yes	no	no
DHG 05-04A	brown	yes	no	no
DHG 01-16	dark grey	yes	yes (< 0.5 mm)	no
DHG 03-16	dark grey	yes	no	no
DHG 03-01A	light grey	yes	no	no
DHG 03-02	dark grey	yes	yes (< 1 mm)	no
SHG 03-01	grey	yes	yes (< 0.5 mm)	no
DHG 01-09	grey	yes	no	no
DHG 04-18 A	grey	no	no	yes
DHG 05-18 a	brown	no	no	yes
DHG 03-18	grey	no	no	yes
DHG 05-18 b	grey	no	no	yes
DHG 01-18	grey	no	no	yes
DHG 02-18 D	brownish grey	no	no	yes
SHG 05-03 *	grey	yes	no	no
DHG 03-04	grey	yes	yes (< 0.5 mm)	no

Table I.3 Petrographic details of samples analysed. These analyses include the sample name, description of groundmass, modal abundance, minerals present and general comments.

Sample Name	Groundmass	Modal abundance	Minerals	General comments
SHG 03-02	Microcrystalline, comprised mostly of microquartz, muscovite and minor clays.	K-feldspar phenocrysts = 35%. Quartz phenocrysts = 3%. Groundmass = 52%.	Phenocrysts: Euhedral rectangular ghost crystals (~0.7 - 2 mm) that are completely replaced by muscovite. These minerals were most likely K-feldspar. Euhedral to subhedral quartz crystals (0.05 - 1 mm) were also observed in thin section.	30% of sample was extensively replaced by chert with ghost K-feldspar still visible.This replacement was not included in modal abundance calculations.
DHG 05-18a	Dominantly cryptocrystalline with some microcrystalline minerals visible that comprise mostly of microquartz and muscovite.	K-feldspar phenocrysts = 32%. Quartz phenocrysts = 1%. Groundmass = 57%.	Phenocrysts: Euhedral rectangular K-feldspar crystals (~0.2 - 1.5 mm) that were replaced by muscovite with intact K-feldspar domains visible. Subhedral to anhedral quartz crystals (0.05 - 0.2 mm) were also observed in thin section.	This felsic porphyritic igneous sample was collected as a clast from an oligomict conglomerate.
CHG 05-03	Microcrystalline, comprised mostly of muscovite and microquartz.	K-feldspar phenocrysts = 35%. Quartz phenocrysts = 10%. Groundmass = 55%.	Phenocrysts: Euhedral rectangular ghost crystals (~0.5 - 2 mm) that are completely replaced by muscovite. These minerals were most likely K-feldspar. Subhedral quartz crystals (0.1 - 1 mm) were also observed in thin section.	This felsic porphyritic igneous sample was collected as a clast from a monomict orthoconglomerate.
CHG 03-02	Microcrystalline, comprised mostly of microquartz, muscovite and minor clays.	K-feldspar phenocrysts = 61%. Quartz phenocrysts = 4%. Groundmass = 35%.	Phenocrysts: Euhedral rectangular K-feldspar crystals (~0.8 - 2 mm) that were replaced by muscovite with intact K-feldspar domains visible. Euhedral to subhedral quartz crystals (0.2 - 0.7 mm) were also observed in thin section.	This felsic porphyritic igneous sample was collected as a clast from a monomict orthoconglomerate.

DHG 04-14	Microcrystalline, comprised mostly of albite, microquartz, muscovite and minor clays.	Albite phenocrysts = 59%. Quartz phenocrysts = 3%. Groundmass = 38%.	Phenocrysts: Euhedral rectangular albite crystals (~0.8 - 3 mm) showing distinct lamellar twinning in crystals. Euhedral to subhedral quartz crystals (0.2 - 0.7 mm) were also observed in thin section.	Felsic porphyritic igneous texture.
DHG 03-01A	Microcrystalline, comprised mostly of muscovite.	K-feldspar phenocrysts = 30%. Quartz phenocrysts = 2%. Groundmass = 68%.	Phenocrysts: Euhedral rectangular ghost crystals (~0.5 - 2 mm) that are completely replaced by muscovite. These minerals were most likely K-feldspar. Subhedral quartz crystals (0.1 - 0.6 mm) were also observed in thin section.	Sample is generally altered intensely, but remnant porphyritic igneous texture is still visible.
DHG 03-02	Microcrystalline, comprised mostly of muscovite and microquartz.	K-feldspar phenocrysts = 40%. Quartz phenocrysts = 5%. Groundmass = 55%.	Phenocrysts: Euhedral to subhedral ghost crystals (~0.7 - 1.5 mm) that are completely replaced by muscovite. These minerals were most likely K-feldspar. Subhedral to anhedral quartz crystals (0.1 - 0.8 mm) were also observed in thin section.	Porphyritic igneous texture.
DHG 05-06	Microcrystalline, comprised mostly of microquartz, muscovite and minor clays.	K-feldspar phenocrysts = 43%. Quartz phenocrysts = 1%. Groundmass = 56%.	Phenocrysts: Euhedral rectangular ghost crystals (~0.7 - 1.4 mm) that are completely replaced by muscovite. These minerals were most likely K-feldspar. Subhedral to anhedral quartz crystals (0.1 - 1 mm) were also observed in thin section.	Sample is generally altered intensely, but remnant porphyritic igneous texture is still visible.

SHG 05-04	Microcrystalline, comprised mostly of microquartz, muscovite and minor clays.	K-feldspar phenocrysts = 28%. Quartz phenocrysts = 7%. Groundmass = 65%.	Phenocrysts: Euhedral rectangular ghost crystals (~0.7 - 1.8 mm) that are completely replaced by muscovite. These minerals were most likely K-feldspar. Subhedral to anhedral quartz crystals (0.1 - 1 mm) were also observed in thin section.	Sample is generally altered intensely, but remnant porphyritic igneous texture is still visible.
SHG 03-02B	Dominantly cryptocrystalline with some microcrystalline minerals visible that comprise mostly of microquartz and muscovite.	K-feldspar phenocrysts = 30%. Quartz phenocrysts = 6%. Groundmass = 64%.	Phenocrysts: Euhedral rectangular K-feldspar crystals (~0.5 - 1.6 mm) that were replaced by muscovite with intact K-feldspar domains visible. Euhedral to subhedral quartz crystals (0.1 - 0.6 mm) were also observed in thin section.	Porphyritic igneous texture.

Figure I.1 Graphical representation of the reflections with peaks indexed, list of d-spacings with relative intensity peaks attributed to a particular mineral.

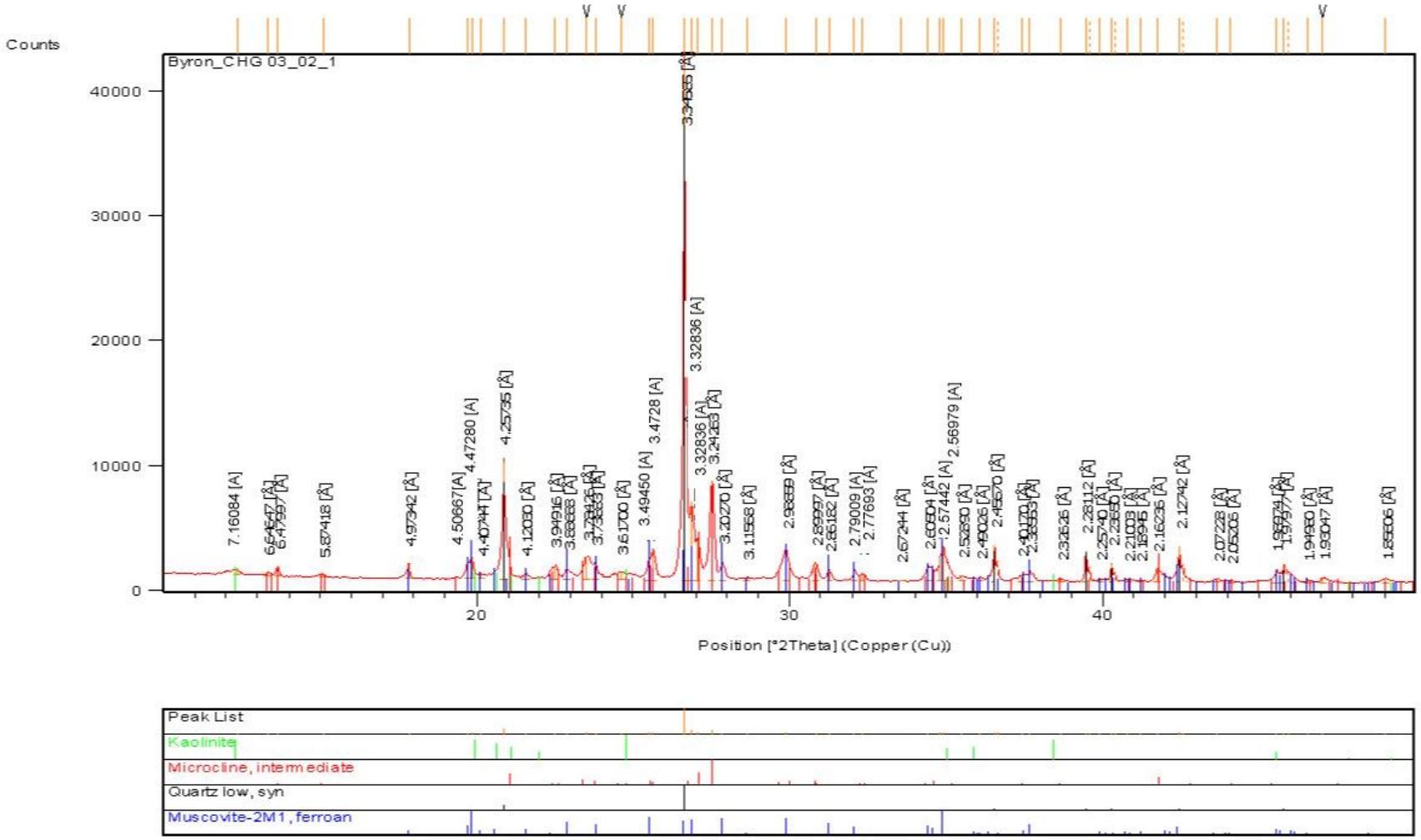

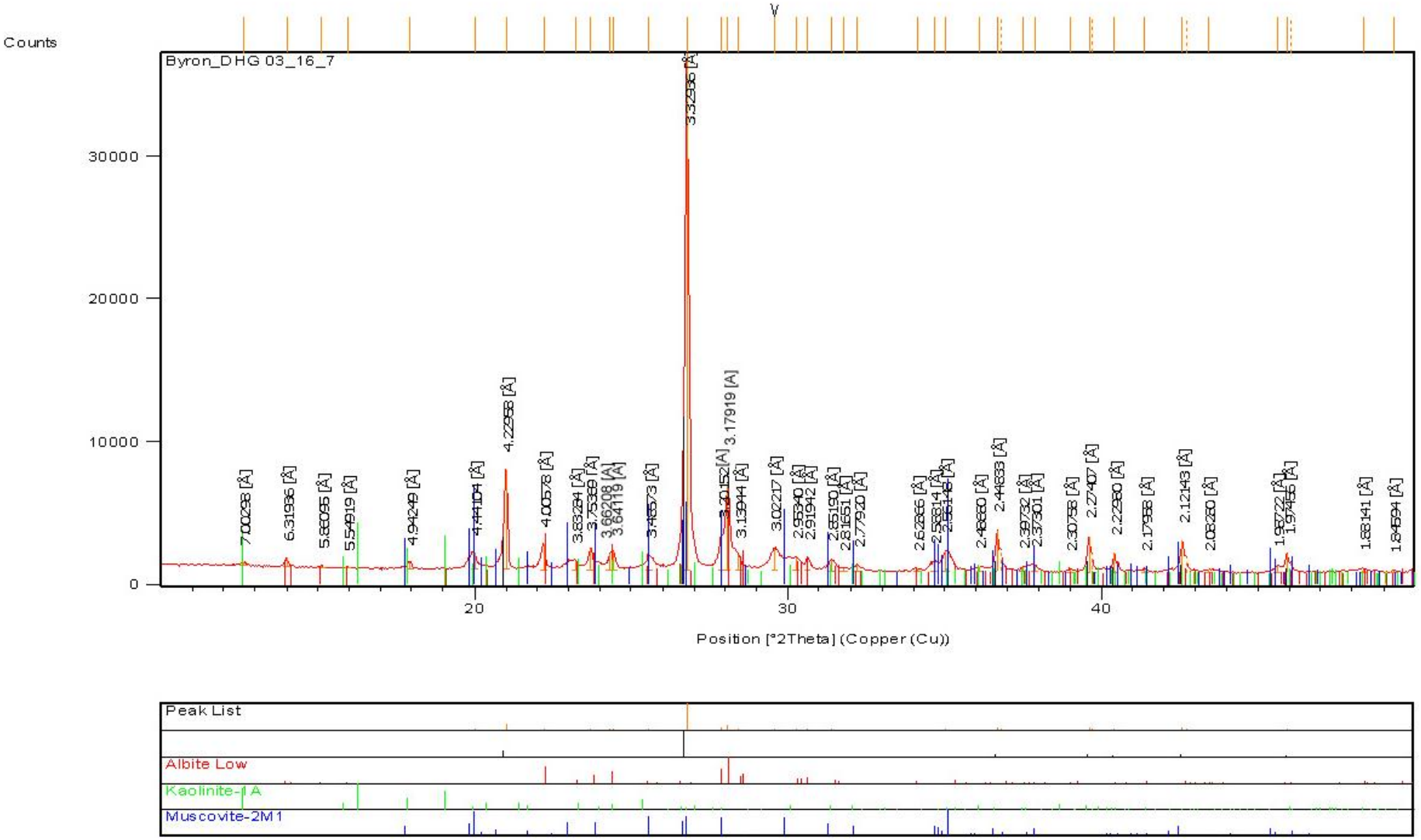
Counts
Byron_DHG 03_16_7
30000
20000
10000
0
20
30
40
Position [°2Theta] (Copper (Cu))
Peak List
Albite Low
Kaolinite-1A
Muscovite-2M1

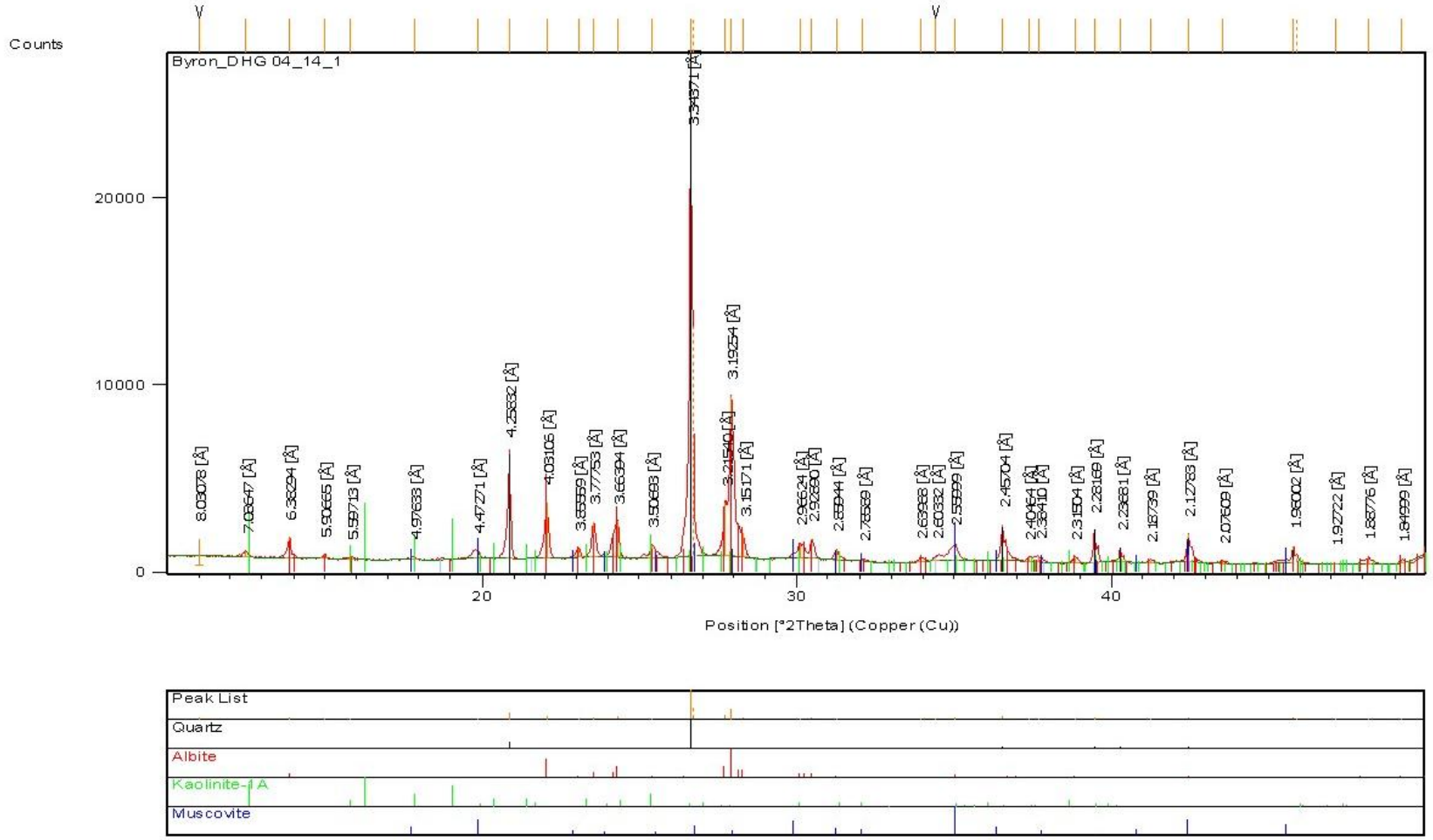
Counts
Byron_DHG 04_14_1
20000
10000
0
20
30
40
Position [°2Theta] (Copper (Cu))
Peak List
Quartz
Albite
Kaolinite-1A
Muscovite

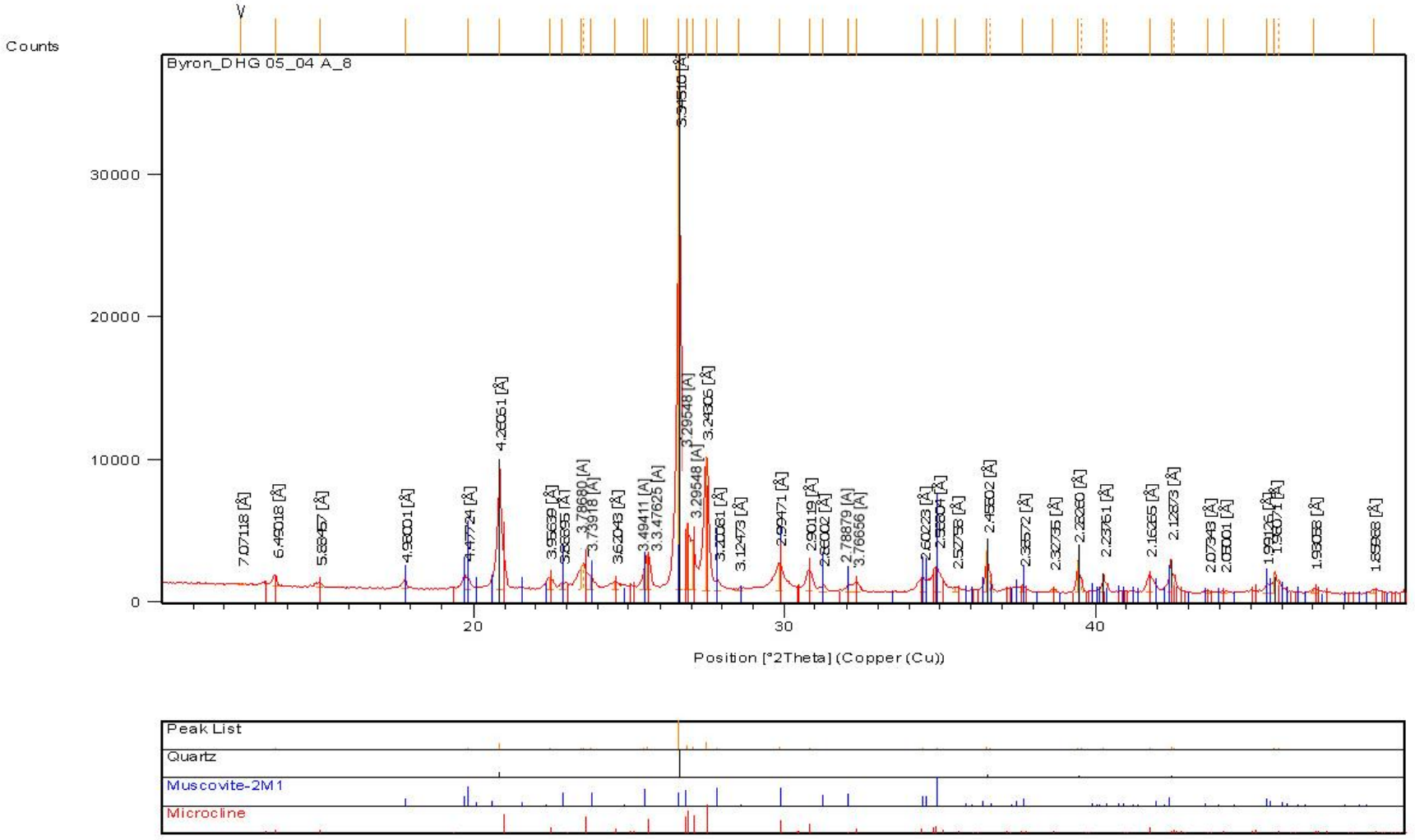
Counts
Byron_DHG 05_04 A_8
30000
20000
10000
0
20
30
40
Position [°2Theta] (Copper (Cu))
Peak List
Quartz
Muscovite-2M1
Microcline

Page: 1 of 1

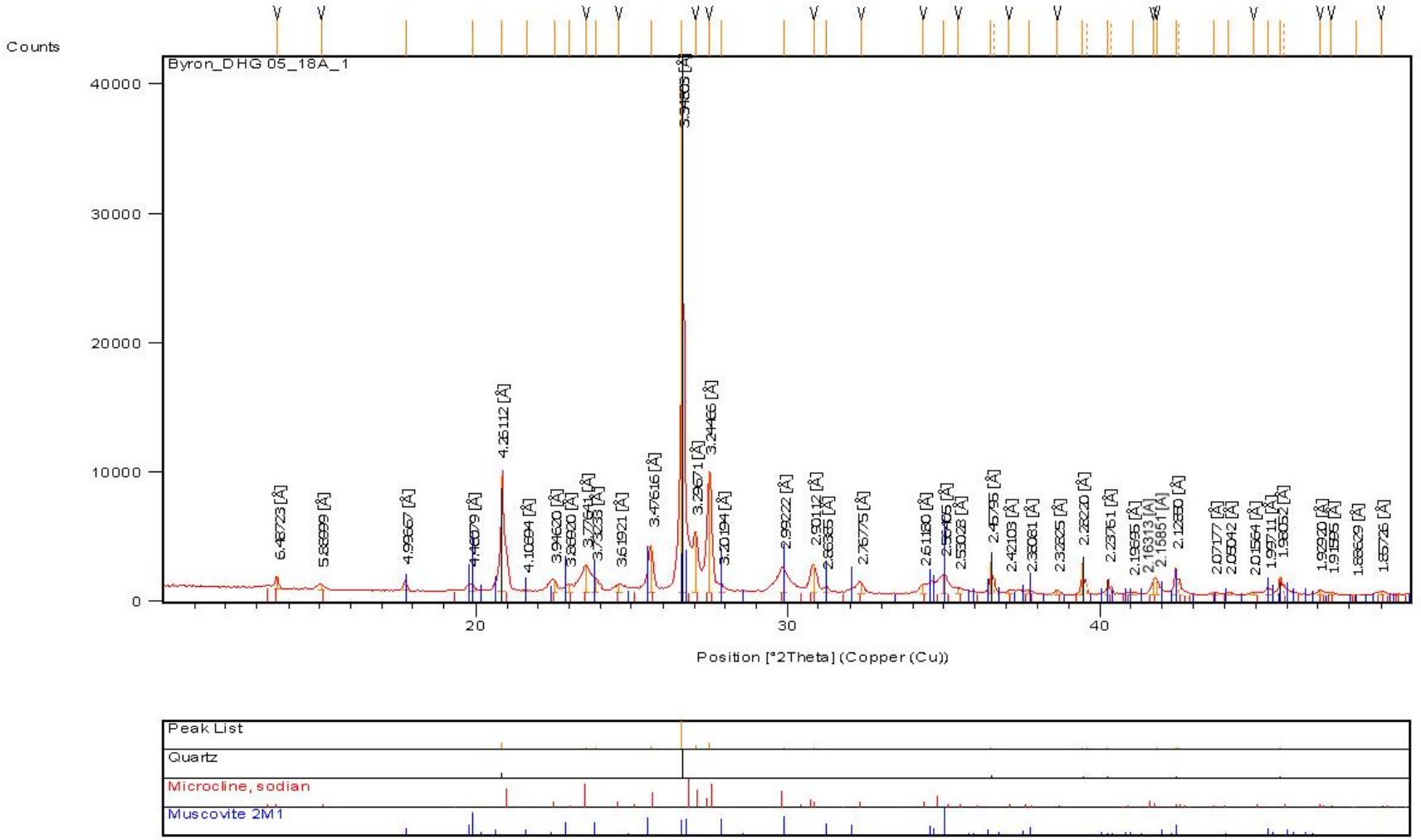
Counts
Byron_DHG 05_18A_1
40000
30000
20000
10000
0
20
30
40
Position [°2Theta] (Copper (Cu))
Peak List
Quartz
Microcline, sodian
Muscovite 2M1

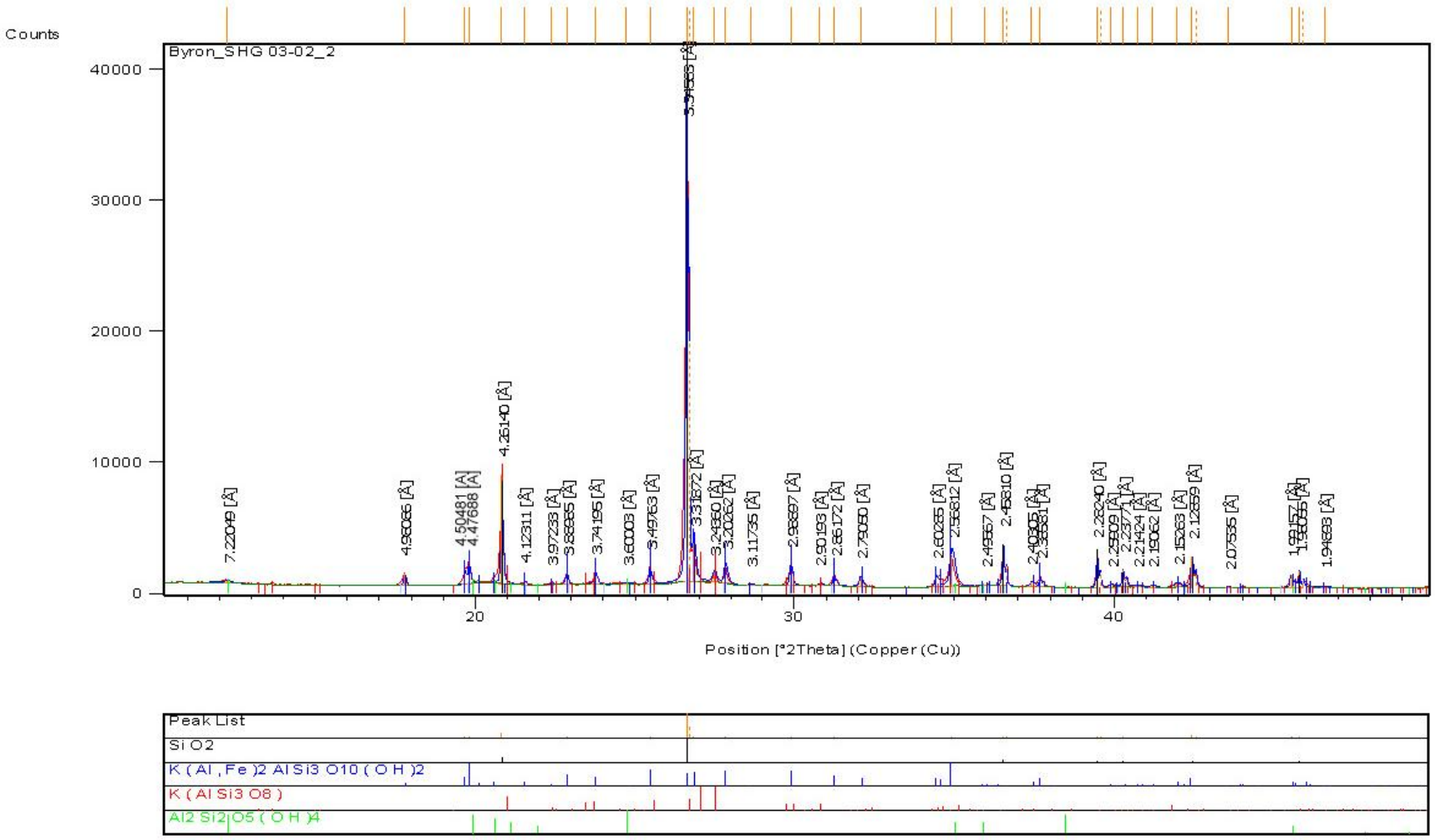
Counts
Byron_SHG 03-02_2
40000
30000
20000
10000
0
20
30
40
Position [°2Theta] (Copper (Cu))
Peak List
Si O2
K (Al , Fe)2 Al Si3 O10 (O H)2
K (Al Si3 O8)
Al2 Si2 O5 (O H)4

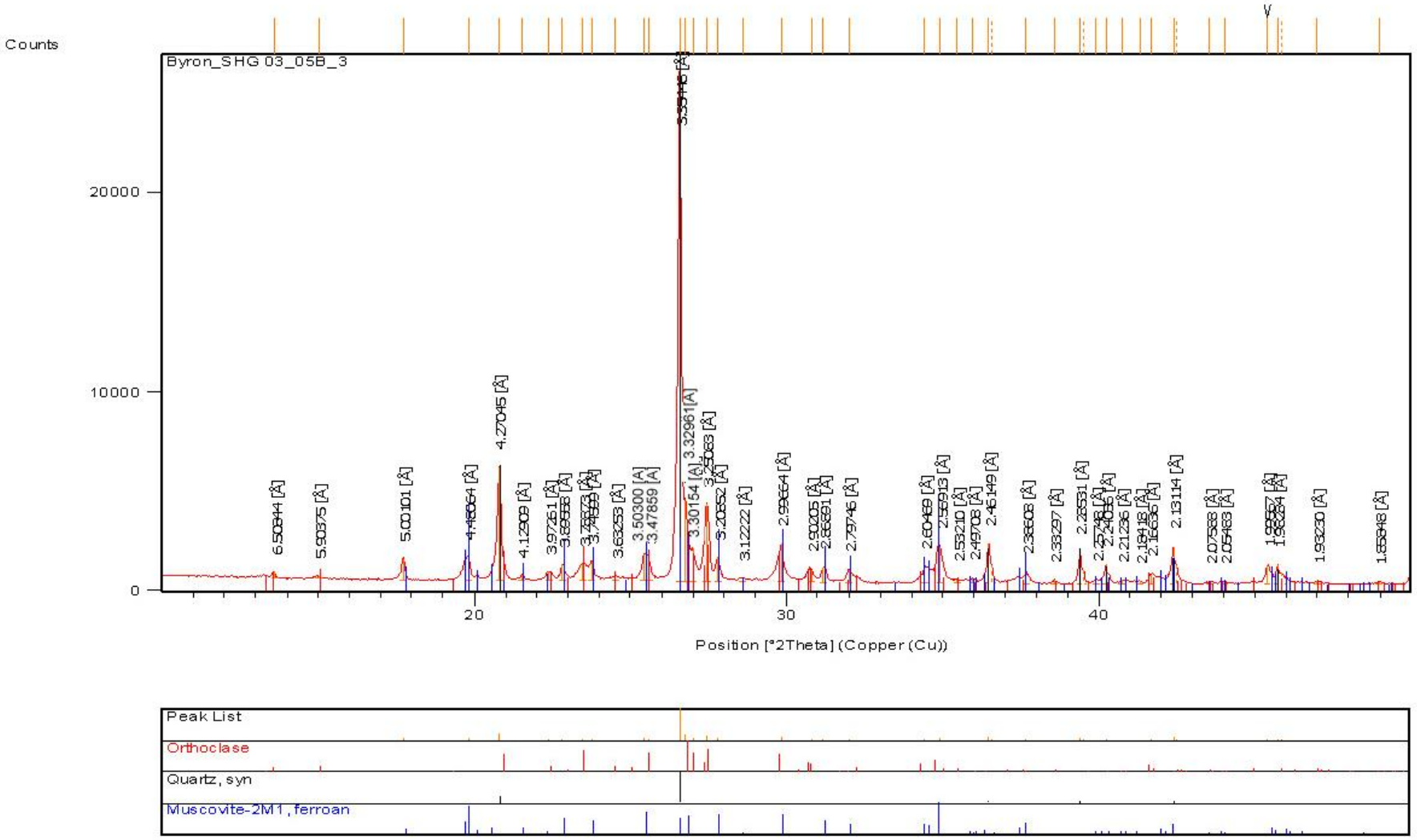
Counts
Byron_SHG 03_05B_3
20000
10000
0
20
30
40
Position [°2Theta] (Copper (Cu))
Peak List
Orthoclase
Quartz, syn
Muscovite-2M1, ferroan

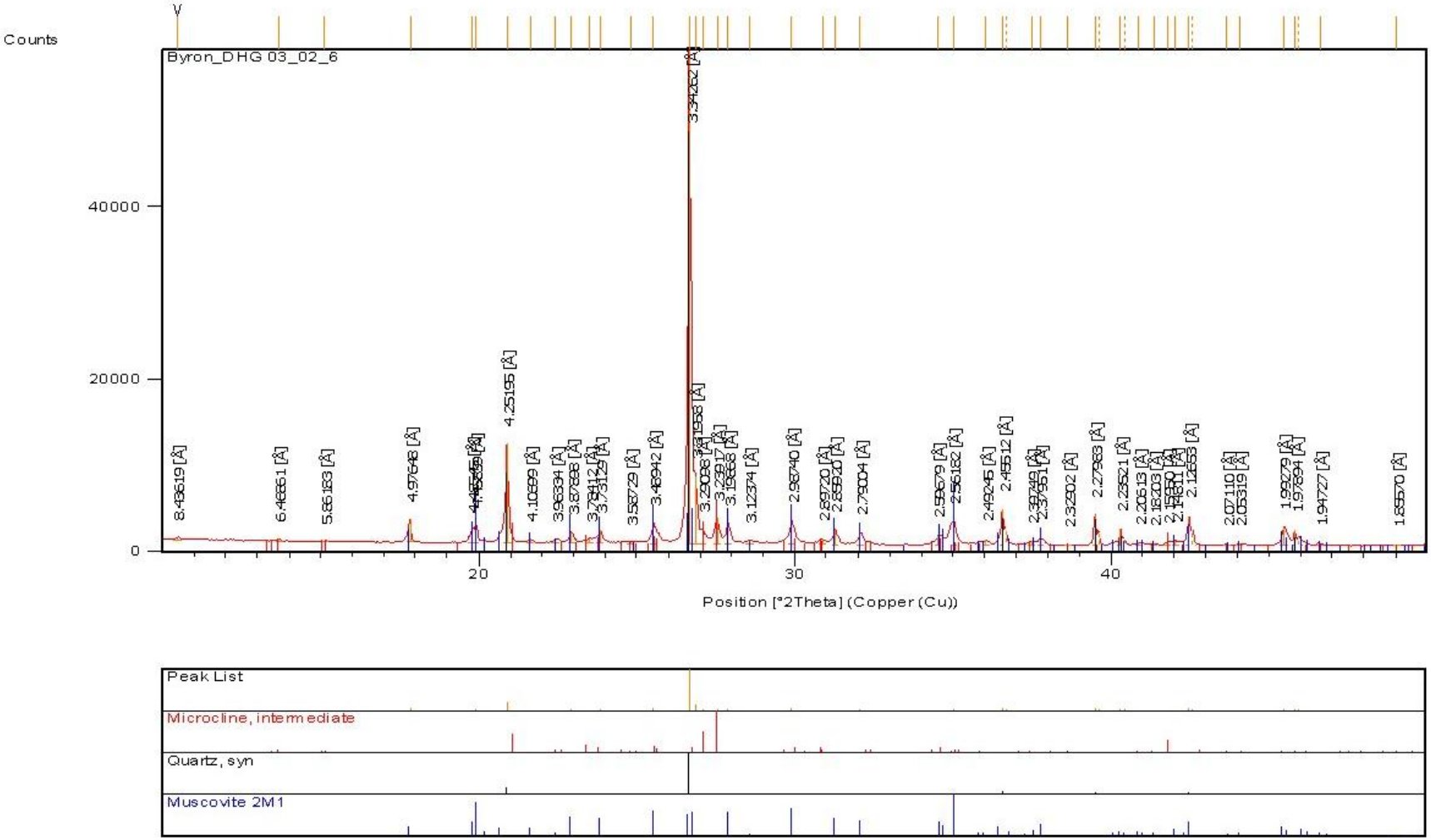
Counts
Byron_DHG 03_02_6
40000
20000
0
20
30
40
Position [°2Theta] (Copper (Cu))
8.43619 [Å]
6.46661 [Å]
5.86183 [Å]
4.97648 [Å]
4.25195 [Å]
4.10899 [Å]
3.96334 [Å]
3.87838 [Å]
3.79112 [Å]
3.73129 [Å]
3.58729 [Å]
3.48942 [Å]
3.34262 [Å]
3.29038 [Å]
3.23917 [Å]
3.19668 [Å]
3.12374 [Å]
2.98740 [Å]
2.89720 [Å]
2.89310 [Å]
2.79004 [Å]
2.59679 [Å]
2.56182 [Å]
2.49245 [Å]
2.45512 [Å]
2.32302 [Å]
2.27963 [Å]
2.23521 [Å]
2.20613 [Å]
2.12653 [Å]
2.07110 [Å]
2.05319 [Å]
1.99279 [Å]
1.97894 [Å]
1.94727 [Å]
1.83570 [Å]
Peak List
Microcline, intermediate
Quartz, syn
Muscovite 2M1

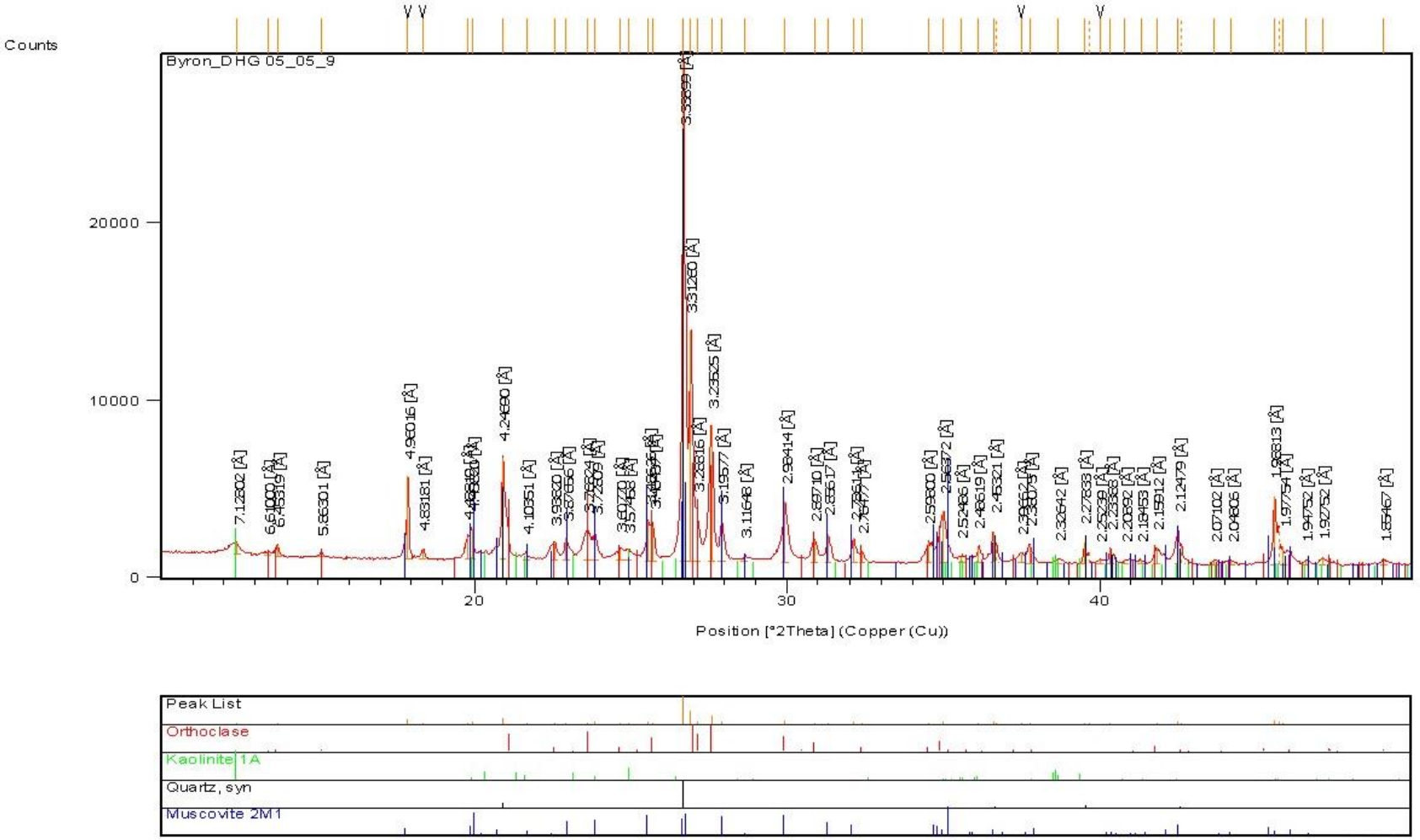
Counts
Byron_DHG 05_05_9
20000
10000
0
20
30
40
Position [°2Theta] (Copper (Cu))
Peak List
Orthoclase
Kaolinite 1A
Quartz, syn
Muscovite 2M1

Table I.4 A. Major- and trace element chemistry of each sample. The raw data from lab together with the unit, LLD (lowest limit of detection), LLD*3 and data in thesis. BDL = below detection limit that is classified in this thesis as LLD*3.

Sample name	DHG 03-04	Unit	LLD	LLD * 3		DHG 03-01A	Unit	LLD	LLD * 3	
Lab	Acme				Thesis data	Acme				Thesis data
SiO2	75.02	%	0.01	0.03	75.02	73.85	%	0.01	0.03	73.85
TiO2	0.20	%	0.01	0.03	0.2	0.22	%	0.01	0.03	0.22
Al2O3	14.09	%	0.01	0.03	14.09	15.24	%	0.01	0.03	15.24
FeOt	1.09	%	0.04	0.12	1.09	0.63	%	0.04	0.12	0.63
MnO	<0.01	%	0.01	0.03	BDL	0.01	%	0.01	0.03	BDL
MgO	0.54	%	0.01	0.03	0.54	1.4	%	0.01	0.03	1.4
CaO	<0.01	%	0.01	0.03	BDL	0.02	%	0.01	0.03	BDL
Na2O	0.04	%	0.01	0.03	0.04	0.04	%	0.01	0.03	0.04
K2O	6.44	%	0.01	0.03	6.44	5.66	%	0.01	0.03	5.66
P2O5	<0.01	%	0.01	0.03	BDL	0.03	%	0.01	0.03	BDL
Sc	3	PPM	1	3	BDL	2	PPM	1	3	BDL
V	15	PPM	8	24	BDL	28	PPM	8	24	28
Cr					BDL				0	
Ni	20	PPM	20	60	BDL	24	PPM	20	60	BDL
Cu	1.5	PPM	0.1	0.3	1.5	0.9	PPM	0.1	0.3	0.9
Zn	2	PPM	1.00	3	BDL	1	PPM	1.00	3	BDL
Ga	15.5	PPM	0.5	1.5	15.5	18.5	PPM	0.5	1.5	18.5
Rb	120.8	PPM	0.1	0.3	120.8	122.4	PPM	0.1	0.3	122.4
Sr	6.6	PPM	0.5	1.5	6.6	9.6	PPM	0.5	1.5	9.6
Y	4.2	PPM	0.1	0.3	4.2	7.9	PPM	0.1	0.3	7.9
Zr	108.4	PPM	0.1	0.3	108.4	114.6	PPM	0.1	0.3	114.6
Nb	4.4	PPM	0.1	0.3	4.4	4.9	PPM	0.1	0.3	4.9
Mo	0.3	PPM	0.10	0.3	0.3	0.1	PPM	0.10	0.3	BDL
Sn	2	PPM	1	3	BDL	2	PPM	1	3	BDL
Cs	1.4	PPM	0.1	0.3	1.4	2.4	PPM	0.1	0.3	2.4
Ba	183	PPM	1	3	183	302	PPM	1	3	302
La	14.6	PPM	0.1	0.3	14.6	22.9	PPM	0.1	0.3	22.9
Ce	28.9	PPM	0.1	0.3	28.9	34.3	PPM	0.1	0.3	34.3
Pr	2.85	PPM	0.02	0.06	2.85	4.7	PPM	0.02	0.06	4.7
Nd	9.8	PPM	0.3	0.9	9.8	17	PPM	0.3	0.9	17
Sm	1.78	PPM	0.05	0.15	1.78	3.03	PPM	0.05	0.15	3.03
Eu	0.49	PPM	0.02	0.06	0.49	0.82	PPM	0.02	0.06	0.82
Gd	1.25	PPM	0.05	0.15	1.25	2.67	PPM	0.05	0.15	2.67
Tb	0.18	PPM	0.01	0.03	0.18	0.35	PPM	0.01	0.03	0.35
Dy	0.72	PPM	0.05	0.15	0.72	1.56	PPM	0.05	0.15	1.56
Ho	0.15	PPM	0.02	0.06	0.15	0.27	PPM	0.02	0.06	0.27
Er	0.4	PPM	0.03	0.09	0.4	0.71	PPM	0.03	0.09	0.71
Tm	0.07	PPM	0.01	0.03	0.07	0.12	PPM	0.01	0.03	0.12
Yb	0.39	PPM	0.05	0.15	0.39	0.62	PPM	0.05	0.15	0.62
Lu	0.06	PPM	0.01	0.03	0.06	0.11	PPM	0.01	0.03	0.11
Hf	2.9	PPM	0.1	0.3	2.9	3.2	PPM	0.1	0.3	3.2
Ta	0.4	PPM	0.1	0.3	0.4	0.5	PPM	0.1	0.3	0.5

Sample name	DHG 03-02	Unit	LLD	LLD * 3		DHG 05-04A	Unit	LLD	LLD * 3	
Lab	Acme				Thesis data	Acme				Thesis data
SiO2	75.77	%	0.01	0.03	75.77	76.49	%	0.01	0.03	76.49
TiO2	0.2	%	0.01	0.03	0.2	0.19	%	0.01	0.03	0.19
Al2O3	13.94	%	0.01	0.03	13.94	12.93	%	0.01	0.03	12.93
FeOt	0.97	%	0.04	0.12	0.97	0.81	%	0.04	0.12	0.81
MnO	0.02	%	0.01	0.03	BDL	0.01	%	0.01	0.03	BDL
MgO	0.53	%	0.01	0.03	0.53	0.89	%	0.01	0.03	0.89
CaO	0.06	%	0.01	0.03	0.06	0.02	%	0.01	0.03	BDL
Na2O	0.04	%	0.01	0.03	0.04	0.04	%	0.01	0.03	0.04
K2O	6.14	%	0.01	0.03	6.14	6.15	%	0.01	0.03	6.15
P2O5	0.06	%	0.01	0.03	0.06	0.03	%	0.01	0.03	BDL
Sc	2	PPM	1	0.03	BDL	3	PPM	1	3	BDL
V	21	PPM	8	0.03	BDL	20	PPM	8	24	BDL
Cr									0	BDL
Ni	20	PPM	20	60	BDL	21	PPM	20	60	BDL
Cu	3.4	PPM	0.1	0.3	3.4	0.5	PPM	0.1	0.3	0.5
Zn	2	PPM	1.00	3	BDL	2	PPM	1	3	BDL
Ga	16.3	PPM	0.5	1.5	16.3	16.8	PPM	0.5	1.5	16.8
Rb	114.6	PPM	0.1	0.3	114.6	139.6	PPM	0.1	0.3	139.6
Sr	8.4	PPM	0.5	1.5	8.4	16.7	PPM	0.5	1.5	16.7
Y	4.6	PPM	0.1	0.3	4.6	6.1	PPM	0.1	0.3	6.1
Zr	103.2	PPM	0.1	0.3	103.2	102.6	PPM	0.1	0.3	102.6
Nb	4.5	PPM	0.1	0.3	4.5	4.3	PPM	0.1	0.3	4.3
Mo	0.1	PPM	0.10	0.3	BDL	0.1	PPM	0.1	0.3	BDL
Sn	1	PPM	1	3	BDL	1	PPM	1	3	BDL
Cs	1.4	PPM	0.1	0.3	1.4	2	PPM	0.1	0.3	2
Ba	395	PPM	1	3	395	319	PPM	1	3	319
La	13.1	PPM	0.1	0.3	13.1	12.8	PPM	0.1	0.3	12.8
Ce	25.3	PPM	0.1	0.3	25.3	23.5	PPM	0.1	0.3	23.5
Pr	2.77	PPM	0.02	0.06	2.77	2.5	PPM	0.02	0.06	2.5
Nd	10.1	PPM	0.3	0.9	10.1	8.8	PPM	0.3	0.9	8.8
Sm	1.8	PPM	0.05	0.15	1.8	1.49	PPM	0.05	0.15	1.49
Eu	0.5	PPM	0.02	0.06	0.5	0.46	PPM	0.02	0.06	0.46
Gd	1.31	PPM	0.05	0.15	1.31	1.23	PPM	0.05	0.15	1.23
Tb	0.17	PPM	0.01	0.03	0.17	0.17	PPM	0.01	0.03	0.17
Dy	0.79	PPM	0.05	0.15	0.79	0.89	PPM	0.05	0.15	0.89
Ho	0.14	PPM	0.02	0.06	0.14	0.18	PPM	0.02	0.06	0.18
Er	0.4	PPM	0.03	0.09	0.4	0.53	PPM	0.03	0.09	0.53
Tm	0.06	PPM	0.01	0.03	0.06	0.08	PPM	0.01	0.03	0.08
Yb	0.39	PPM	0.05	0.15	0.39	0.51	PPM	0.05	0.15	0.51
Lu	0.06	PPM	0.01	0.03	0.06	0.07	PPM	0.01	0.03	0.07
Hf	2.9	PPM	0.1	0.3	2.9	3	PPM	0.1	0.3	3
Ta	0.5	PPM	0.1	0.3	0.5	0.4	PPM	0.1	0.3	0.4

Sample name	DHG 05-04	Unit	LLD	LLD * 3		DHG 05-06	Unit	LLD	LLD * 3	
Lab	Acme				Thesis data	Acme				Thesis data
SiO2	74.95	%	0.01	0.03	74.95	70.43	%	0.01	0.03	70.43
TiO2	0.19	%	0.01	0.03	0.19	0.23	%	0.01	0.03	0.23
Al2O3	12.99	%	0.01	0.03	12.99	15.87	%	0.01	0.03	15.87
FeOt	0.94	%	0.04	0.12	0.94	1.51	%	0.04	0.12	1.51
MnO	0.01	%	0.01	0.03	BDL	0.02	%	0.01	0.03	BDL
MgO	0.57	%	0.01	0.03	0.57	0.71	%	0.01	0.03	0.71
CaO	0.05	%	0.01	0.03	0.05	0.03	%	0.01	0.03	BDL
Na2O	0.07	%	0.01	0.03	0.07	0.27	%	0.01	0.03	0.27
K2O	8.57	%	0.01	0.03	8.57	8.58	%	0.01	0.03	8.58
P2O5	0.06	%	0.01	0.03	0.06	0.05	%	0.01	0.03	0.05
Sc	3	PPM	1	3	BDL	3	PPM	1	3	BDL
V	17	PPM	8	24	BDL	18	PPM	8	24	BDL
Cr				0	BDL				0	BDL
Ni	20	PPM	20	60	BDL	20	PPM	20	60	BDL
Cu	2	PPM	0.1	0.3	2	1.7	PPM	0.1	0.3	1.7
Zn	5	PPM	1	3	5	4	PPM	1	3	4
Ga	14.7	PPM	0.5	1.5	14.7	19.4	PPM	0.5	1.5	19.4
Rb	136.2	PPM	0.1	0.3	136.2	160.5	PPM	0.1	0.3	160.5
Sr	10.1	PPM	0.5	1.5	10.1	23.7	PPM	0.5	1.5	23.7
Y	4.9	PPM	0.1	0.3	4.9	6.2	PPM	0.1	0.3	6.2
Zr	96.5	PPM	0.1	0.3	96.5	129.8	PPM	0.1	0.3	129.8
Nb	4.2	PPM	0.1	0.3	4.2	5.5	PPM	0.1	0.3	5.5
Mo	0.2	PPM	0.1	0.3	0.2	0.1	PPM	0.1	0.3	BDL
Sn	1	PPM	1	3	BDL	1	PPM	1	3	BDL
Cs	2.2	PPM	0.1	0.3	2.2	3	PPM	0.1	0.3	3
Ba	389	PPM	1	3	389	360	PPM	1	3	360
La	12.9	PPM	0.1	0.3	12.9	18.3	PPM	0.1	0.3	18.3
Ce	23.2	PPM	0.1	0.3	23.2	31	PPM	0.1	0.3	31
Pr	2.51	PPM	0.02	0.06	2.51	3.71	PPM	0.02	0.06	3.71
Nd	9.2	PPM	0.3	0.9	9.2	13.3	PPM	0.3	0.9	13.3
Sm	1.55	PPM	0.05	0.15	1.55	2.19	PPM	0.05	0.15	2.19
Eu	0.48	PPM	0.02	0.06	0.48	0.65	PPM	0.02	0.06	0.65
Gd	1.28	PPM	0.05	0.15	1.28	1.82	PPM	0.05	0.15	1.82
Tb	0.17	PPM	0.01	0.03	0.17	0.24	PPM	0.01	0.03	0.24
Dy	0.86	PPM	0.05	0.15	0.86	1.17	PPM	0.05	0.15	1.17
Ho	0.15	PPM	0.02	0.06	0.15	0.19	PPM	0.02	0.06	0.19
Er	0.43	PPM	0.03	0.09	0.43	0.54	PPM	0.03	0.09	0.54
Tm	0.06	PPM	0.01	0.03	0.06	0.08	PPM	0.01	0.03	0.08
Yb	0.43	PPM	0.05	0.15	0.43	0.47	PPM	0.05	0.15	0.47
Lu	0.06	PPM	0.01	0.03	0.06	0.07	PPM	0.01	0.03	0.07
Hf	2.8	PPM	0.1	0.3	2.8	3.6	PPM	0.1	0.3	3.6
Ta	0.4	PPM	0.1	0.3	0.4	0.5	PPM	0.1	0.3	0.5

Sample name	CHG 03-02	Unit	LLD	LLD * 3		CHG 05-03	Unit	LLD	LLD * 3	
Lab	Acme				Thesis data	Acme				Thesis data
SiO2	74.46	%	0.01	0.03	74.46	74.4	%	0.01	0.03	74.4
TiO2	0.2	%	0.01	0.03	0.2	0.21	%	0.01	0.03	0.21
Al2O3	13.62	%	0.01	0.03	13.62	13.66	%	0.01	0.03	13.66
FeOt	1.3	%	0.04	0.12	1.3	0.83	%	0.04	0.12	0.83
MnO	0.01	%	0.01	0.03	BDL	0.01	%	0.01	0.03	BDL
MgO	0.61	%	0.01	0.03	0.61	0.54	%	0.01	0.03	0.54
CaO	0.01	%	0.01	0.03	BDL	0.02	%	0.01	0.03	BDL
Na2O	0.06	%	0.01	0.03	0.06	0.18	%	0.01	0.03	0.18
K2O	6.77	%	0.01	0.03	6.77	7.94	%	0.01	0.03	7.94
P2O5	0.05	%	0.01	0.03	0.05	0.03	%	0.01	0.03	BDL
Sc	3	PPM	1	3	BDL	3	PPM	1	3	BDL
V	15	PPM	8	24	BDL	14	PPM	8	24	BDL
Cr				0	BDL				0	BDL
Ni	5	PPM	20	60	BDL	20	PPM	20	60	BDL
Cu	1	PPM	0.1	0.3	1	0.6	PPM	0.1	0.3	0.6
Zn	2	PPM	1	3	BDL	3	PPM	1	3	3
Ga	15.6	PPM	0.5	1.5	15.6	16.8	PPM	0.5	1.5	16.8
Rb	126.8	PPM	0.1	0.3	126.8	144.6	PPM	0.1	0.3	144.6
Sr	9.1	PPM	0.5	1.5	9.1	22.8	PPM	0.5	1.5	22.8
Y	4.6	PPM	0.1	0.3	4.6	13.5	PPM	0.1	0.3	13.5
Zr	105.6	PPM	0.1	0.3	105.6	116.8	PPM	0.1	0.3	116.8
Nb	4.3	PPM	0.1	0.3	4.3	5	PPM	0.1	0.3	5
Mo	0.1	PPM	0.1	0.3	BDL	0.1	PPM	0.1	0.3	BDL
Sn	3	PPM	1	3	BDL	1	PPM	1	3	BDL
Cs	2.9	PPM	0.1	0.3	2.9	2.4	PPM	0.1	0.3	2.4
Ba	279	PPM	1	3	279	365	PPM	1	3	365
La	12.5	PPM	0.1	0.3	12.5	39.6	PPM	0.1	0.3	39.6
Ce	22.5	PPM	0.1	0.3	22.5	31.8	PPM	0.1	0.3	31.8
Pr	2.5	PPM	0.02	0.06	2.5	7.58	PPM	0.02	0.06	7.58
Nd	8.7	PPM	0.3	0.9	8.7	27.3	PPM	0.3	0.9	27.3
Sm	1.49	PPM	0.05	0.15	1.49	4.18	PPM	0.05	0.15	4.18
Eu	0.48	PPM	0.02	0.06	0.48	1.18	PPM	0.02	0.06	1.18
Gd	1.18	PPM	0.05	0.15	1.18	3.75	PPM	0.05	0.15	3.75
Tb	0.16	PPM	0.01	0.03	0.16	0.5	PPM	0.01	0.03	0.5
Dy	0.82	PPM	0.05	0.15	0.82	2.39	PPM	0.05	0.15	2.39
Ho	0.15	PPM	0.02	0.06	0.15	0.42	PPM	0.02	0.06	0.42
Er	0.44	PPM	0.03	0.09	0.44	1.12	PPM	0.03	0.09	1.12
Tm	0.06	PPM	0.01	0.03	0.06	0.15	PPM	0.01	0.03	0.15
Yb	0.4	PPM	0.05	0.15	0.4	0.86	PPM	0.05	0.15	0.86
Lu	0.06	PPM	0.01	0.03	0.06	0.12	PPM	0.01	0.03	0.12
Hf	3	PPM	0.1	0.3	3	3.5	PPM	0.1	0.3	3.5
Ta	0.5	PPM	0.1	0.3	0.5	0.5	PPM	0.1	0.3	0.5

Sample name	SHG 03-01	Unit	LLD	LLD * 3		SHG 03-02B	Unit	LLD	LLD * 3	
Lab	Acme				Thesis data	Acme				Thesis data
SiO2	71.48	%	0.01	0.03	71.48	73.89	%	0.01	0.03	73.89
TiO2	0.23	%	0.01	0.03	0.23	0.22	%	0.01	0.03	0.22
Al2O3	15.99	%	0.01	0.03	15.99	14.54	%	0.01	0.03	14.54
FeOt	1.26	%	0.04	0.12	1.26	0.71	%	0.04	0.12	0.71
MnO	0.01	%	0.01	0.03	BDL	0.01	%	0.01	0.03	BDL
MgO	0.87	%	0.01	0.03	0.87	0.49	%	0.01	0.03	0.49
CaO	0.01	%	0.01	0.03	BDL	0.02	%	0.01	0.03	BDL
Na2O	0.03	%	0.01	0.03	BDL	0.06	%	0.01	0.03	0.06
K2O	6.56	%	0.01	0.03	6.56	7.73	%	0.01	0.03	7.73
P2O5	0.01	%	0.01	0.03	BDL	0.01	%	0.01	0.03	BDL
Sc	3	PPM	1	3	BDL	3	PPM	1	3	BDL
V	15	PPM	8	24	BDL	16	PPM	8	24	BDL
Cr				0	BDL				0	BDL
Ni	26	PPM	20	60	BDL	20	PPM	20	60	BDL
Cu	4.7	PPM	0.1	0.3	4.7	1.4	PPM	0.1	0.3	1.4
Zn	4	PPM	1	3	4	3	PPM	1	3	BDL
Ga	19.3	PPM	0.5	1.5	19.3	17	PPM	0.5	1.5	17
Rb	129.4	PPM	0.1	0.3	129.4	128.7	PPM	0.1	0.3	128.7
Sr	5.8	PPM	0.5	1.5	5.8	11.7	PPM	0.5	1.5	11.7
Y	4.6	PPM	0.1	0.3	4.6	4.4	PPM	0.1	0.3	4.4
Zr	118.5	PPM	0.1	0.3	118.5	109.3	PPM	0.1	0.3	109.3
Nb	4.6	PPM	0.1	0.3	4.6	4.5	PPM	0.1	0.3	4.5
Mo	0.1	PPM	0.1	0.3	BDL	0.1	PPM	0.1	0.3	BDL
Sn	1	PPM	1	3	BDL	1	PPM	1	3	BDL
Cs	2.1	PPM	0.1	0.3	2.1	1.4	PPM	0.1	0.3	1.4
Ba	204	PPM	1	3	204	497	PPM	1	3	497
La	19	PPM	0.1	0.3	19	13.4	PPM	0.1	0.3	13.4
Ce	30.3	PPM	0.1	0.3	30.3	24.5	PPM	0.1	0.3	24.5
Pr	3.62	PPM	0.02	0.06	3.62	2.56	PPM	0.02	0.06	2.56
Nd	13.5	PPM	0.3	0.9	13.5	9	PPM	0.3	0.9	9
Sm	2.17	PPM	0.05	0.15	2.17	1.41	PPM	0.05	0.15	1.41
Eu	0.63	PPM	0.02	0.06	0.63	0.52	PPM	0.02	0.06	0.52
Gd	1.71	PPM	0.05	0.15	1.71	1.16	PPM	0.05	0.15	1.16
Tb	0.21	PPM	0.01	0.03	0.21	0.15	PPM	0.01	0.03	0.15
Dy	0.98	PPM	0.05	0.15	0.98	0.76	PPM	0.05	0.15	0.76
Ho	0.16	PPM	0.02	0.06	0.16	0.15	PPM	0.02	0.06	0.15
Er	0.42	PPM	0.03	0.09	0.42	0.42	PPM	0.03	0.09	0.42
Tm	0.07	PPM	0.01	0.03	0.07	0.07	PPM	0.01	0.03	0.07
Yb	0.43	PPM	0.05	0.15	0.43	0.38	PPM	0.05	0.15	0.38
Lu	0.06	PPM	0.01	0.03	0.06	0.06	PPM	0.01	0.03	0.06
Hf	3.5	PPM	0.1	0.3	3.5	3.2	PPM	0.1	0.3	3.2
Ta	0.4	PPM	0.1	0.3	0.4	0.4	PPM	0.1	0.3	0.4

Sample name	SHG 05-04	Unit	LLD	LLD * 3		DHG 05-05	Unit	LLD	LLD * 3	
Lab	Acme				Thesis data	Acme				Thesis data
SiO2	69.48	%	0.01	0.03	69.48	70.95	%	0.01	0.03	70.95
TiO2	0.24	%	0.01	0.03	0.24	0.23	%	0.01	0.03	0.23
Al2O3	16.03	%	0.01	0.03	16.03	15.85	%	0.01	0.03	15.85
FeOt	1.84	%	0.04	0.12	1.84	1.24	%	0.04	0.12	1.24
MnO	0.02	%	0.01	0.03	BDL	0.01	%	0.01	0.03	BDL
MgO	1.21	%	0.01	0.03	1.21	0.72	%	0.01	0.03	0.72
CaO	0.03	%	0.01	0.03	BDL	0.01	%	0.01	0.03	BDL
Na2O	0.11	%	0.01	0.03	0.11	0.06	%	0.01	0.03	0.06
K2O	7.01	%	0.01	0.03	7.01	7.5	%	0.01	0.03	7.5
P2O5	0.05	%	0.01	0.03	0.05	0.02	%	0.01	0.03	BDL
Sc	3	PPM	1	3	BDL	3	PPM	1	3	BDL
V	16	PPM	8	24	BDL	16	PPM	8	24	BDL
Cr				0	BDL				0	BDL
Ni	24	PPM	20	60	BDL	34	PPM	20	60	BDL
Cu	1.2	PPM	0.1	0.3	1.2	3.2	PPM	0.1	0.3	3.2
Zn	9	PPM	1	3	9	4	PPM	1	3	4
Ga	17.5	PPM	0.5	1.5	17.5	18.7	PPM	0.5	1.5	18.7
Rb	147.3	PPM	0.1	0.3	147.3	149.1	PPM	0.1	0.3	149.1
Sr	19.6	PPM	0.5	1.5	19.6	9.9	PPM	0.5	1.5	9.9
Y	6.9	PPM	0.1	0.3	6.9	4.9	PPM	0.1	0.3	4.9
Zr	124.7	PPM	0.1	0.3	124.7	134.8	PPM	0.1	0.3	134.8
Nb	5	PPM	0.1	0.3	5	5.4	PPM	0.1	0.3	5.4
Mo	0.1	PPM	0.1	0.3	BDL	0.1	PPM	0.1	0.3	BDL
Sn	1	PPM	1	3	BDL	1	PPM	1	3	BDL
Cs	4	PPM	0.1	0.3	4	2.9	PPM	0.1	0.3	2.9
Ba	371	PPM	1	3	371	243	PPM	1	3	243
La	40.7	PPM	0.1	0.3	40.7	17.3	PPM	0.1	0.3	17.3
Ce	52.1	PPM	0.1	0.3	52.1	26.2	PPM	0.1	0.3	26.2
Pr	8.61	PPM	0.02	0.06	8.61	3.43	PPM	0.02	0.06	3.43
Nd	31.4	PPM	0.3	0.9	31.4	12.6	PPM	0.3	0.9	12.6
Sm	5.34	PPM	0.05	0.15	5.34	2.19	PPM	0.05	0.15	2.19
Eu	1.37	PPM	0.02	0.06	1.37	0.58	PPM	0.02	0.06	0.58
Gd	3.72	PPM	0.05	0.15	3.72	1.86	PPM	0.05	0.15	1.86
Tb	0.45	PPM	0.01	0.03	0.45	0.24	PPM	0.01	0.03	0.24
Dy	1.93	PPM	0.05	0.15	1.93	1.05	PPM	0.05	0.15	1.05
Ho	0.27	PPM	0.02	0.06	0.27	0.18	PPM	0.02	0.06	0.18
Er	0.7	PPM	0.03	0.09	0.7	0.48	PPM	0.03	0.09	0.48
Tm	0.11	PPM	0.01	0.03	0.11	0.08	PPM	0.01	0.03	0.08
Yb	0.69	PPM	0.05	0.15	0.69	0.45	PPM	0.05	0.15	0.45
Lu	0.1	PPM	0.01	0.03	0.1	0.07	PPM	0.01	0.03	0.07
Hf	3.4	PPM	0.1	0.3	3.4	3.5	PPM	0.1	0.3	3.5
Ta	0.5	PPM	0.1	0.3	0.5	0.5	PPM	0.1	0.3	0.5

Sample name	CHG 03-07	LLD	LLD*3		DHG 01-09	LLD	LLD*3	
Lab	Stel2			Thesis data	Stel1			Thesis data
SiO2	75.95	0.03	0.09	75.95	73.27	0.03	0.09	73.27
TiO2	0.21	0.02	0.06	0.21	0.22	0.02	0.06	0.22
Al2O3	14.16	0.06	0.18	14.16	14.60	0.06	0.18	14.6
FeOt	1.04	0.01	0.03	1.04	1.55	0.01	0.03	1.55
MnO	0.01	0.01	0.03	BDL	0.03	0.01	0.03	BDL
MgO	0.55	0.04	0.12	0.55	0.97	0.04	0.12	0.97
CaO	0.05	0.04	0.12	0.05	0.01	0.04	0.12	BDL
Na2O	bd	0.01	0.03	BDL	bd	0.01	0.03	BDL
K2O	5.95	0.01	0.03	5.95	6.88	0.01	0.03	6.88
P2O5	0.08	0.01	0.03	0.08	0.03	0.01	0.03	BDL
Sc	6.03	0.15	0.44	6.03	7.74	0.15	0.44	7.74
V	20.30	0.13	0.38	20.30	34.74	0.13	0.38	34.74
Cr	28.83	3.13	9.39	28.83	54.58	3.13	9.39	54.58
Ni	16.06	0.41	1.22	16.06	73.23	0.41	1.22	73.23
Cu	5.71	0.52	1.55	5.71	19.98	0.52	1.55	19.98
Zn	17.28	0.59	1.78	17.28	103.55	0.59	1.78	103.55
Rb	92.67	0.04	0.12	92.67	85.77	0.04	0.12	85.77
Sr	8.15	0.00	0.00	8.15	4.19	0.00	0.00	4.19
Y	4.28	0.01	0.04	4.28	14.13	0.01	0.04	14.13
Zr	83.02	0.00	0.00	83.02	125.82	0.00	0.00	125.82
Nb	3.81	0.01	0.04	3.81	5.47	0.01	0.04	5.47
Mo	0.50	0.05	0.14	0.50	0.43	0.05	0.14	0.43
Cs	1.76	0.01	0.02	1.76	1.93	0.01	0.02	1.93
Ba	164.07	0.00	0.00	164.07	310.54	0.00	0.00	310.54
La	12.01	0.00	0.00	12.01	13.63	0.00	0.00	13.63
Ce	21.04	0.00	0.00	21.04	25.13	0.00	0.00	25.13
Pr	1.93	0.00	0.00	1.93	2.74	0.00	0.00	2.74
Nd	6.93	0.00	0.00	6.93	11.97	0.00	0.00	11.97
Sm	1.20	0.00	0.00	1.20	2.72	0.00	0.00	2.72
Eu	0.50	0.00	0.00	0.50	0.89	0.00	0.00	0.89
Gd	0.91	0.00	0.00	0.91	2.61	0.00	0.00	2.61
Tb	0.13	0.01	0.02	0.13	0.32	0.01	0.02	0.32
Dy	0.80	0.02	0.06	0.80	2.19	0.02	0.06	2.19
Ho	0.15	0.00	0.00	0.15	0.50	0.00	0.00	0.50
Er	0.47	0.02	0.07	0.47	1.42	0.02	0.07	1.42
Tm	0.07	0.00	0.00	0.07	0.23	0.00	0.00	0.23
Yb	0.46	0.00	0.00	0.46	1.28	0.00	0.00	1.28
Lu	0.07	0.00	0.00	0.07	0.17	0.00	0.00	0.17
Hf	2.15	0.04	0.11	2.15	3.47	0.04	0.11	3.47
Ta	0.37	0.00	0.00	0.37	0.55	0.00	0.00	0.55

Sample name	DHG 01-12	LLD	LLD*3		DHG 01-16	LLD	LLD*3	
Lab	Stel1			Thesis data	Stel1			Thesis data
SiO2	72.30	0.03	0.09	72.3	69.85	0.03	0.09	69.85
TiO2	0.22	0.02	0.06	0.22	0.23	0.02	0.06	0.23
Al2O3	14.88	0.06	0.18	14.88	14.57	0.06	0.18	14.57
FeOt	1.41	0.01	0.03	1.41	2.27	0.01	0.03	2.27
MnO	0.09	0.01	0.03	0.09	0.03	0.01	0.03	BDL
MgO	0.69	0.04	0.12	0.69	0.89	0.04	0.12	0.89
CaO	0.00	0.04	0.12	BDL	1.79	0.04	0.12	1.79
Na2O	0.01	0.01	0.03	BDL	6.30	0.01	0.03	6.3
K2O	7.66	0.01	0.03	7.66	0.87	0.01	0.03	0.87
P2O5	0.04	0.01	0.03	0.04	0.06	0.01	0.03	0.06
Sc	5.91	0.15	0.44	5.91	5.22	0.15	0.44	5.22
V	20.12	0.13	0.38	20.12	24.75	0.13	0.38	24.75
Cr	30.04	3.13	9.39	30.04	72.11	3.13	9.39	72.11
Ni	26.17	0.41	1.22	26.17	20.47	0.41	1.22	20.47
Cu	14.47	0.52	1.55	14.47	39.11	0.52	1.55	39.11
Zn	33.44	0.59	1.78	33.44	25.72	0.59	1.78	25.72
Rb	144.38	0.04	0.12	144.38	71.74	0.04	0.12	71.74
Sr	11.96	0.00	0.00	11.96	20.56	0.00	0.00	20.56
Y	5.56	0.01	0.04	5.56	4.10	0.01	0.04	4.10
Zr	123.67	0.00	0.00	123.67	78.94	0.00	0.00	78.94
Nb	5.88	0.01	0.04	5.88	2.48	0.01	0.04	2.48
Mo	0.57	0.05	0.14	0.57	0.34	0.05	0.14	0.34
Cs	2.45	0.01	0.02	2.45	1.38	0.01	0.02	1.38
Ba	392.76	0.00	0.00	392.76	151.73	0.00	0.00	151.73
La	14.43	0.00	0.00	14.43	7.33	0.00	0.00	7.33
Ce	25.06	0.00	0.00	25.06	14.07	0.00	0.00	14.07
Pr	2.52	0.00	0.00	2.52	1.65	0.00	0.00	1.65
Nd	9.75	0.00	0.00	9.75	6.89	0.00	0.00	6.89
Sm	1.75	0.00	0.00	1.75	1.42	0.00	0.00	1.42
Eu	0.46	0.00	0.00	0.46	0.33	0.00	0.00	0.33
Gd	1.32	0.00	0.00	1.32	0.92	0.00	0.00	0.92
Tb	0.18	0.01	0.02	0.18	0.14	0.01	0.02	0.14
Dy	0.99	0.02	0.06	0.99	0.84	0.02	0.06	0.84
Ho	0.20	0.00	0.00	0.20	0.14	0.00	0.00	0.14
Er	0.54	0.02	0.07	0.54	0.47	0.02	0.07	0.47
Tm	0.08	0.00	0.00	0.08	0.09	0.00	0.00	0.09
Yb	0.52	0.00	0.00	0.52	0.45	0.00	0.00	0.45
Lu	0.09	0.00	0.00	0.09	0.08	0.00	0.00	0.08
Hf	3.15	0.04	0.11	3.15	2.07	0.04	0.11	2.07
Ta	0.60	0.00	0.00	0.60	0.23	0.00	0.00	0.23

Sample name	DHG 02-10	LLD	LLD*3		DHG 02-12	LLD	LLD*3	
Lab	Stel3			Thesis data	Stel1			Thesis data
SiO2	71.68	0.03	0.09	71.68	70.5447	0.03	0.09	70.54
TiO2	0.22	0.02	0.06	0.22	0.2718	0.02	0.06	0.27
Al2O3	15.81	0.06	0.18	15.81	12.4497	0.06	0.18	12.45
FeOt	1.69	0.01	0.03	1.69	7.5888	0.01	0.03	7.59
MnO	0.01	0.01	0.03	BDL	0.0981	0.01	0.03	0.1
MgO	0.86	0.04	0.12	0.86	2.376	0.04	0.12	2.38
CaO	0.02	0.04	0.12	BDL	0.0693	0.04	0.12	BDL
Na2O	0.00	0.01	0.03	BDL	bd	0.01	0.03	BDL
K2O	7.29	0.01	0.03	7.29	3.0366	0.01	0.03	3.04
P2O5	0.05	0.01	0.03	0.05	0.0693	0.01	0.03	0.07
Sc	5.98	0.15	0.44	5.98	5.83	0.15	0.44	5.83
V	20.95	0.13	0.38	20.95	21.45	0.13	0.38	21.45
Cr	70.21	3.13	9.39	70.21	34.27	3.13	9.39	34.27
Ni	17.58	0.41	1.22	17.58	25.50	0.41	1.22	25.50
Cu	24.60	0.52	1.55	24.60	8.90	0.52	1.55	8.90
Zn	18.66	0.59	1.78	18.66	22.05	0.59	1.78	22.05
Rb	105.59	0.04	0.12	105.59	146.16	0.04	0.12	146.16
Sr	25.66	0.00	0.00	25.66	4.72	0.00	0.00	4.72
Y	3.87	0.01	0.04	3.87	5.26	0.01	0.04	5.26
Zr	84.78	0.00	0.00	84.78	120.91	0.00	0.00	120.91
Nb	3.60	0.01	0.04	3.60	4.89	0.01	0.04	4.89
Mo	0.51	0.05	0.14	0.51	0.80	0.05	0.14	0.80
Cs	2.07	0.01	0.02	2.07	3.47	0.01	0.02	3.47
Ba	209.10	0.00	0.00	209.10	186.88	0.00	0.00	186.88
La	10.54	0.00	0.00	10.54	14.66	0.00	0.00	14.66
Ce	17.85	0.00	0.00	17.85	23.86	0.00	0.00	23.86
Pr	1.83	0.00	0.00	1.83	2.61	0.00	0.00	2.61
Nd	6.52	0.00	0.00	6.52	9.69	0.00	0.00	9.69
Sm	1.52	0.00	0.00	1.52	1.67	0.00	0.00	1.67
Eu	0.44	0.00	0.00	0.44	0.59	0.00	0.00	0.59
Gd	1.09	0.00	0.00	1.09	1.30	0.00	0.00	1.30
Tb	0.13	0.01	0.02	0.13	0.19	0.01	0.02	0.19
Dy	0.78	0.02	0.06	0.78	1.02	0.02	0.06	1.02
Ho	0.17	0.00	0.00	0.17	0.21	0.00	0.00	0.21
Er	0.45	0.02	0.07	0.45	0.45	0.02	0.07	0.45
Tm	0.05	0.00	0.00	0.05	0.09	0.00	0.00	0.09
Yb	0.31	0.00	0.00	0.31	0.49	0.00	0.00	0.49
Lu	0.05	0.00	0.00	0.05	0.09	0.00	0.00	0.09
Hf	2.10	0.04	0.11	2.10	2.95	0.04	0.11	2.95
Ta	0.32	0.00	0.00	0.32	0.55	0.00	0.00	0.55

Sample name	DHG 02-16	LLD	LLD*3		DHG 03-16	LLD	LLD*3	
Lab	Stel2			Thesis data	Stel2			Thesis data
SiO2	72.97	0.03	0.09	72.97	66.82	0.03	0.09	66.82
TiO2	0.20	0.02	0.06	0.2	0.28	0.02	0.06	0.28
Al2O3	14.56	0.06	0.18	14.56	14.00	0.06	0.18	14
FeOt	1.74	0.01	0.03	1.74	2.08	0.01	0.03	2.08
MnO	0.03	0.01	0.03	BDL	0.04	0.01	0.03	0.04
MgO	1.13	0.04	0.12	1.13	1.08	0.04	0.12	1.08
CaO	0.62	0.04	0.12	0.62	3.61	0.04	0.12	3.61
Na2O	4.03	0.01	0.03	4.03	2.34	0.01	0.03	2.34
K2O	1.59	0.01	0.03	1.59	3.51	0.01	0.03	3.51
P2O5	0.06	0.01	0.03	0.06	0.06	0.01	0.03	0.06
Sc	3.70	0.15	0.44	3.70	4.13	0.15	0.44	4.13
V	17.52	0.13	0.38	17.52	15.57	0.13	0.38	15.57
Cr	37.21	3.13	9.39	37.21	29.90	3.13	9.39	29.90
Ni	11.77	0.41	1.22	11.77	16.52	0.41	1.22	16.52
Cu	11.00	0.52	1.55	11.00	31.38	0.52	1.55	31.38
Zn	14.31	0.59	1.78	14.31	16.14	0.59	1.78	16.14
Rb	139.26	0.04	0.12	139.26	115.13	0.04	0.12	115.13
Sr	10.80	0.00	0.00	10.80	10.16	0.00	0.00	10.16
Y	6.74	0.01	0.04	6.74	8.09	0.01	0.04	8.09
Zr	115.07	0.00	0.00	115.07	130.38	0.00	0.00	130.38
Nb	7.42	0.01	0.04	7.42	7.78	0.01	0.04	7.78
Mo	0.47	0.05	0.14	0.47	0.36	0.05	0.14	0.36
Cs	3.08	0.01	0.02	3.08	3.04	0.01	0.02	3.04
Ba	387.94	0.00	0.00	387.94	442.70	0.00	0.00	442.70
La	12.92	0.00	0.00	12.92	15.66	0.00	0.00	15.66
Ce	25.07	0.00	0.00	25.07	26.99	0.00	0.00	26.99
Pr	2.53	0.00	0.00	2.53	2.84	0.00	0.00	2.84
Nd	9.05	0.00	0.00	9.05	11.64	0.00	0.00	11.64
Sm	1.81	0.00	0.00	1.81	1.86	0.00	0.00	1.86
Eu	0.59	0.00	0.00	0.59	0.55	0.00	0.00	0.55
Gd	1.42	0.00	0.00	1.42	1.68	0.00	0.00	1.68
Tb	0.20	0.01	0.02	0.20	0.22	0.01	0.02	0.22
Dy	1.28	0.02	0.06	1.28	1.81	0.02	0.06	1.81
Ho	0.27	0.00	0.00	0.27	0.32	0.00	0.00	0.32
Er	0.73	0.02	0.07	0.73	0.82	0.02	0.07	0.82
Tm	0.10	0.00	0.00	0.10	0.13	0.00	0.00	0.13
Yb	0.68	0.00	0.00	0.68	0.82	0.00	0.00	0.82
Lu	0.10	0.00	0.00	0.10	0.14	0.00	0.00	0.14
Hf	2.98	0.04	0.11	2.98	3.45	0.04	0.11	3.45
Ta	0.64	0.00	0.00	0.64	0.86	0.00	0.00	0.86

Sample name	DHG 04-14	LLD	LLD*3		DHG 06-13	LLD	LLD*3	
Lab	Stel3			Thesis data	Stel3			Thesis data
SiO2	71.92	0.03	0.09	71.92	76.34	0.03	0.09	76.34
TiO2	0.19	0.02	0.06	0.19	0.18	0.02	0.06	0.18
Al2O3	14.73	0.06	0.18	14.73	13.03	0.06	0.18	13.03
FeOt	1.58	0.01	0.03	1.58	0.23	0.01	0.03	0.23
MnO	0.03	0.01	0.03	BDL	0.00	0.01	0.03	BDL
MgO	1.34	0.04	0.12	1.34	0.22	0.04	0.12	0.22
CaO	0.53	0.04	0.12	0.53	0.09	0.04	0.12	0.09
Na2O	4.60	0.01	0.03	4.6	0.03	0.01	0.03	BDL
K2O	2.23	0.01	0.03	2.23	8.48	0.01	0.03	8.48
P2O5	0.06	0.01	0.03	0.06	0.11	0.01	0.03	0.11
Sc	4.24	0.15	0.44	4.24	8.05	0.15	0.44	8.05
V	12.41	0.13	0.38	12.41	22.09	0.13	0.38	22.09
Cr	16.66	3.13	9.39	16.66	31.01	3.13	9.39	31.01
Ni	19.06	0.41	1.22	19.06	25.23	0.41	1.22	25.23
Cu	4.22	0.52	1.55	4.22	8.95	0.52	1.55	8.95
Zn	14.69	0.59	1.78	14.69	25.79	0.59	1.78	25.79
Rb	41.78	0.04	0.12	41.78	87.44	0.04	0.12	87.44
Sr	32.39	0.00	0.00	32.39	7.04	0.00	0.00	7.04
Y	3.25	0.01	0.04	3.25	6.39	0.01	0.04	6.39
Zr	75.63	0.00	0.00	75.63	114.44	0.00	0.00	114.44
Nb	3.07	0.01	0.04	3.07	5.02	0.01	0.04	5.02
Mo	0.67	0.05	0.14	0.67	1.08	0.05	0.14	1.08
Cs	1.58	0.01	0.02	1.58	3.03	0.01	0.02	3.03
Ba	99.38	0.00	0.00	99.38	190.71	0.00	0.00	190.71
La	9.52	0.00	0.00	9.52	14.99	0.00	0.00	14.99
Ce	18.64	0.00	0.00	18.64	26.14	0.00	0.00	26.14
Pr	2.03	0.00	0.00	2.03	2.63	0.00	0.00	2.63
Nd	7.20	0.00	0.00	7.20	9.83	0.00	0.00	9.83
Sm	1.28	0.00	0.00	1.28	1.81	0.00	0.00	1.81
Eu	0.35	0.00	0.00	0.35	0.50	0.00	0.00	0.50
Gd	0.86	0.00	0.00	0.86	1.45	0.00	0.00	1.45
Tb	0.13	0.01	0.02	0.13	0.19	0.01	0.02	0.19
Dy	0.55	0.02	0.06	0.55	0.97	0.02	0.06	0.97
Ho	0.13	0.00	0.00	0.13	0.22	0.00	0.00	0.22
Er	0.29	0.02	0.07	0.29	0.72	0.02	0.07	0.72
Tm	0.03	0.00	0.00	0.03	0.10	0.00	0.00	0.10
Yb	0.28	0.00	0.00	0.28	0.57	0.00	0.00	0.57
Lu	0.04	0.00	0.00	0.04	0.09	0.00	0.00	0.09
Hf	1.93	0.04	0.11	1.93	2.88	0.04	0.11	2.88
Ta	0.29	0.00	0.00	0.29	0.54	0.00	0.00	0.54

Sample name	SHG 03-16	LLD	LLD*3		DHG 05-18a	LLD	LLD*3	
Lab	Stel2			Thesis data	Stel2			Thesis data
SiO2	71.15	0.03	0.09	71.15	70.67	0.03	0.09	70.67
TiO2	0.25	0.02	0.06	0.25	0.24	0.02	0.06	0.24
Al2O3	15.03	0.06	0.18	15.03	14.46	0.06	0.18	14.46
FeOt	2.07	0.01	0.03	2.07	0.31	0.01	0.03	0.31
MnO	0.02	0.01	0.03	BDL	BDL	0.01	0.03	BDL
MgO	0.88	0.04	0.12	0.88	0.41	0.04	0.12	0.41
CaO	0.25	0.04	0.12	0.25	0.53	0.04	0.12	0.53
Na2O	6.63	0.01	0.03	6.63	0.028	0.01	0.03	BDL
K2O	0.45	0.01	0.03	0.45	10.1	0.01	0.03	10.1
P2O5	0.06	0.01	0.03	0.06	0.08	0.01	0.03	0.08
Sc	6.35	0.15	0.44	6.35	3.71	0.15	0.44	3.71
V	18.91	0.13	0.38	18.91	14.94	0.13	0.38	14.94
Cr	28.35	3.13	9.39	28.35	46.68	3.13	9.39	46.68
Ni	6.39	0.41	1.22	6.39	9.24	0.41	1.22	9.24
Cu	5.17	0.52	1.55	5.17	10.27	0.52	1.55	10.27
Zn	10.55	0.59	1.78	10.55	14.55	0.59	1.78	14.55
Rb	45.84	0.04	0.12	45.84	141.12	0.04	0.12	141.12
Sr	11.54	0.00	0.00	11.54	6.36	0.00	0.00	6.36
Y	5.94	0.01	0.04	5.94	5.34	0.01	0.04	5.34
Zr	87.02	0.00	0.00	87.02	77.04	0.00	0.00	77.04
Nb	6.48	0.01	0.04	6.48	5.84	0.01	0.04	5.84
Mo	0.41	0.05	0.14	0.41	0.49	0.05	0.14	0.49
Cs	1.27	0.01	0.02	1.27	1.93	0.01	0.02	1.93
Ba	215.56	0.00	0.00	215.56	165.68	0.00	0.00	165.68
La	13.52	0.00	0.00	13.52	8.47	0.00	0.00	8.47
Ce	25.60	0.00	0.00	25.60	19.20	0.00	0.00	19.20
Pr	2.82	0.00	0.00	2.82	1.81	0.00	0.00	1.81
Nd	10.93	0.00	0.00	10.93	6.55	0.00	0.00	6.55
Sm	2.10	0.00	0.00	2.10	1.32	0.00	0.00	1.32
Eu	0.62	0.00	0.00	0.62	0.42	0.00	0.00	0.42
Gd	1.63	0.00	0.00	1.63	1.18	0.00	0.00	1.18
Tb	0.21	0.01	0.02	0.21	0.16	0.01	0.02	0.16
Dy	1.18	0.02	0.06	1.18	0.98	0.02	0.06	0.98
Ho	0.23	0.00	0.00	0.23	0.19	0.00	0.00	0.19
Er	0.62	0.02	0.07	0.62	0.46	0.02	0.07	0.46
Tm	0.09	0.00	0.00	0.09	0.07	0.00	0.00	0.07
Yb	0.52	0.00	0.00	0.52	0.43	0.00	0.00	0.43
Lu	0.09	0.00	0.00	0.09	0.07	0.00	0.00	0.07
Hf	2.02	0.04	0.11	2.02	1.99	0.04	0.11	1.99
Ta	0.53	0.00	0.00	0.53	0.46	0.00	0.00	0.46

Sample name	DHG 05-18b	LLD	LLD*3		DHG 03-18	LLD	LLD*3	
Lab	Stel1			Thesis data	Stel3			Thesis data
SiO2	71.39	0.03	0.09	71.39	70.987	0.03	0.09	70.99
TiO2	0.22	0.02	0.06	0.22	0.239	0.02	0.06	0.24
Al2O3	13.25	0.06	0.18	13.25	13.531	0.06	0.18	13.53
FeOt	0.37	0.01	0.03	0.37	0.551	0.01	0.03	0.55
MnO	0.04	0.01	0.03	0.04	0.033	0.01	0.03	BDL
MgO	0.60	0.04	0.12	0.6	0.613	0.04	0.12	0.61
CaO	1.11	0.04	0.12	1.11	1.613	0.04	0.12	1.61
Na2O	0.04	0.01	0.03	0.04	0.035	0.01	0.03	0.04
K2O	9.32	0.01	0.03	9.32	7.974	0.01	0.03	7.97
P2O5	0.07	0.01	0.03	0.07	0.076	0.01	0.03	0.08
Sc	8.17	0.15	0.44	8.17	3.92	0.15	0.44	3.92
V	30.98	0.13	0.38	30.98	13.11	0.13	0.38	13.11
Cr	33.60	3.13	9.39	33.60	30.44	3.13	9.39	30.44
Ni	12.23	0.41	1.22	12.23	14.84	0.41	1.22	14.84
Cu	18.90	0.52	1.55	18.90	4.68	0.52	1.55	4.68
Zn	19.43	0.59	1.78	19.43	21.68	0.59	1.78	21.68
Rb	95.33	0.04	0.12	95.33	120.20	0.04	0.12	120.20
Sr	15.55	0.00	0.00	15.55	17.50	0.00	0.00	17.50
Y	10.81	0.01	0.04	10.81	7.76	0.01	0.04	7.76
Zr	115.64	0.00	0.00	115.64	128.81	0.00	0.00	128.81
Nb	7.07	0.01	0.04	7.07	7.51	0.01	0.04	7.51
Mo	0.60	0.05	0.14	0.60	0.41	0.05	0.14	0.41
Cs	1.13	0.01	0.02	1.13	2.68	0.01	0.02	2.68
Ba	127.29	0.00	0.00	127.29	595.05	0.00	0.00	595.05
La	15.38	0.00	0.00	15.38	16.43	0.00	0.00	16.43
Ce	27.82	0.00	0.00	27.82	27.91	0.00	0.00	27.91
Pr	3.03	0.00	0.00	3.03	2.96	0.00	0.00	2.96
Nd	11.72	0.00	0.00	11.72	11.32	0.00	0.00	11.32
Sm	2.45	0.00	0.00	2.45	2.08	0.00	0.00	2.08
Eu	0.64	0.00	0.00	0.64	0.59	0.00	0.00	0.59
Gd	2.14	0.00	0.00	2.14	1.70	0.00	0.00	1.70
Tb	0.33	0.01	0.02	0.33	0.21	0.01	0.02	0.21
Dy	1.81	0.02	0.06	1.81	1.40	0.02	0.06	1.40
Ho	0.40	0.00	0.00	0.40	0.25	0.00	0.00	0.25
Er	1.06	0.02	0.07	1.06	0.82	0.02	0.07	0.82
Tm	0.15	0.00	0.00	0.15	0.14	0.00	0.00	0.14
Yb	1.04	0.00	0.00	1.04	0.66	0.00	0.00	0.66
Lu	0.12	0.00	0.00	0.12	0.11	0.00	0.00	0.11
Hf	2.88	0.04	0.11	2.88	3.25	0.04	0.11	3.25
Ta	0.61	0.00	0.00	0.61	0.65	0.00	0.00	0.65

Sample name	DHG 01-18	LLD	LLD*3		DHG 04-18a	LLD	LLD*3	
Lab	Stel3			Thesis data	Stel2			Thesis data
SiO2	66.09	0.03	0.09	66.09	70.81	0.03	0.09	70.81
TiO2	0.36	0.02	0.06	0.36	0.28	0.02	0.06	0.28
Al2O3	9.68	0.06	0.18	9.68	14.05	0.06	0.18	14.05
FeOt	1.74	0.01	0.03	1.74	0.57	0.01	0.03	0.57
MnO	0.20	0.01	0.03	0.2	0.05	0.01	0.03	0.05
MgO	2.53	0.04	0.12	2.53	0.51	0.04	0.12	0.51
CaO	4.74	0.04	0.12	4.74	0.58	0.04	0.12	0.58
Na2O	0.01	0.01	0.03	BDL	0.03	0.01	0.03	BDL
K2O	6.11	0.01	0.03	6.11	9.69	0.01	0.03	9.69
P2O5	0.08	0.01	0.03	0.08	0.08	0.01	0.03	0.08
Sc	3.95	0.15	0.44	3.95	6.11	0.15	0.44	6.11
V	10.74	0.13	0.38	10.74	12.41	0.13	0.38	12.41
Cr	42.17	3.13	9.39	42.17	25.04	3.13	9.39	25.04
Ni	7.78	0.41	1.22	7.78	9.44	0.41	1.22	9.44
Cu	5.10	0.52	1.55	5.10	13.46	0.52	1.55	13.46
Zn	12.17	0.59	1.78	12.17	17.84	0.59	1.78	17.84
Rb	121.18	0.04	0.12	121.18	124.49	0.04	0.12	124.49
Sr	9.02	0.00	0.00	9.02	11.98	0.00	0.00	11.98
Y	3.52	0.01	0.04	3.52	8.31	0.01	0.04	8.31
Zr	86.04	0.00	0.00	86.04	141.79	0.00	0.00	141.79
Nb	4.60	0.01	0.04	4.60	8.49	0.01	0.04	8.49
Mo	0.38	0.05	0.14	0.38	0.42	0.05	0.14	0.42
Cs	1.42	0.01	0.02	1.42	1.94	0.01	0.02	1.94
Ba	171.44	0.00	0.00	171.44	237.89	0.00	0.00	237.89
La	10.57	0.00	0.00	10.57	15.80	0.00	0.00	15.80
Ce	19.59	0.00	0.00	19.59	29.60	0.00	0.00	29.60
Pr	1.82	0.00	0.00	1.82	3.06	0.00	0.00	3.06
Nd	7.01	0.00	0.00	7.01	11.74	0.00	0.00	11.74
Sm	1.20	0.00	0.00	1.20	2.38	0.00	0.00	2.38
Eu	0.37	0.00	0.00	0.37	0.54	0.00	0.00	0.54
Gd	1.07	0.00	0.00	1.07	1.84	0.00	0.00	1.84
Tb	0.12	0.01	0.02	0.12	0.28	0.01	0.02	0.28
Dy	0.65	0.02	0.06	0.65	1.66	0.02	0.06	1.66
Ho	0.12	0.00	0.00	0.12	0.29	0.00	0.00	0.29
Er	0.35	0.02	0.07	0.35	0.87	0.02	0.07	0.87
Tm	0.06	0.00	0.00	0.06	0.13	0.00	0.00	0.13
Yb	0.27	0.00	0.00	0.27	0.78	0.00	0.00	0.78
Lu	0.04	0.00	0.00	0.04	0.11	0.00	0.00	0.11
Hf	2.23	0.04	0.11	2.23	3.61	0.04	0.11	3.61
Ta	0.38	0.00	0.00	0.38	0.73	0.00	0.00	0.73

Sample name	DHG 02-18d	LLD	LLD*3		SHG 05-03*	LLD	LLD*3	
Lab	Stel2			Thesis data	Acme			Thesis data
SiO2	71.10	0.03	0.09	71.1	78.5	0.01	0.03	78.5
TiO2	0.27	0.02	0.06	0.27	0.21	0.01	0.03	0.21
Al2O3	13.87	0.06	0.18	13.87	13.26	0.01	0.03	13.26
FeOt	0.74	0.01	0.03	0.74	0.42	0.04	0.12	0.42
MnO	0.03	0.01	0.03	BDL	0.01	0.01	0.03	BDL
MgO	0.68	0.04	0.12	0.68	0.57	0.01	0.03	0.57
CaO	1.28	0.04	0.12	1.28	0.01	0.01	0.03	BDL
Na2O	BD	0.01	0.03	BDL	0.04	0.01	0.03	0.04
K2O	8.04	0.01	0.03	8.04	4.52	0.01	0.03	4.52
P2O5	0.07	0.01	0.03	0.07	0.01	0.01	0.03	BDL
Sc	5.14	0.15	0.44	5.14	3.00	1.00	3.00	BDL
V	22.55	0.13	0.38	22.55	17.00	8.00	24.00	BDL
Cr	29.07	3.13	9.39	29.07			0.00	BDL
Ni	30.28	0.41	1.22	30.28	20.00	20.00	60.00	BDL
Cu	35.00	0.52	1.55	35.00	0.30	0.10	0.30	0.30
Zn	50.98	0.59	1.78	50.98	2.00	1.00	3.00	BDL
Ga					16.10	0.50	1.50	16.10
Rb	94.87	0.04	0.12	94.87	86.30	0.10	0.30	86.30
Sr	119.12	0.00	0.00	119.12	4.30	0.50	1.50	4.30
Y	4.82	0.01	0.04	4.82	4.40	0.10	0.30	4.40
Zr	112.48	0.00	0.00	112.48	101.70	0.10	0.30	101.70
Nb	4.77	0.01	0.04	4.77	4.00	0.10	0.30	4.00
Mo	0.88	0.05	0.14	0.88	0.10	0.10	0.30	BDL
Sn					1.00	1.00	3.00	BDL
Cs	3.01	0.01	0.02	3.01	1.30	0.10	0.30	1.30
Ba	357.15	0.00	0.00	357.15	257.00	1.00	3.00	257.00
La	16.27	0.00	0.00	16.27	12.40	0.10	0.30	12.40
Ce	28.17	0.00	0.00	28.17	23.50	0.10	0.30	23.50
Pr	2.97	0.00	0.00	2.97	2.35	0.02	0.06	2.35
Nd	10.97	0.00	0.00	10.97	8.00	0.30	0.90	8.00
Sm	2.22	0.00	0.00	2.22	1.25	0.05	0.15	1.25
Eu	0.61	0.00	0.00	0.61	0.28	0.02	0.06	0.28
Gd	1.46	0.00	0.00	1.46	0.98	0.05	0.15	0.98
Tb	0.18	0.01	0.02	0.18	0.15	0.01	0.03	0.15
Dy	0.91	0.02	0.06	0.91	0.79	0.05	0.15	0.79
Ho	0.15	0.00	0.00	0.15	0.14	0.02	0.06	0.14
Er	0.48	0.02	0.07	0.48	0.42	0.03	0.09	0.42
Tm	0.08	0.00	0.00	0.08	0.07	0.01	0.03	0.07
Yb	0.42	0.00	0.00	0.42	0.40	0.05	0.15	0.40
Lu	0.07	0.00	0.00	0.07	0.06	0.01	0.03	0.06
Hf	2.91	0.04	0.11	2.91	3.20	0.10	0.30	3.20
Ta	0.47	0.00	0.00	0.47	0.40	0.10	0.30	0.40

References

Anhaeusser, C. R., (1973), The geology and geochemistry of the Archaean granites and gneisses of the Johannesburg-Pretoria Dome, *Geology Society of South Africa*, Special Publication, 3, 361-385.

Anhaeusser, C. R., Robb, L. J., Viljoen, M. J., (1981), Provisional geological map of the Barberton Greenstone Belt and surrounding granitic terrane, eastern Transvaal and Swaziland, *Geological Society of South Africa*, scale 1:250,000, Geological Society of South Africa, Special Publication 9.

Armstrong, R. A., Compston, W., de Wit, M. J. and Williams, I. S., (1990), The stratigraphy of the 3.5-3.2 Ga Barberton Greenstone Belt revisited: a single zircon ion microprobe study, *Earth and Planetary Science Letters*, 101, 90-106.

Alfonso, P., Melgarejo, J.C., Yusta, I., Velasco, F., (2003), Geochemistry of feldspars and muscovite in granitic pegmatite from the Cap de Creus field, Catalonia, Spain,*Canadian Mineralogist*, 41, 103–116.

Barker, F., Arth, J.G., (1976), Generation of trondhjemitic-tonalitic liquids and Archean bimodal trondjemite-basalt suites, *Geology*, 4, 596-600.

Barker, F., (1979), Trondhjemite: Definition, environment and hypotheses of origin, *in* Barker, F., (Eds.), Trondhjemites, dacites and related rocks, Elsevier, Amsterdam, 1-12.

Belcher, R.W., Kisters, A.F.M., (2006a), Syntectonic emplacement and deformation of the Heerenveen batholith: Conjectures on the structural setting of the 3.1 Ga granite magmatism in the Barberton granite-greenstone terrain, South Africa. In: Reimold, W.U.,

Belcher, R.W., Kisters, A.F.M., (2006b), Progressive adjustments of ascent and emplacement controls during the incremental construction of the 3.1 Ga Heerenveen batholith, South Africa. *Journal of Structural Geology 28*, 1406–1421.

Berman, R.G., (1988), Internally consistent thermodynamic data for minerals in the system Na_2O- K_2O- CaO- MgO- FeO- Fe_2O_3- Al_2O_3-SiO_2- TiO_2- H_2O- CO_2. *Journal of Petrology*, 29, 445–522.

Smith, J.V., Brown, W.L., (1988) Feldspar minerals: Crystal Structures, Physical, Chemical, and Microtextural Properties, Second revised and extended Edition, Springer-Verlag.

Byerly, G.R., Kröner, A., Lowe, D.R., Todt, W., Walsh, M.M., (1996), Prolonged magmatism and time constraints for sediments deposition in the Early Archean Barberton greenstone belt: evidence from the upper Onverwacht and Fig Tree groups. *Precambrian Research* 78, 125–138.

Cloete, M., (1999), Aspects of volcanism and metamorphism of the Onverwacht Group lavas in the southwestern portion of the Barberton Greenstone Belt. *Memoir of the Geological Society of South Africa*, 84, 232 pp.

de Ronde, C.E.J., Kamo, S.L., (2000), An Archean Arc-Arc collisional event: a short-lived (ca. 3 Myr) episode, Weltevreden area, Barberton greenstone belt, South Africa. *Journal of African Earth Sciences*, 30 (2), 219-248.

de Vries, S.T., Nijman, W., Armstrong, R.A., 2006, Growth-fault structure and stratigraphic architecture of the Buck Ridge volcano-sedimentary complex, upper Hooggenoeg Formation, Barberton Greenstone Belt, South Africa., *Precambrian Research*, 149, 77-98.

de Vries, S.T., Touret, J.L.R., (2007). Early Archaean hydrothermal fluids; a study of inclusions from the similar to 3.4 Ga Buck Ridge Chert, Barberton Greenstone Belt, South Africa. *Chemical Geology*. 237 (3–4), 289–302.

de Wit, M.J., 1982, Gliding and overthrust nappe tectonics in the Barberton greenstone belt. *Journal of Structural Geology*, 4, 117-136.

de Wit, M.J., Armstrong, R.J., Wilson, A.H., (1987a), Felsic igneous rocks within the 3.3- to 3.5 Ga Barberton greenstone belt: high crustal level equivalents of the surrounding tonalite-trondhjemite terrain, emplaced during thrusting. *Tectonics*, 6, 529-549.

de Wit, M.J., Furnes, H., Robins, B., (2011), Geology and tectonostratigraphy of the Onverwacht Suite, Barberton Greenstone Belt, South Africa. *Precambrian Research*, 186, 1-27.

Diener, J., Stevens, G., and Kisters, A.F.M. (2006), High-pressure intermediate-temperature metamorphism in the Southern Barberton granitoid-greenstone terrain, South Africa: a consequence of subduction-driven overthickening and collapse of mid-Archean continental crust. In: Benn, K., Mareschal, J-C., Condie, K.C. (Eds.), Archean Geodynamics and Environments. Geophysical Monograph 164. American Geophysical Union, Washington, DC, pp.239-254.

Diener, J.F.A., Stevens, G., Kisters, A.F.M., Poujol, M., 2005. Metamorphism andexhumation of the basal parts of the Barberton greenstone belt, South Africa: constraining the rates of Mesoarchaean tectonism, *Precambrian Research*, 143,87–112.

Duchac, K.C., Hanor, J.S., (1987), Origin and timing of the metasomatic silicification of an Early Archean Komatiite Sequence, Barberton Mountain Land, South-Africa,*Precambrian Research*, 37 (2), 125–146.

Dziggel, A., Stevens, G., Poujol, M., Anhaeusser, C.R., Armstrong, R.A., (2002), Metamorphism of the granite-greenstone terrane south of the Barberton greenstone belt, South Africa: an insight into the tectono-thermal evolution of the 'lower' portions of the Onverwacht Group. *Precambrian Research*, 114, 221-247.

Foley, S., Tiepolo, M., and Vannucci, R., (2002), Growth of early continental crust controlled by melting of amphibolite in subduction zones,*Nature*, 417, 837–840.

Grant, J.A., (1986), The isocon diagram: a simple solution to Gresen's equation for metasomatic alteration. *Economic Geology*, 81, 1976–1982.

Grant, J.A., (2005), Isocon analysis: a brief review of the method and applications. *Physics and Chemistry of the Earth, 30*, 997–1004.

Gibson, R.L. (Eds.), Processes on the Early Earth. Geological Society of America, Special Publication 405, pp. 211-231.

Hall, A.L., (1918). The geology of the Barberton gold mining district. *Geological Survey of South Africa Memoir*, 9, 347.

Heubeck, C., Lowe, D.R., (1994a), Depositional and tectonic setting of the Archean Moodies Group, Barberton Greenstone Belt, South Africa, *Precambrian Research*, 68, 257-290.

Heubeck, C. and Lowe, D. R., (1994b), Late syndepositional deformation and detachment tectonics in the Barberton Greenstone Belt, South Africa, *Tectonics*, 13, 1514-1536.

Hofmann, A., (2005), The geochemistry of sedimentary rocks from the Fig Tree Group, Barberton greenstone belt: implications for tectonic, hydrothermal and surface processes during mid-Archaean times. *Precambrian Research*, 143 (1–4), 23–49.

Hofmann, A., Harris, C., (2008), Stratiform alteration zones in the Barbertongreenstone belt: a windowinto subseafloor processes 3.5–3.3 Ga ago. *Chemical Geology*, 257, 224–242.

Kamo, S.L., Davis, D.W., (1994), Reassessment of Archaean crustal development in the Barberton Mountain Land, South Africa, based on U–Pb dating. *Tectonics*, 13, 167–192.

Kisters, A. F. M., Stevens, G., Dziggel, A., Armstrong, R. A., (2003), Extensional detachment faulting and core-complex formation in the southern Barberton granite-greenstone terrain, South Africa: Evidence for a 3.2 Ga orogenic collapse, *Precambrian Research*, 127, 355-378.

Kitajima, K., Maruyama, S., Utsunomiya, S., Liou, J.G., (2001), Seafloor hydrothermal alteration at an Archaean mid-ocean ridge,*Journal of Metamorphic Geology*, 19, 581–597.

Knauth, L.P., Lowe, D.R., (2003), High Archean climatic temperature inferred from oxygen isotope geochemistry of cherts in the 3.5 Ga Swaziland Supergroup, South Africa. *Geological Society of America Bulletin*.115(5), 566–580.

Kröner, A., Byerly, G.R., Lowe, D.T., (1991a), Chronology of early Archaean granite-greenstone evolution in the Barberton Mountain Land, South Africa, based on precise dating by single zircon evaporation. *Earth and Planetary Sciences Letters*, 103, 41-54.

Kröner, A., Byerly, G.R., Lowe, D.T., (1992), Chronology of early Archaean granite-greenstone evolution in the Barberton Mountain Land, South Africa, based on precise dating by single zircon evaporation. *Earth and Planetary Sciences Letters.*, 103, 41-54.

Kroner, A., Hegner, E., Wendt, J. I., Byerly, G. R., (1996), The oldest part of the Barberton granitoid-greenstone terrain, South Africa: evidence for crust formation between 3.5 and 3.7 Ga, *Precambrian Research*, 78, 105-124.

Le Bas, M.J., Le Maitre, R.W., Streckeisen, A., Zanettin, B., (1986), A chemical classification of volcanic rocks based on the total alkali-silica diagram,*Journal of Petrology*, 27, 745-750.

Le Maitre, R.W, (2002), Igneous Rocks: A classification and Glossary of Terms. Cambridge University Press, Cambridge, pp. 236.

Lowe, D.R., Byerly, G.R., Ransom, B.L., Nocita, B.R., (1985), Stratigraphic and sedimentological evidence bearing on structural repetition in Early Archaean rocks of the Barberton Greenstone Belt, South Africa, *Precambrian Research*, 27, 165-186.

Lowe, D.R., Byerly, G.R., (1986b), Early archaean silicate spherules of probable impact origin, South Africa and western Australia,*Geology*, 14, 83-86.

Lowe, D.R., Byerly, G.R., (1999), Stratigraphy of the west-central part of the Barberton Greenstone Belt, South Africa. In: Lowe, D.R., Byerly, G.R. (Eds), Geologic Evolution of the Barberton Greenstone Belt, South Africa. *Geological Society of America, Special Paper*, 329, 1-36.

Lowe, D.R., Fisher Worrell, G.F., (1999), Sedimentology, mineralogy, and implications of silicified evaporites in the Kromberg Formation, Barberton Greenstone Belt, South Africa,*Geological Society of America Special Paper*, 329, 167–169.

Lowe, D.R., 1999b. Shallow-water sedimentation of accresionary lapilli-bearing strata of the Msuali Chert: Evidence of explosive hydromagmatic komatiitic volcanism. In: Lowe, D.R., Byerly, G.R. (Eds), Geologic Evolution of the Barberton Greenstone Belt, South Africa. *Geological Society of America, Special Paper*, 329, 213-232.

Lowe, D.R., (1999c), Geological evolution of the Barberton greenstone belt and vicinity. In: Lowe, D.R., G.R. Byerly. (Eds), Geologic Evolution of the Barberton Greenstone Belt, South Africa,*Geological Society of America, Special Paper*, 329, 287-312.

Lowe, D.R., Byerly, G.B., (2007), An overview of the geology of the Barberton Greenstone Belt and vicinity: implications for early crustal development. In: Van Kranendonk, M.J., Smithies, R.H., Bennett, V. (Eds.), Earth's Oldest rocks. : Developments in Precambrian geology. Elsevier, pp. 481-526.

Martin, H., 1994. The Archean grey gneisses and the genesis of the continental crust. In: Condie, K.C. (Ed.), Archean crustal evolution. Developments in Precambrian Geology. Elsevier, Amsterdam, pp. 205–259.

Martin, H., Moyen, J.-F., (2002), Secular changes in TTG composition as markers of the progressive cooling of the Earth,*Geology*,30 (4), 319–322.

Moyen, J-F., Stevens, G., (2006), Experimental constraints on TTG petrogenesis: Implications for Archean geodynamics. In: Benn, K., Mareschal, J-C., Condie, K.C. (Eds.), Archean Geodynamics and Environments. Geophysical Monograph 164. American Geophysical Union, Washington, DC, pp. 149-175.

Moyen, J.-F., Stevens, G., Kisters, A.F.M., Belcher, R.W., (2007), TTG plutons of the Barberton granitoid-greenstone terrain, South Africa. In: Van Kranendonk, M.J., Smithies, R.H., Bennett, V. (Eds.), Earth's Oldest rocks. : Developments in Precambrian geology. Elsevier, pp. 606–668.

Moyen, J-F., (2011), The composite Archaean grey gneisses: Petrological significance, and evidence for a non-unique tectonic setting for Archaean crustal growth,*Lithos*, 123, 21-36.

Mergoil-Daniel, J., Chevalier, R., (1984), Les feldspaths potassiques partiellement ordonnés: structure cristallographique et signification géologique = Partially ordered potassic feldspars: cristallographic structure and geological occurrence,*Bulletin de mineralogy*, 107, 401-410.

O'Connor, J.T., (1965). A classification of quartz-rich igneous rocks based on feldspar ratios. Washington US Government Printing Office, *Geological Survey Professional Papers*, 525, 79–84.

Patiño Douce, A.E., Johnston, A.D., (1991), Phase equilibria and melt productivity in the politic system: Implications for the origin of peraluminous granitoids and aluminous granulites: *Contributions to Mineralogy and Petrology*, 107, 202–218.

Paris, I., Stanistreet, I.G., Hughes, M.J., (1985), Cherts of the Barberton greenstone belt interpreted as products of submarine exhalative activity. *Journal of Geology*, 93, 111–129.

Petit, J-C., (1992), Reasoning by analogy. Rational foundation of natural analogue studies, *Applied Geochemistry*, Issue supplementary, 9-14.

Rapp, R.P., Shimizu, N., Norman, M.D., (2003), Growth of early continental crust by partial melting of eclogite.*Nature*, 425,605–609.

Rapp, R.P., Watson, E.B., Miller, C.F., (1991), Partial melting of amphibolite/eclogite and the origin of Archaean trondhjemites and tonalities, *Precambrian Research*, 51, 1–25.

Robb, L. J., Anhaeusser, C. R., (1983), Chemical and petrogenetic characteristics of Archaean tonalite-trondhjemite gneiss plutons in the Barberton Mountain Land, *Geological Societyof South Africa*, Special Publication, 9, 103-117.

Rouchon, V., Orberger, B., (2008), Origin and mechanism of K–Si metasomatism of ca. 3.4–3.3 Ga volcaniclastic depostits and implication for Archean seawater evolution: examples form cherts of Kittys Gap (Pilbara craton, Australia) and Msauli (Barberton Greenstone Belt, South Africa),*Precambrian Research.* 165, 169–189.

Rouchon, V., Orberger, B., Hofman, A., Pinty, D.L, (2009), Diagenetic Fe-carbonates in Paleoarchean felsic sedimentary rocks (HooggenoegFormation, Barberton greenstone belt, South Africa): Implications for CO2sequestration and the chemical budget of seawater,*Precambrian Research*, 172, 255-278.

Sanchez-Garrido, C.J.M.G., Stevens, G., Moyen, J-F., Martin, H., Doucelance, R., 2011, Diversity in Earth's early felsic crust: Paleoarchean peraluminous granites of the Barberton Greenstone Belt. *Geology*, 39, 963-966.

Schermerhorn, L.J.G., (1973), What is keratophyre?, *Lithos*, 6, 1–11.

Schmidt, M.W., Vielzeuf, D., Auzanneau, E., (2004), Melting and dissolution of subducting crust at high pressures: The key role of white mica. *Earth and Planetary Science Letters*, 228, 65–84.

Tarduno, J.A., Cottrell , R.D., Watkeys , M.K., Hofmann, A., Doubrovine, P.V., Mamajek , E.E., Lui, D., Silbeck, D.G., Neukirch, L.P., Usui, Y., (2010), Geodynamo, solar wind, and magnetopause 3.4–3.45 billion years ago, *Science* 327, 1238–1240.

Tegtmeyer, A.R., Kröner, A., (1987), U–Pb zircon ages bearing on the nature of early Archaean greenstone belt evolution, Barberton Mountainland, Southern Africa. *Precambrian Reseach*, 36, 1–20.

Terabayashi, M., Masada, Y., Ozawa, H., (2003), Archean ocean-floor metamorphism in the North Pole area, Pilbara Craton, Western Australia,*Precambrian Research*, 127, 167–180.

Van Kranendonk, M.J., Pirajno, F., (2004), Geological setting and geochemistry of metabasalts and alteration zones associated with hydrothermal chert ± barite deposits in the ca. 3.45 Ga Warrawoona Group, Pilbara Craton, Australia, Geochemistry: Exploration, Environment, *Analysis*, 4, 253-278.

Viljoen, M. J., Viljoen, R. P., (1969a), An introduction to the geology of the Barberton granite-greenstone terrain, *Geological Society of South Africa*, Special Publication 2, 9–28.

Viljoen, M. J., Viljoen, R. P., (1969b), The geology and geochemistry of the lower ultramafic unit of the Onverwacht Group and a proposed new class of igneous rocks, *Geological Society of South Africa*, Special Publication 2, 55-86.

Visser, D.J.L., et al., (1956). The geology of the Barberton Area. *Geological Survey of South Africa Special Publication*, 15, 1–253.

Westraat, J.D., Kisters, A.F.M., Poujol, M., Stevens, G., (2005), Transcurrent shearing, granite sheeting and the incremental construction of the tabular 3.1 Ga Mpuluzi batholith, Barberton granite- greenstone terrain, South Africa. *Journal of the Geological Society of London 162*, 373–388.

Usui, Y., Tarduno, J.A., Watkeys, M., Hofmann, A., Cottrell, R.D., (2009), Evidence for a 3.45-billion-year-old magnetic remanence: hints of an ancient geodynamo from conglomerates of South Africa,*Geochemistry Geophysics Geosystems*,10, 9.

Xie, X., Byerly, G.R., Ferrel, R.E., (1997), 2b trioctahedral chlorite from the Barberton Greenstone Belt: crystal structure and rock composition constraints with implications for geothermometry. *Contributions Mineralogy and Petrology*, 126, 275-291.

Yearron, L.M., (2003), Archaean granite petrogenesis and implications for the evolution of the Barberton Mountain Land, South Africa. Unpublished PhD Thesis, Kingston University, Kingtson, UK, 315 pp.

Zamora, D., 2000. Fusion de la croûte océanique subductée : approche expérimentale et géochimique. Thèse d'université Thesis, Université Blaise-Pascal, Clermont-Ferrand, France, 314 pp.